Exploring the Versatility of

Dithieno[2,3-*b*;3',2'-*e*]-4-keto-1,4-dihydrophosphinines

Amaar Hussein

A thesis submitted to the Faculty of Graduate Studies in partial fulfillment of the requirements for the degree of Masters in Chemistry

Department of Chemistry, York University
Toronto, Canada
June 2025

Abstract

A less studied alteration of the dithienophosphole is the dithieno[2,3-*b*;3',2'-*e*]-4-keto-1,4-dihydrophosphinine. Its relatively untouched chemistry and various sites for functionalization, makes it an appealing scaffold that can be tailored to the needs of various applications. Herein we report a range of targeted approaches to functionalizing each site of the dithienoketophosphinine with an emphasis on understanding the resulting properties. Based on the innate ability of phosphorus to be functionalized and alter the properties of entire molecular scaffolds, the first series of compounds focuses on phosphorus functionalization. The second series is derived from the synthetic versatility of carbonyl groups wherein Knoevenagel condensation was performed to create a series of dicyanomethylene-dithienophosphinines with enhanced acceptor character. Finally, a third series focusing on extending the conjugation of the dithienoketophosphinine by various aryl groups differing in their donor/acceptor behaviour and unlocking emission are presented. For each of the three series we report the optical, electrochemical, structural and synthetic details.

Dedication

To Dr. Ayub Reayi, your guidance has been invaluable.

Acknowledgments

For the completion of this thesis and the journey to get there I owe many thanks to people inside and outside the lab. I am deeply appreciative to my supervisor Dr. Thomas Baumgartner; his confidence in my potential as an undergraduate up until now has been invaluable throughout the journey and this thesis would not be possible without him. His endless support, mentorship and patience have led to the betterment of me as a researcher, and academic. Many thanks to Dr. Christopher Caputo and Dr. Ryan Hili for being members on my committee and for their guidance and knowledge throughout the course of this research. I would like to thank my mother, my uncle, aunts, grandparents and my wife Mariam for their constant support, in ensuring that I have the best environment to grow and come to such achievements, with unconditional love and understanding. Although many have come through the lab in my time as a graduate student as well as in the department, I am grateful to everyone for the chemistry and non-chemistry related discussions during the day, the support, encouragement and many laughs throughout the years. Although there are many people to name, I would like to especially thank Dr. Nayanthara Asok, Reza Dadgaryeganeh, Dr. Joshua Gaffen, Dr.Vanessa Béland, Dr. Matthew Gradiski, Dr. Avik Battacharjee, Taylor Cosby, Casey Lenart, Lucas Torres, Dusty Cadwallader, Maryam Jabbarpoor , Jesse LeBlanc, Dr. Howard Hunter, Cheryl Cai Hui Tan and Madison Diamantopoulos . I would also like to thank the support staff, administration and instrumentation staff at York University, for their efforts to ensure we always have the resources needed to get the research done. I am eternally grateful for this opportunity and fulfilling journey.

Table of Contents

Abstract ..... *ii*

Dedication ..... *iii*

Acknowledgments ..... *iv*

Table of Contents ..... *v*

List of Tables ..... *viii*

List of Figures ..... *x*

List of Schemes ..... *xvi*

List of Abbreviations and Symbols ..... *xviii*

Chapter One: Introduction *1*

1.1 π-Conjugated Organic Materials **1**

1.2 Phosphorus-based Organic Conjugated Materials **2**

1.2.1 Phospholes 3

1.2.2 The Dithieno[3,2-b:2',3'-d]phosphole 4

1.2.3 Backbone Modifications of Dithieno[3,2-b:2',3'-d]phosphole 6

1.3 Notable Phosphorus-based Compounds with Increased Electron-Accepting Properties **7**

1.3.1 Lower LUMO Energies via Addition of Select Groups to the Backbone 8

1.3.2 Substitution of the Backbone with Nitrogen-containing Aryl Groups 10

1.3.3 Phosphaviologens 11

1.3.4 Increased Electron-affinity through Addition of Carbonyl Groups 12

1.4 Phosphinines **16**

1.5 Scope of thesis **18**

1.6 References **20**

Chapter 2: Phosphorus Modifications on the Dithieno[2,3-b:3',2'-e]-4-keto-1,4-dihydrophosphinine *25*

Acknowledgements **25**

2.1 Introduction **25**

2.2 Results and Discussion **29**

2.2.1 Synthesis of Precursor Compounds 29

2.2.2 Further Phosphorus-Functionalization 30

2.2.3 Solid-State Structures of Select Compounds 32

2.2.4 Optical Properties 36

2.2.5 Density Functional Theory Calculations 38

2.2.6 Time-dependent Density Functional Theory (TDDFT) Calculations 39

2.2.7 Cyclic Voltammetry 42

2.3 Conclusion and Outlook **43**

2.4 Experimental Section **44**

2.4.1 General Methods 44

2.4.2 Synthesis and Characterization 44

2.5 References **48**

Chapter 3: Ketone Modifications of the Dithieno[2,3-b; 3',2'-e]-4-keto-1,4-dihydrophosphinine Toward Stronger Electron Acceptors ***51***

Acknowledgements **51**

3.1 Introduction **51**

3.2 Results and Discussion **55**

3.2.1 Synthesis 55

3.2.2 Solid-state structures 56

3.2.3 Optical Properties 59

3.2.4 Density Functional Theory Calculations 60

3.2.5 Time-dependent Density Functional Theory (TDDFT) Calculations 62

3.2.6 Cyclic Voltammetry 64

3.3 Conclusion and Future Outlook **66**

3.4 Experimental Section **67**

3.4.1 General Methods 67

3.4.2 Synthetic procedures 68

3.5 References **70**

Chapter Four: Extending the Conjugation of the Dithieno[2,3-b;3',2'-e]-4-keto-1,4-dihydrophosphinine Core ***72***

Acknowledgements **72**

4.1 Introduction **72**

4.2 Results and Discussion 77
4.2.1 Synthesis 77
4.2.2 Solid State Structures 80
4.2.3 Optical properties 82
4.2.4 Solvatochromism 85
4.2.5 Density Functional Theory (DFT) Calculations 92
4.2.6 Time-dependent Density Functional Theory (TDDFT) Calculations 93
4.2.7 Cyclic Voltammetry 96
4.3 Conclusion and Future Outlook 97
4.4 Experimental Section 98
4.4.1 General Methods 98
4.4.2 Synthetic Procedures 98
4.5 References 102

Chapter 5: Conclusions and Future Outlook 105
5.1 Conclusions 105
5.2 Future outlook 106
5.2.1 Chemical reductions 106
5.2.2 Solid state emission 107
5.2.3 4-Pyridyl Functionalized Dithienoketophosphinine 108
5.2.4 Dicyanomethylene Functionalization of Tetra-substituted Species 110
5.2.5. Analyte Sensing 112
5.2.6 Nitro-substituted Species 114
5.2.7 Addition of Cationic Phosphonium Groups on Dithieno-backbone 115
5.2.8 Polycyclic Aromatic Hydrocarbon-type Dithienoketophosphinines 117
5.2.9 Keto-modifications of Dithienoketophosphinines with Donor Groups 118
5.3 References 121

List of Tables

Table 2-1. (a) Absorption wavelengths and (b) molar extinction coefficients of all P-functionalized species in CH_2Cl_2 at $5x10^{-5}$ M. (c) Reduction potentials obtained from cyclic voltammetry experiments (vs. Fc/Fc^+) with NBu_4PF_6 as supporting electrolyte in CH_3CN. (d) Computational values of frontier molecular orbitals B3LYP/6-31G+(d) basis set and a LANL2MB for 2-3Au using PCM solvation model in CH_2Cl_2. (e) Optical bandgap (HOMO-LUMO). 37

Table 2-2. Time-dependent density functional theory calculation results for phosphorus-functionalized species using TD-SCF CAM-B3LYP/6-31G+(d) using PCM solvation model in CH_2Cl_2. (a) Oscillator strengths used to determine (b) dominant transitions. 40

Table 3-1. (a) Absorption wavelengths and (b) molar extinction coefficients of all species in CH_2Cl_2 at $5x10^{-5}$ M. (c) Reduction potentials obtained from cyclic voltammetry experiments (vs Fc/Fc^+) with NBu_4PF_6 as supporting electrolyte in CH_3CN. (d) Computational values of frontier molecular orbitals B3LYP/6-31G+(d) basis set using the PCM solvation model in CH_2Cl_2. (e) Optical bandgap (HOMO-LUMO). 60

Table 3-2. Time-dependent density functional theory calculation results for the dicyanomethylene-functionalized species using TD-SCF CAM-B3LYP 6-31G+(d) using PCM solvation model in CH_2Cl_2. (a) Oscillator strengths used to determine dominant transitions(b). 62

Table 4-1. (a) Absorption and emission maxima c = $5x10^{-6}$ M in CH_2Cl_2. (b) Molar extinction coefficient. (c) Stokes shift in wavenumbers. (d) Quantum yield in CH_2Cl_2 (e) cyclic voltammetry in CH_3CN, vs. Fc/Fc^+, NBu_4PF_6 as supporting electrolyte. (f) B3LYP/6-31G+(d) level of theory using the PCM solvation model in CH_2Cl_2. (g) optical gap HOMO-LUMO..... 82

Table 4-2. (a) Quantitative absorption, (b) molar extinction, and (c) emission values of 4-7 and 4-9 in various solvents ($5x10^{-6}$ M). 91

Table 4-3. Time-dependent density functional theory calculation results for tetra cross-coupled species using TD-SCF CAM-B3LYP/6-31G+(d) using a PCM solvation model in CH_2Cl_2. (a) oscillator strengths used to determine dominant transitions (b) 94

List of Figures

Figure 1-1. Comparison of phosphole and pyrrole geometries (A); Depiction of the σ*-π* interaction between phosphorus and butadiene fragment lowering the LUMO energy (B).[9] 3

Figure 1-2. Compound 1-1 phosphole system synthesized by Réau et al; Compound 1-2 dithienophosphole synthesized by Baumgartner et al.[9] 4

Figure 1-3. Dithienophosphole P-modifications (left); Metal-coordinated and cationic dithienophospholes (right).[9,15–18] 6

Figure 1-4. Various P-functionalized and cross-coupled species and their varying emission throughout the visible light spectrum.[9] (© Georg Thieme Verlag KG) 7

Figure 1-5. Various phenyl conjugated dithieno[3,2-*b*:2',3'-*d*]phospholes.[20] 8

Figure 1-6. Pentafluorophenyl dithienophospholes with various fluorophenyl groups on the backbone (left);[8] 4-pyridyl-substituted dithieno[3,2-*b*:2',3'-*d*]phosphole and its methylated congener (middle);[21] Benzothieno-annulated dithienophospholes (right).[10] 10

Figure 1-7. Dithiazolo[5,4-*b*:4',5'-*d*]phosphole with various backbone modifications (left); thiazole extended dithiazolo[5,4-*b*:4',5'-*d*]phosphole (right).[22] 11

Figure 1-8. From left to right: Native viologen, and phosphaviologens with oxidized, methylated and sulfidated phosphorus centres.[23,25] 12

Figure 1-9. Various phosphorus functionalized dithieno[3,2-*c*:2',3'-*e*]-2,7-diketophosphepins (top); Triazole-extended dithienodiketophosphepin (1-25; bottom); Dicationic triazole-extended dithienodiketophosphepin (1-26; bottom).[4,26] 14

Figure 1-10. Oxidized and cationic trisdodecyloxybenzyl functionalized dithieno[2,3-*b*:3',2'-*e*]-4-keto-1,4-dihydrophosphinine (1-27, 1-28) reported by Baumgartner et al.[27] Backbone-modified dithieno[2,3-*b*:3',2'-*e*]-4-keto-1,4-dihydrophosphinine (1-29, 1-30) reported by Xiao at al.[28] ... 15

Figure 1-11. Comparison of phosphinine and pyridine (left). First phosphinine reported by Märkl and coworkers (right).[7] 16

Figure 1-12. Dithieno-fused phosphinine compounds reported by Mathey and coworkers (compounds 1-32 to 1-34, top);[30,31] Benzo-fused phosphinines reported in the 1970s (1-35 and 1-36, bottom);[7] Acridophosphine reported by Kivala et al. (1-37, bottom).[32] 18

Figure 2-1. Diphosphahexaarenes with various phosphorus modifications (left);[5] phosphaphenalenes with fused thiophene and multiple phosphorus functionalizations (middle);[6] dicyanomethylene functionalized acridophosphine with various phosphorus functionalities (right).[3] 26

Figure 2-2. Previous dithieno[2,3-*b*:3,2-*e*]-4-keto-1,4-dihydrophosphinine systems reported by the Baumgartner group (2-3O and 2-3Bn):[8] Proposed P-functionalization of the dithienoketophosphinine system as part of this thesis (2-3, 2-3Me, 2-3Au). 28

Figure 2-3. (A) Solid-state structure of single molecule of 2-3O (thermal ellipsoids at 50% probability); (B) intermolecular hydrogen bonding interactions of 2-3O; (C) packing of 2-3O with evident π-stacking between adjacent compounds. 33

Figure 2-4. (A) Solid-state structure of single molecule of 2-3Me (thermal ellipsoids at 50% probability); (B) intermolecular hydrogen bonding interactions in 2-3Me; (C) packing of 2-3Me with evident π-stacking between adjacent compounds and interpenetrating triflate counter anions. 34

Figure 2-5. (A) Solid-state structure of single molecule of 2-3Au (thermal ellipsoids at 50% probability); (B) aurophilic interaction between adjacent molecules of 2-3Au; (C) packing of 2-3Au with hydrogen-bonding interactions between adjacent compounds. 35

Figure 2-6. Absorption spectra of the phosphorus-functionalized species (CH_2Cl_2; c = $5x10^{-5}$ M). 38

Figure 2-7. Frontier molecular orbitals of 2-3, 2-3O, 2-3Me, and 2-3Au with respective HOMO and LUMO energies (eV). B3LYP6-31G+(d) with LanL2MB level of theory for 2-3Au using a PCM solvation model in CH_2Cl_2. 39

Figure 2-8. Select molecular orbitals for phosphorus functionalized species. 41

Figure 2-9. Cyclic voltammograms of 2-3O (red), 2-3 (green), 2-3Me (blue) and 2-3Au (yellow). Potentials are referenced to Fc/Fc^+. Scan rate 100 mV/s with NBu_4PF_6 as supporting electrolyte. All experiments performed in dry CH_3CN under argon. 42

Figure 3-1. Select scaffolds based on 7,7,8,8-tetracyano-*p*-quinodimethane. Compounds 3-1 to 3-4 reported by Kobayashi et al.[4] 52

Figure 3-2. Dicyanomethylene functionalized acridophosphines (left)[5] and arylborane-based systems reported by Yin et al. (middle, right)[6]. 53

Figure 3-3. Dicyanomethylene functionalized dithienophosphinines. 54

Figure 3-4. A) Solid-state structure of 3-7O (thermal ellipsoids 50% probability); B) front-image depicting non-planarity of dicyanomethylene; C) dihedral angle; D) intermolecular π-stacking; E) O-H and N-H hydrogen-bonding interactions..... 56

Figure 3-5. A) Solid-state structure of 3-7Me (thermal ellipsoids 50% probability); B) image depicting non planarity of dicyanomethylene and dithieno-backbone; C) dihedral angle; D) intermolecular π-stacking and NH hydrogen-bonding interactions..... 58

Figure 3-6. Absorption spectra of the dicyanomethylene species (CH_2Cl_2; c = $5x10^{-5}$ M)..... 59

Figure 3-7. Frontier molecular orbitals of 3-7, 3-7O and 3-7Me with respective HOMO and LUMO energies (eV). B3LYP 6-31G+(d) using a PCM solvation model in CH_2Cl_2..... 61

Figure 3-8. Select molecular orbitals for the dicyanomethylene functionalized species. 63

Figure 3-9. Cyclic voltammograms displaying the reduction regime for 3-7O, 3-7, and 3-7Me. Potentials are references to Fc/Fc^+. Scan rate is 100 mV/s with NBu_4PF_6 as supporting electrolyte. All experiments performed in dry CH_3CN. 65

Figure 3-10. Cyclic voltammogram of 3-7O with varying scan rates from 0.01 V/s to 1 V/s/ Potentials are references to Fc/Fc^+ with NBu_4PF_6 as supporting electrolyte; all experiments performed in dry CH_3CN under argon. 66

Figure 4-1. A) α-Bromination of the dithieno[3,2-*b*:2,3′-*d*]phosphole;[2] (B) various cross-coupled dithieno[3,2-*b*:2′,3′-*d*]phospholes.[2,4,5] 73

Figure 4-2. Fluorescent probes based on the dithienoketophosphinine reported by Xiao et al.[9] .. 74

Figure 4-3. Targeted tetra-substituted dithienoketophosphinines with various donor/acceptor termini. 76

Figure 4-4. (A) Structure of 4-7 in the solid state, thermal ellipsoids at 50% probability; (B) intramolecular π-stacking and hydrogen bonding interactions; (C) intermolecular π-stacking; (D) bulk packing with some intermolecular hydrogen-bonding interactions shown as red dashes. ... 80

Figure 4-5. Absorption spectra of the tetra cross-coupled derivatives (CH_2Cl_2; $5x10^{-6}$ M) 84

Figure 4-6. (A) Emission spectra of all derivatives (CH_2Cl_2; $5x10^{-6}$ M); (B) emission colours of all species in CH_2Cl_2. 85

Figure 4-7. Normalized low-energy absorption (A) and emission (B) spectra of 4-7 in various solvents (c = $5x10^{-6}$ M) 86

Figure 4-8. Normalized low-energy absorption (A) and emission (B) spectra of 4-9 in various solvents (c = $5x10^{-6}$ M). 87

Figure 4-9. (A) Emission of 4-7 in various solvents under UV irradiation; (B) Different colours of 4-9 in various solutions non-irradiated; (C) Emission of 4-9 in various solvents under UV-irradiation. Solutions from left to right in order of increasing $E_T(30)$ value. 88

Figure 4-10. Emission maxima plotted against $E_T(30)$ value for 4-7 (A) and 4-9 (B). 90

Figure 4-11. Frontier molecular orbitals of 4-7, 4-8, and 4-9 with respective HOMO and LUMO energies (eV). Level: B3LYP/6-31G+(d) using a PCM solvation model in CH_2Cl_2. 92

Figure 4-12. Select molecular orbitals for tetra cross-coupled species. 95

Figure 4-13. Cyclic voltammograms of 4-7, 4-8 and 4-9. Potentials are references to Fc/Fc^+. Scan rate 100 mV/s with $NBuPF_6$ as supporting electrolyte. All experiments performed in dry CH_3CN under argon. 96

Figure 5-1. Solid state emission of cross coupled species from Chapter 4. From left to right (4-6, 4-7, 4-8, 4-9). 108

Figure 5-2. 4-Pyridyl dithienophospholes 1-14 and 1-14a; viologen and phosphaviologen 1-18 and 1-19a; 4-pyridyl extended dithienoketophosphinine 4-6 and methylated congener 5-1.[1,5] . 109

Figure 5-3. Frontier molecular orbitals of 4-6 and 5-1 with respective HOMO and LUMO energies (eV). Level: B3LYP/6-31G+(d) using a PCM solvation model in CH_2Cl_2. 110

Figure 5-4. (A) Reaction conditions to prepare compound 5-2; (B) solid-state structure of 5-2 thermal ellipsoids with 50% probability; (C) emission of 5-2 in $CDCl_3$; (D) frontier molecular orbitals of 5-2 with respective HOMO and LUMO energies (eV). B3LYP/6-31G+(d) level of theory using a PCM solvation model in CH_2Cl_2. 111

Figure 5-5. Proposed tetra-cross-coupled dithienophosphinine systems with dicyanomethylene functionality. 111

Figure 5-6. Frontier molecular orbitals of 5-13 with respective HOMO and LUMO energies (eV). Level: B3LYP/6-31G+(d) using a PCM solvation model in CH_2Cl_2..... 117

Figure 5-7. Phosphorus-incorporated vat orange 3 systems reported by our group (A); Formation of polycyclic aromatic hydrocarbon type dithienoketophosphinine 5-14 with generic Scholl reaction conditions (B); Proposed dithienoketophosphinine systems 5-15 to 5-17..... 118

List of Schemes

Scheme 2-1. Synthetic pathway to form dithieno[2,3-*b*:3′,2′-*e*]-4-keto-1,4-dihydrophosphinine oxide 2-3O. 30

Scheme 2-2. Methylation of protected phosphinine (A); aurylation of protected phosphinine and failed deprotection attempt (B); reduction followed by successful aurylation and methylation of dithienoketophosphinine (C). 31

Scheme 3-1. (A) Synthesis of 3-7O from dithienoketophosphinine precursor 2-3O (B) reduction of 3-7O to form 3-7 and methylation to form 3-7Me. 55

Scheme 4-1. (A) Attempted bromination of the dithienoketophosphinine using conditions previously employed on the dithienophosphole; (B) New conditions for the bromination of the dithienoketophosphinine; (C) Molecular structure of 4-5 in the solid state, thermal ellipsoids at 50% probability. 75

Scheme 4-2. Attempted tetra-bromination using various literature methods. 78

Scheme 4-3. Synthesis and reaction conditions toward cross-coupled species 4-6 – 4-9. 79

Scheme 5-1. Previously reported dimethylamino-functionalized dithienophosphole protonation (A);[6] Proposed protonation of dimethylamino-functionalized dithienoketophosphinine and the respective emissions after addition of acid (B). 113

Scheme 5-2. (A) Previously reported B(pin)-functionalized dithienophosphole 5-7 and fluoride coordinated species 5-7a;[7] (B) proposed B(pin)-functionalized dithienoketophosphinine 5-8 and fluoride coordinated species 5-8a; (pin: pinacolate). 114

Scheme 5-3. Proposed reaction toward 4-nitrobenzene- and 3-nitrobenzene-functionalized dithienoketophosphinines. 115

Scheme 5-4. Addition of cationic side groups to pyrometallic diimides reported by Cao et al.[11] 116

Scheme 5-5. (A) Horner-Wadsworth-Emmons (HWE) reaction performed by Nielson at all to form TTF-functionalized 5-18; (B) proposed dithienoketophosphinine with TTF-type functionality. 119

List of Abbreviations and Symbols

Symbol	Definition
Å	Angstrom (10^{-10} m)
Ag/AgCl	Silver/ silver chloride
CV	Cyclic Voltammetry
DFT	Density functional theory
EPR	Electron paramagnetic resonance
$E_T(30)$	Solvent polarity parameter
ε	Molar extinction coefficient ($M^{-1}cm^{-1}$)
Fc/Fc^+	Ferrocene/ Ferrocenium
HOMO	Highest occupied molecular orbital
J	Coupling constant
LUMO	Lowest unoccupied molecular orbital
NMR	Nuclear magnetic resonance
OFET	Organic field-effect transistor
OLED	Organic light-emitting diode
PCM	Polarizable continuum model
ppm	Parts per million
R.T.	Room temperature
SCE	Saturated calomel electrode
TDDFT	Time-dependent density functional theory
UV Vis	Ultra-violet visible
XRD	X-ray Diffraction
λ_{MaxABS}	Absorption maxima wavelength
λ_{MaxEM}	Emission maxima wavelength

Chapter One: Introduction

1.1 π-Conjugated Organic Materials

The research and development of novel π-conjugated organic architectures plays an important role in the field of functional organic materials. Organic conjugated materials are cheaper and less toxic compared to predominately used metal- and silicon-based materials, making them good candidates for use in applications such as, organic field effect transistors (OFETs), organic light emitting diodes (OLEDs), fluorescent sensors, and as chromophores in other organic devices to name a few.[1,2] Molecules with small and tunable energy gaps between their highest occupied molecular orbital (HOMO) and lowest unoccupied molecular orbital (LUMO) have thus been highly researched for to their beneficial optoelectronic properties such as; the ability to absorb and emit light across the visible light spectrum, and their ability to gain or lose electrons depending on the energy of their respective HOMO or LUMO levels.[3] Some of the aforementioned devices also require specific electronic properties from molecules since they are comprised of two semiconductor components: a p-type component, which conducts positive charges or holes as a result of donating an electron and an n-type component that then transports negative charges as the result of its electron-accepting nature.[4] Until recently, materials researched globally have predominately been p-type, meaning there are less n-type materials in existence, thus making the creation of n-type materials a major focus area of research.[5] An important factor in determining the suitability of a material as n-type semiconductor is the energy of the LUMO level; a lower LUMO suggests higher affinity for electrons and as a result could enhance electron transport.[4] A common approach to obtaining a low LUMO has been through addition of electron-withdrawing groups such as cyano, carbonyl, trifluoromethyl or pentafluoro groups to purely carbon-based

scaffolds.[4] An alternative approach implemented in the last few decades to modulate the properties of carbon-based conjugated materials more effectively involves substituting one or more carbon atoms with heteroatoms such as N, S, B, Si, P etc., which has allowed for the creation of a wide array of tunable materials, due in part to heavier main-group elements having the ability to non-hybridize and in-turn interact with the π-orbitals of the carbon-based back-bone using antibonding orbitals.[1,6,7]

1.2 Phosphorus-based Organic Conjugated Materials

Among these heteroatoms, phosphorus is intriguing due to its unique electronics and highly versatile reactivity especially when incorporated into five- and six-membered carbon-based heterocycles. The latter is of particular interest for the scope of this thesis research. The impact of a phosphorus-based building block, when used to replace a carbon centre in conjugated heterocycles, is accredited to its size, hybridization, stability and electronics. Phosphorus has a radius that is 0.33Å larger than that of carbon and nitrogen, which when incorporated into five- and six-membered heterocycles, causes the C-P-C angle to be smaller than a purely carbon-based system.[7] Also related to the phosphorus atom's size, it its inability to hybridize. As a result of a larger effective nuclear charge of phosphorus, the energy and size differences between the 3s and 3p orbitals do not favour hybridization, instead it retains a pyramidal geometry in molecules, due to a high inversion barrier leading to increased stability overall.[7] The pyramidal nature of the phosphorus centre in phospholes specifically (and on occasion in phosphinines) prevents efficient overlap between the phosphorus lone pair and the conjugated system unlike in pyrrole, the five-membered nitrogen analog which does not have a pyramidal geometry (Figure 1-1). In turn, a unique σ*-π* interaction occurs between the phosphorus and the conjugated system leading to a

lower energy LUMO, making a stronger acceptor compound by simple addition of phosphorus (Figure 1-1). Another feature of phosphorus is when it is in the trivalent λ^3 state, it can react with Lewis acids, metals and other electrophilic species that in turn tune the electronics at the phosphorus to create different materials, one of which is the highly sought-after n-type.[8]

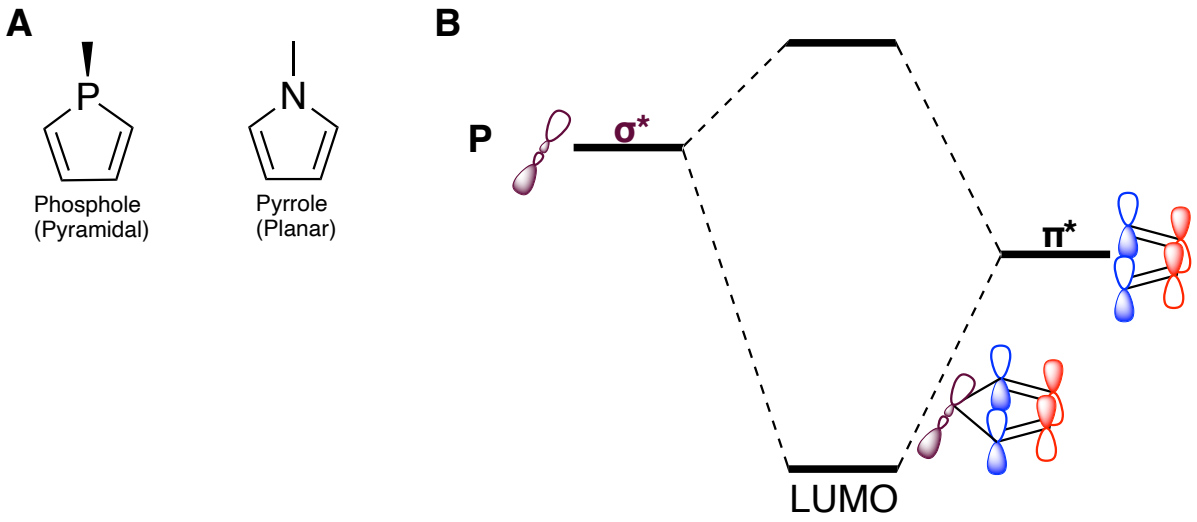

Figure 1-1. Comparison of phosphole and pyrrole geometries (A); Depiction of the σ*-π* interaction between phosphorus and butadiene fragment lowering the LUMO energy (B).[9]

1.2.1 Phospholes

First described in the 1950s, phospholes are five-membered phosphorus containing heterocycles that can be viewed as a phosphorus bridged butadiene (Figure 1-1). The parent phosphole has weak aromatic character in comparison to other heteroatom congeners, i.e., pyrrole, due to a less efficient interaction between the butadiene π-system and the phosphorus lone pair.[9,10] To further display the advantageous electronics of phosphorus incorporation, as a result of its σ*-π* interaction, phospholes have a high electron affinity with a low energy LUMO compared to that of the purely

carbon-based cyclopentadiene (Figure 1-1). Phospholes have been used in oligo- and polymeric systems as well as in fused systems wherein they exhibit properties otherwise not seen in purely carbon-based systems.[11] Although first discovered in 1959, phospholes have not been researched for their material applications until 2000.[9] The first example demonstrating the tunability of a phosphole-based system was done by Réau et al. wherein a 2,5-diarylphosphole **1-1** (Figure 1-2) was modified at R and Ar, which in turn varied the optical and electrochemical properties of the system.[9] In 2004, our group reported the dithienophosphole **1-2** (Figure 1-2), a highly luminescent and tunable system that is composed of a phosphorus-bridged bithiophene.[12] The rigid and planar structure of the thiophenes creates a high degree of π-conjugation within the scaffold and lowers the energy of the HOMO-LUMO gap of the molecule making a highly blue emissive compound with a near unity quantum yield. By having a highly modifiable phosphorus centre as well as the thieno groups on either side, this system has been extensively modified to vary its optoelectronic properties.[13]

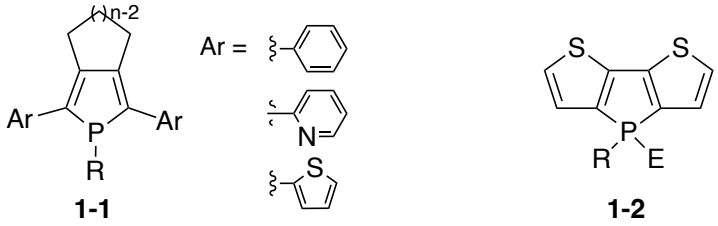

1-1 **1-2**

Figure 1-2. Compound **1-1** phosphole system synthesized by Réau et al; Compound **1-2** dithienophosphole synthesized by Baumgartner et al.[9]

1.2.2 The Dithieno[3,2-b:2',3'-d]phosphole

One of the features of the dithienophosphole **1-3** that highlights its remarkable versatility, are the two opportunities for phosphorus functionalization denoted as E and R (Figure 1-3). Different

exocyclic substituents R can be introduced via various dichlorophosphanes during the ring annulation step.[9] The typical species used is dichlorophenylphosphane, leading to fairly stable phenyl-phospholes. Other groups such as *tert*-butyl as well as acceptor groups such as pentafluorophenyl, or donor groups such as triphenylamino have been added to name a few.[9,14] A second site for functionalization at the phosphorus is the lone pair, denoted as E (Figure 1-3). Simple modifications of E include oxidation, sulfidation as well as reactions with Lewis acids (BH_3) that all result in changes of the HOMO-LUMO gap of these compounds and in turn influencing the optical and electronic properties.[9] Interestingly, the dithienophosphole has also been used as a ligand when reacted with various metals such as iron, tungsten, copper, palladium etc. where, depending on the metal's oxidation state, the complex can comprise up to three dithienophosphole units in different geometries as shown by compounds **1-4**, **1-5**, and **1-6** (Figure 1-3).[15,16] The nucleophilic lone pair can also react with alkyl halides and aryliodonium species to form cationic phospholium compounds **1-7** and **1-8** (Figure 1-3).[16–18] Lastly, benzyl groups with dodecyl substituents have been added as well to afford cationic compound **1-9** that enables applications in self-assembly, unlocking liquid crystalline behaviour. Overall, by functionalization of the phosphorus, it has been reported by our group that the HOMO-LUMO gap, solid-state packing and electrochemical properties can all be varied quite effectively.

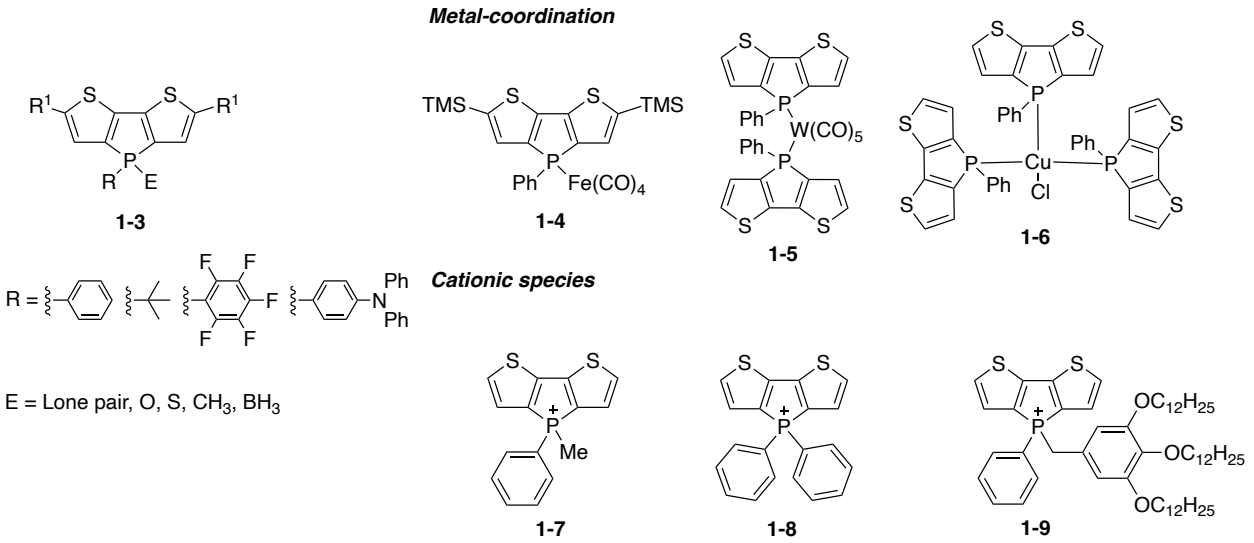

Figure 1-3. Dithienophosphole P-modifications (left); Metal-coordinated and cationic dithienophospholes (right).[9,15–18]

1.2.3 Backbone Modifications of Dithieno[3,2-b:2',3'-d]phosphole

As useful as phosphorus functionalization is, it limits the degree of tunability of the system. Although, in the case of the dithienophosphole system, it is not the only available site for modifications. To further modulate the HOMO-LUMO gap, the α-positions on the thieno backbone denoted as R^1 in Figure 1-3 are also convenient sites for halogenation that can later be used in cross-coupling reactions. The extension of the conjugation of the central conjugated backbone with various different aryl groups has shown to alter the supramolecular organization, luminescence properties, and electrochemistry of the dithienophosphole more dramatically than phosphorus modifications alone.[9] In 2007, our group reported a series of compounds that were made through Suzuki- and Stille-type cross-coupling to afford different emission colours across the visible light spectrum with different structural organizations.[13] Additionally, compounds containing the trisdodecyloxy benzyl motif; compound **1-9** shown in Figure 1-3, have shown to display different emission colours in their liquid crystalline phase as a function of the backbone

modification.[17] Additional features, such as useful electrochemical properties have also been seen post cross-coupling but will be mentioned in the coming sections. Figure 1-4 depicts the varying emission colours obtained throughout select modifications made to the dithienophosphole core.

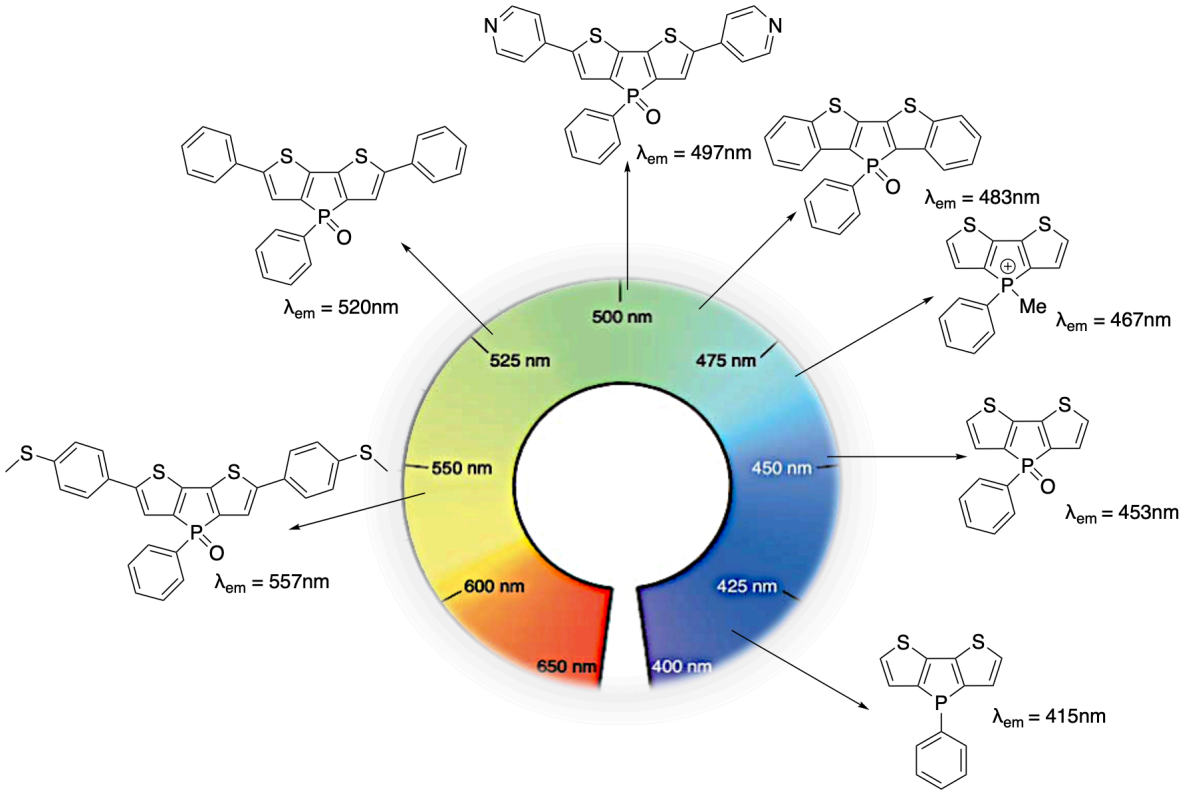

Figure 1-4. Various P-functionalized and cross-coupled species and their varying emission throughout the visible light spectrum.[9] (© Georg Thieme Verlag KG)

1.3 Notable Phosphorus-based Compounds with Increased Electron-Accepting Properties

Thus far, our group has shown that by altering the substituents at the phosphorus and the conjugated backbone, the electrochemical and optical properties can be effectively tuned. To further expand the library of n-type materials, our group has also reported a range of extended derivatives centered around the dithienophosphole core, as the core itself has limited redox

features. The next sections will discuss other pertinent architectures with focus of increasing electron affinity, as reported by our group in the last two decades. A useful characterization method to determine the electron affinity of our compounds is cyclic voltammetry. In an ideal scenario, a compound accepting an electron (or more) should involve a reversible process so that in can be applied in real-world electronics applications. Additionally, the reduction potential of the compound in an ideal case should be close to zero or at low voltage to indicate that it has a small energy barrier to accept electrons.[19] The design strategies implemented by our group for better electron acceptance include; P-functionalization, addition of electron-accepting moieties onto the conjugated backbone, changing the aryl-backbone and lastly, one of most importance to this thesis, ring-expansion via incorporation of a carbonyl group into the P-heterocycle.

1.3.1 Lower LUMO Energies via Addition of Select Groups to the Backbone

The first set of examples on redox-active dithienophospholes involves cross-coupled species. The simplest example is the diphenyl-substituted dithienophosphole **1-10** (Figure 1-5) synthesized by our group already in 2007 but only explored for its redox chemistry in 2016.[13,20] Essentially, a phenyl group is a good placeholder for studying the redox events of extended dithienophospholes as it is only very mildly electron donating and balances out the acceptor character of the phosphole.

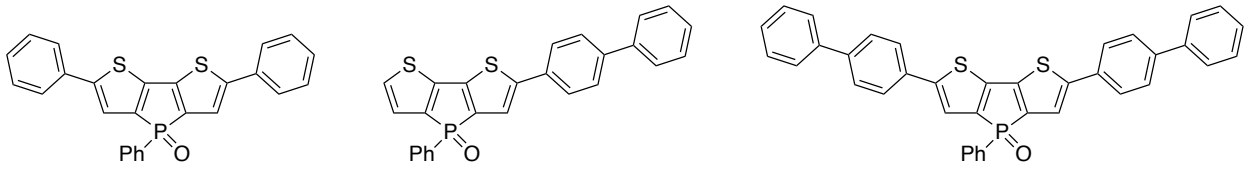

1-10 **1-11** **1-12**

Figure 1-5. Various phenyl conjugated dithieno[3,2-*b*:2',3'-*d*]phospholes.[20]

Compounds **1-10**, **1-11**, and **1-12** were reported to have ambipolar redox properties where, depending on the number and extension of the phenyl groups, the quasi-reversible reduction events decreased in potential. For compound **1-10** the reduction potential is -2.08 V , for **1-11** it is -2.18 V, and for **1-12** it is -2.04 V (vs Fc/Fc^{+}).[20] Although not involving fully reversible events, this initial study sets the stage for understanding the impact of a neutral extension to the dithienophosphole scaffold to gauge the effect of other groups, and in particular, electron-accepting groups that are to be introduced in a similar fashion. Another example was reported by our group in 2009, where the scaffold of a dithienophosphole with a pentafluorophenyl group at the phosphorus centre was extended with different cross-coupled difluorophenyl groups (compounds **1-13a-c**; Figure 1-6).[8] The different isomers only show small differences in their redox properties, with reductions occurring between -1.59 V and -1.52 V (vs. Ag/AgCl), all of which are quasi-reversible.[8] A more recent example for electron-accepting dithienophospholes was reported in 2020, that involved cross-coupled 4-pyridyl groups at the α-positions of the dithienophosphole (**1-14**, Figure 1-6).[21] By addition of these electron accepting groups, **1-14** exhibits two quasi-reversible reduction processes at -1.22 V and -1.53 V (vs. Ag/AgCl) and when the nitrogen atoms were methylated (**1-14a**, Figure 1-6), one reduction occurred at -0.59 V (vs. Ag/AgCl).[21] Although the aforementioned backbone-extended species all show quasi-reversibility, it is an asset to have these modifications impact the properties of the compounds towards n-type materials, in addition to their fantastic luminescent properties.

The final example for backbone modification dates back to 2008 where our group synthesized a series of P-functionalized phospholes **1-15**, **1-15a**, **1-15b** all with an benzo-annulated thiophene backbone.[10] The takeaway from this study, aside from the varying optical features, was that P-functionalization also plays a major role in modifying the redox properties of the system. The

overall comparison in this study was between a trivalent **1-15**, oxidized **1-15a** and methylated **1-15b** species. The trivalent species had the most negative potential whereas P-oxidation lowered the threshold by 0.5 V and made the quasi-reversibility seen in the trivalent species **1-15** fully reversible in **1-15a**. For the methylated species, reversibility was not seen, however, the reduction potential is lowered by another 0.2 V relative to that of the oxidized species.[10]

Essentially, when targeting new scaffolds, it is important to focus on both the conjugated backbone and the phosphorus substituents to change the electronic properties of the system and as a result, their photophysics and redox behaviour.

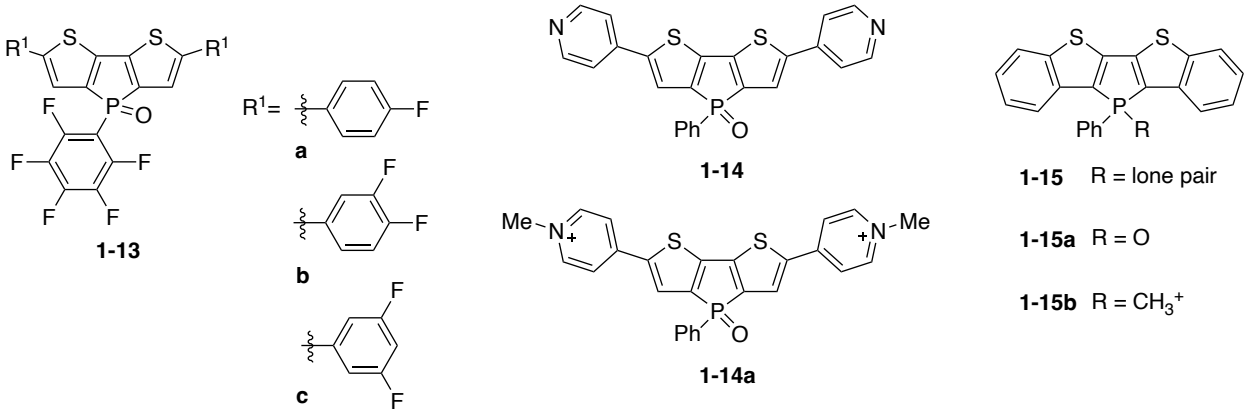

Figure 1-6. Pentafluorophenyl dithienophospholes with various fluorophenyl groups on the backbone (left);[8] 4-pyridyl-substituted dithieno[3,2-*b*:2',3'-*d*]phosphole and its methylated congener (middle);[21] Benzothieno-annulated dithienophospholes (right).[10]

1.3.2 Substitution of the Backbone with Nitrogen-containing Aryl Groups

Over the last decade, further enhancement of the phospholes' electron-accepting nature was achieved by addition of nitrogen-containing aryl groups in place of the purely thiophene-based groups (Compound **1-16**; Figure 1-7).[22] The first series of nitrogen-incorporated compounds involved thiazole, a more electron-accepting analog of thiophene. The effect of the nitrogen is

reflected in the energies of the frontier molecular orbitals where the LUMO of **1-16** is -2.21 eV, lower than that of the related dithienophosphole (-1.86 eV). Consequentially, in the cyclic voltammetry (CV) all derivatives **1-16** (**a-d**) and the triazole extended **1-17** (Figure 1-7) show one quasi-reversible reduction.[22] The reduction potentials of the compounds are varied from -2.07 V to -1.68 V (vs. Fc/Fc^{+}). Although not significantly different from the dithienophosphole in terms of the electrochemical processes (i.e., no full reversibility), the addition of the nitrogen centres overall decreased the LUMO energy.

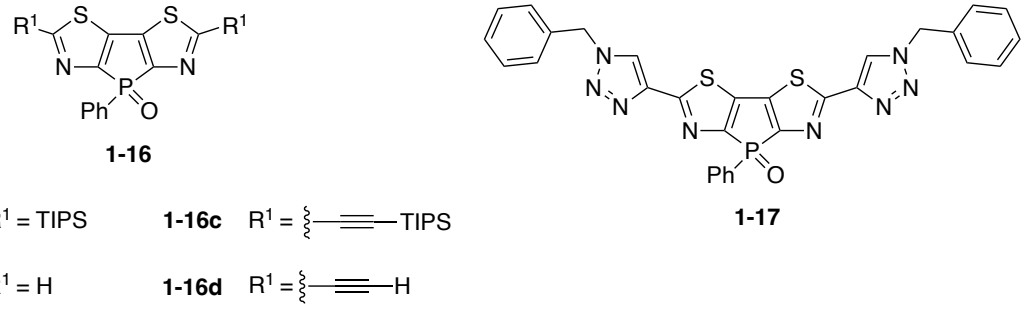

Figure 1-7. Dithiazolo[5,4-*b*:4',5'-*d*]phosphole with various backbone modifications (left); thiazole extended dithiazolo[5,4-*b*:4',5'-*d*]phosphole (right).[22]

1.3.3 Phosphaviologens

The most prominent electron-accepting scaffold made in the group thus far has been the bridging of viologens **1-18** with a phosphorus-based group to create the so-called "phosphaviologen" **1-19** (Figure 1-8).[23] The rationale behind using viologen as a backbone is due to its exceptionally reversible redox chemistry and potential for the pyrido-nitrogen to be further functionalized to create cationic species, further enhancing their electron-acceptor character. The phosphaviologens have dramatically enhanced electron-accepting features in comparison to their thiophene analogues, with reduction potentials as low as -0.5 V alongside full reversibility for both redox

processes allowing them to be excellent n-type materials that have also been employed in battery applications.[24] The nitrogen centres were also functionalized to created water-soluble cationic species maintaining the electrochemical properties. Recently, our group also reported a detailed study on the electrochemical properties of the P-methylated species **1-20** (Figure 1-8) and a P-sulfidated species **1-21** (Figure 1-8) with nitrogen centres methylated in both species as well.[25] Interestingly, these compounds were two- and three-electron acceptors with reversible reduction events that were exceptionally low in energy. The sulfidated species **1-21** has two reversible reductions at -0.6 V and -1.0 V (vs. Fc/Fc^+) whereas the methylated congener **1-20** reduces at even lower potentials of -0.3 V and -0.8 V (vs. Fc/Fc^+), respectively.[25] Although this scaffold is not a major compound of interest for the scope of this thesis, its outstanding properties are an ideal benchmark for comparison with some of the target compounds in this thesis.

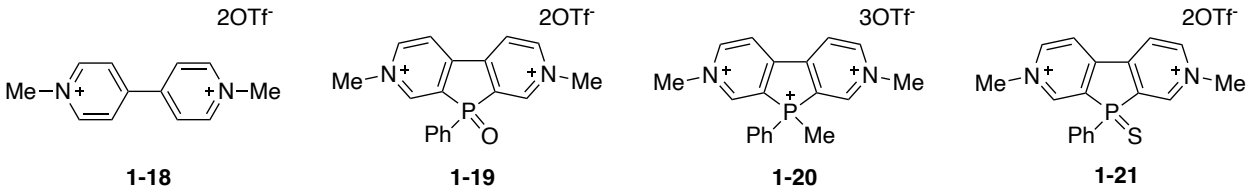

Figure 1-8. From left to right: Native viologen, and phosphaviologens with oxidized, methylated and sulfidated phosphorus centres.[23,25]

1.3.4 Increased Electron-affinity through Addition of Carbonyl Groups

Thus far, the modifications made to the phospholes reported in our group have retained the central five-membered phosphole unit. Other strategies we employed within the last decade have involved insertion of carbonyl groups to the central ring leading to ring expansion and in turn changing the core at the central P-heterocycle. The first example reported in 2013 introduced a seven-membered extension of the dithienophosphole **1-22** (Figure 1-9) termed dithieno[3,2-*c*:2',3'-*e*]-2,7-

diketophosphepin with two carbonyl groups at each α-position adjacent to the phosphorus.[4] The addition of the carbonyl groups decreased the LUMO energy of the P-oxidized system to -3.21 eV overall. The phosphorus modifications of the system involved oxidization and aurylation toward compounds **1-23** and **1-24**, respectively (Figure 1-9). The oxidized species **1-23** has two reversible reductions at -1.17 V (vs. Fc/Fc^+) and -1.65 V (vs. Fc/Fc^+), whereas the aurylated compound **1-24** displays three irreversible reductions at -1.15 V, -1.59 V, and -1.99 V (vs. Fc/Fc^+).[4] The improvement in electron-acceptor character is evident in both species **1-23** and **1-24** that have lower reduction potentials by ~1 V to that the trivalent compound **1-22**. However, the triazole-extended backbone **1-25** exhibits more quasi-reversibility in the reduction events, when compared to that of the phosphorus modified species. Methylation of the triazole units toward the dicationic species **1-26** (Figure 1-9) leads to a remarkable improvement for the reduction events in terms of their reversibility as well as lowered potential.[26] The only pitfall of this system was that by having two carbonyl groups adjacent to the phosphorus centre, quaternization of the phosphorus became quite difficult and limited further enhancements.

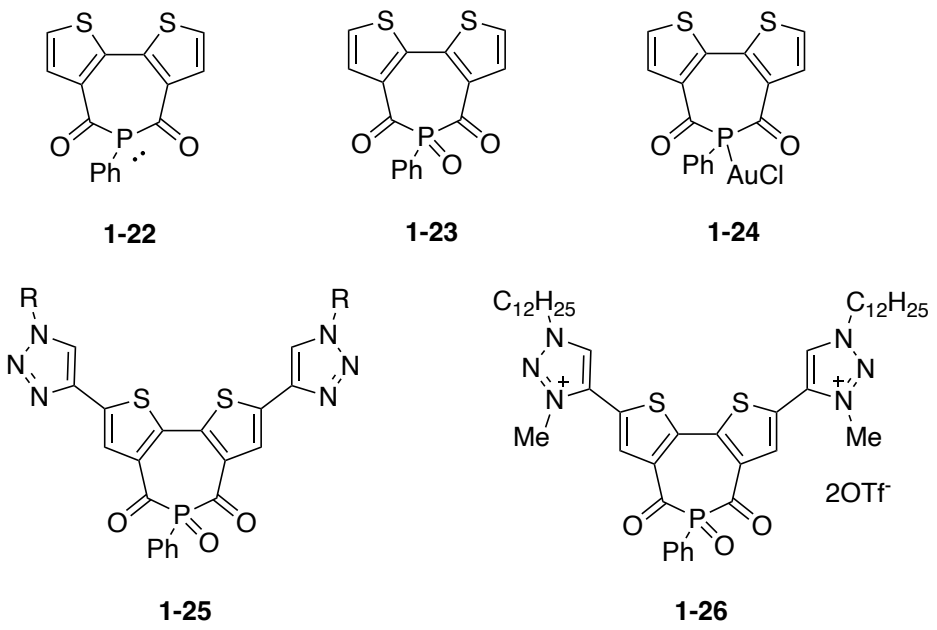

Figure 1-9. Various phosphorus functionalized dithieno[3,2-*c*:2',3'-*e*]-2,7-diketophosphepins (top); Triazole-extended dithienodiketophosphepin (**1-25**; bottom); Dicationic triazole-extended dithienodiketophosphepin (**1-26**; bottom).[4,26]

In 2013, our group also introduced the dithieno[2,3-*b*:3',2'-*e*]-4-keto-1,4-dihydrophosphinine scaffold that is based on the dithienophosphole but with an additional carbonyl at the *para* position creating a six-membered phosphinine **1-27** (Figure 1-10).[27] The idea behind having the carbonyl at the *para* position to the phosphorus was to make a stronger electron-accepting scaffold compared to dithienophosphole but one that does not inhibit the reactivity of the phosphorus centre like the diketophosphepin system. As a result of the strong electron-accepting features, compound **1-27** indeed displays promising electronic properties, namely one reversible reduction event at -1.5 V (vs. Fc/Fc^{+}) when P-oxidized, making it a better n-type material relative to dithienophospholes. However, **1-27** is not emissive unlike the corresponding dithienophosphole.[27] Moreover, the dominant focus of the initial study was the self-assembly for this system. To this end, dithienoketophosphinine was P-functionalized with trisdodecyloxybenzylbromide to create a

cationic phosphenium species **1-28** (Figure 1-10). Without getting into the self-assembly properties of **1-28**, simple quaternization of the phosphorus dropped the LUMO energy by almost 3 eV compared to **1-27** and this was reflected in the CV where a second, reversible reduction process was introduced at a lower potential of -1.12 V next to another at -1.75 V (vs. Fc/Fc^{+}).[27] Other than these initial investigations, this compound has remained relatively unexplored for its potential as an n-type material. There is much possibility for it to be functionalized at both the phosphorus centre, the conjugated backbone, and the carbonyl group to broadly establish its applicability as a redox active compound.

It is, however, important to mention that the dithienoketophosphinine was also studied by Xiao et al. in 2022 for use as a fluorescent probe in biological applications. In essence, the dithienoketophosphinine was brominated at the α-positions of the thiophene and thereafter it was functionalized with diamines to make compounds **1-29** and **1-30** (Figure 1-10). The internal charge-transfer process led to these compounds being useful as luminescent supramolecular probes.[28] Compounds **1-29** and **1-30** were not studied for any of their electrochemical properties, however, functionalization of the α-positions unlocked the emission of this scaffold, which varied in solvents between 453 nm and 501 nm.

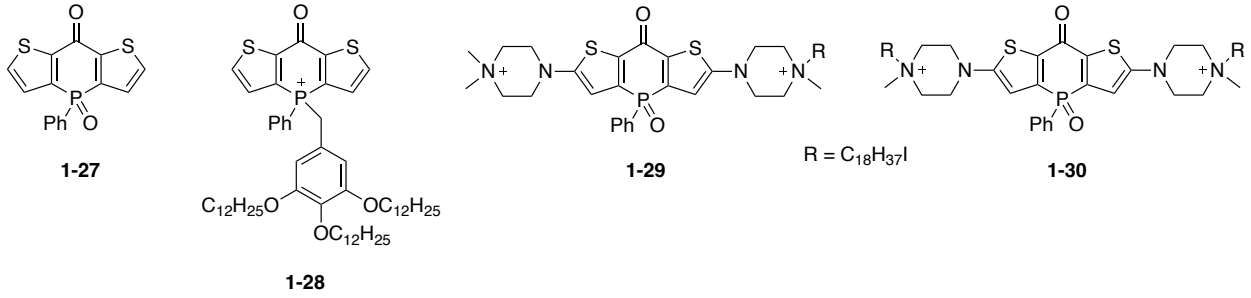

Figure 1-10. Oxidized and cationic trisdodecyloxybenzyl functionalized dithieno[2,3-*b*:3',2'-*e*]-4-keto-1,4-dihydrophosphinine (**1-27**, **1-28**) reported by Baumgartner et al.[27] Backbone-modified dithieno[2,3-*b*:3',2'-*e*]-4-keto-1,4-dihydrophosphinine (**1-29**, **1-30**) reported by Xiao at al.[28]

1.4 Phosphinines

First synthesized in 1966 by Märkl and coworkers, phosphinines are the phosphorus analog of pyridine (Figure 1-11). Trivalent and pentavalent phosphinines are six-membered planar systems containing six π-electrons with a varying degrees of aromaticity.[29] Unlike the dihydrophosphinine and phospholes introduced previously, trivalent phosphinines have 88% of the aromaticity of benzene as a result of highly efficient p-orbital overlap between the phosphorus and endocyclic carbons. In comparison to pyridine, phosphinines have a lower LUMO level owing to the interaction of the phosphorus atom and carbon-based system. The HOMO is, however, higher in energy and its dominant contribution is at the phosphorus lone pair. As a result of these electronic features, phosphinines are strong electron acceptors (low-lying LUMO) but at the same time can be good electron donors (high HOMO) making them useful in the field of coordination chemistry in metal complexation and in catalysis.[29] However, as a result of the high reactivity of the system, it lacks the stability to be useful in materials applications and has thus made them less studied than phospholes. To overcome these stability issues, substitution of the α-carbons has been reported to kinetically stabilize the system as well as extension of the π-system via addition of aryl groups, both of which are shown in the original 2,4,6-triphenyl phosphinine **1-31** reported by Märkl et al.[29]

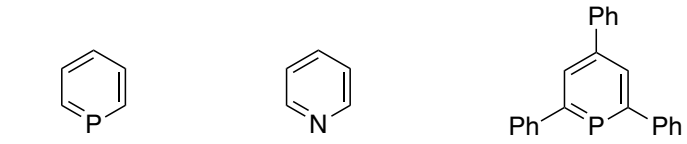

Phosphinine **Pyridine** **1-31**

Figure 1-11. Comparison of phosphinine and pyridine (left). First phosphinine reported by Märkl and coworkers (right).[7]

The phosphinine examples moving forward are to be focused around phosphinines fused with thieno groups to correlate this work with that of the scaffold of interest **1-27** (Figure 1-10). The first examples of thiophene-fused phosphinines were introduced by Mathey and coworkers in 2007 (**1-32** and **1-33;** Figure 1-12).[30] The focus of the research was on the synthesis of these species with a brief mention of the photophysics and electronics. In brief, compound **1-32** has a smaller HOMO-LUMO gap than **1-33** and thus was the dominantly studied compound. A few highlighting features include a reversible reduction at -1.9 V (vs. SCE) and the compound also had blue emission at 426 nm.[30]

In follow-up study by Mathey et al.[31] in 2008, a thiophene unit in compound **1-32** was substituted at the α-carbon adjacent to the phosphorus in place of the phenyl giving compound **1-34** (Figure 1-12). This compound was reported to have a more red-shifted absorption as a result of a lower HOMO-LUMO gap.[31] Other closely studied fused systems containing a central phosphinine core are compounds **1-35** and **1-36** (Figure 1-12). These compounds were reported in 1974 but only for their synthesis.[7] In 2017, Kivala et al. reported a series of compounds based on **1-35** but with a dicyanomethylene in place of the carbonyl group (**1-37**, Figure 1-12).[32] In their study, they took advantage of the phosphorus functionalization to vary the electronics of the compounds. These acridophopshinine derivatives were primarily functionalized at the phosphorus via oxidation (**1-37O**), methylation (**1-37Me**), and sulfidation (**1-37S**) from a trivalent species. The compounds were studied predominately for their electrochemical and optical properties, along with a nitrogen-based analog. All of the phosphorus containing systems have two one-electron reductions at lower reduction potentials when compared to the nitrogen analog. Quantitatively replacing the heteroatom in the nitrogen analog with a reduction potential of -1.6 V lowers the potential to -1.49 V in the phosphorus species (both vs Fc/Fc^{+}).[32] Sulfidation changes the potential to -1.30 V, then

oxidation further decreases it to -1.26 V. Lastly, the methylated species has a reduction potential of -0.96 V, which was the lowest of all compounds in the study. The optical features of these species also experienced changes according to the substituent at the phosphorus. Overall, the study done by the Kivala group is a small preview on the impact of simple modifications at the phosphorus centre on the properties of systems containing phosphorus.

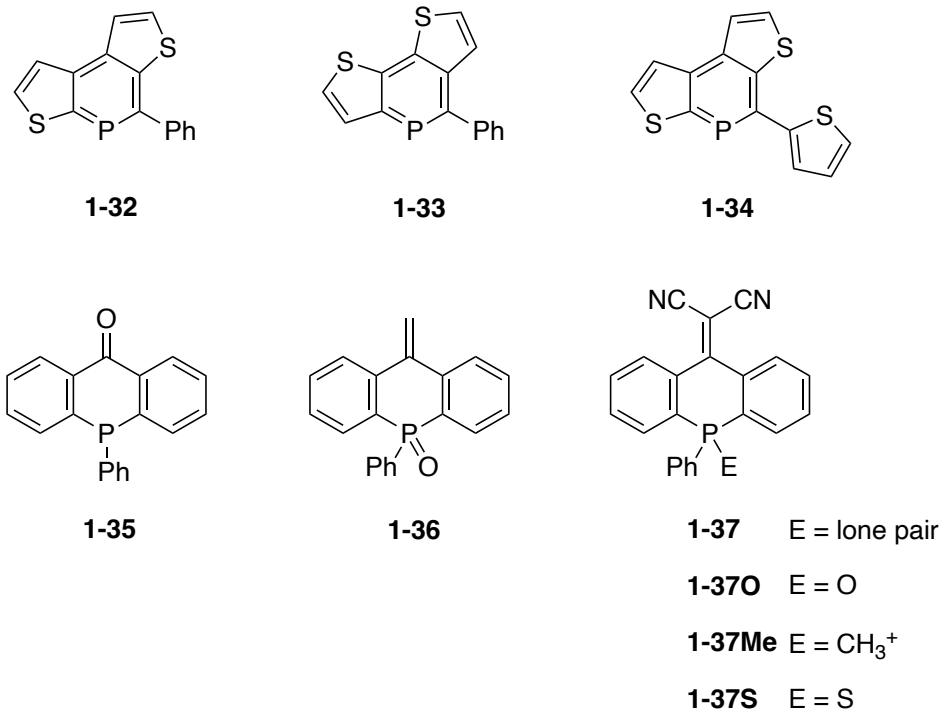

Figure 1-12. Dithieno-fused phosphinine compounds reported by Mathey and coworkers (compounds **1-32** to **1-34**, top);[30,31] Benzo-fused phosphinines reported in the 1970s (**1-35** and **1-36**, bottom);[7] Acridophosphine reported by Kivala et al. (**1-37**, bottom).[32]

1.5 Scope of thesis

This thesis revolves around modifications of the dithieno[2,3-*b*:3',2'-*e*]-4-keto-1,4-dihydro-phosphinine to establish a broad new materials platform by comprehensively verifying its optical and electrochemical properties and ultimately, gauging its use for n-type materials. The thesis

explores phosphorus and ketone functionalization, as well as extension of the conjugated backbone. The characterization of all new derivatives reported herein is fairly consistent throughout the chapters, including cyclic voltammetry to study the electron-accepting qualities of the molecules, as well as UV-Vis (and fluorescence) spectroscopy to fully study their absorption and potential emission properties. Single crystal X-ray crystallography determines the solid-state structures of the compounds in order to have an in depth look at the molecular and supramolecular features (packing, bond lengths and angles). Lastly, density-functional theory (DFT) calculations have been performed to understand the orbital distribution as well as the HOMO and LUMO energies for the different new compounds.

Chapter 2 exclusively covers simple P-functionalization of the dithienoketophosphinine and takes a look at how the parent system's properties can be altered upon metal complexation as well as alkylation. Chapter 3 focuses on converting the carbonyl into a dicyanomethylene group to evaluate the resulting electron-acceptor properties of the scaffold. Phosphorus functionalization is performed on this compound as well. Chapter 4 then focuses on the bromination of the thieno groups, followed by Suzuki-Miyaura cross coupling to extend the core with aryl groups that are either electron-accepting to electron-donating. Chapter 5 provides a future outlook on the project and will discuss some directions that this chemistry can head towards. It also highlights some miscellaneous reactions performed that have not led to conclusive or complete results but are noteworthy to mention for future projects.

1.6 References

(1) Stolar, M.; Baumgartner, T. Phosphorus-Containing Materials for Organic Electronics. *Chem. Asian J.* **2014**, *9* (5), 1212–1225. https://doi.org/10.1002/asia.201301670.

(2) Zucchero, A. J.; McGrier, P. L.; Bunz, U. H. F. Cross-Conjugated Cruciform Fluorophores. *Acc. Chem. Res.* **2010**, *43* (3), 397–408. https://doi.org/10.1021/ar900218d.

(3) Shimizu, A.; Ishizaki, Y.; Horiuchi, S.; Hirose, T.; Matsuda, K.; Sato, H.; Yoshida, J. HOMO–LUMO Energy-Gap Tuning of π-Conjugated Zwitterions Composed of Electron-Donating Anion and Electron-Accepting Cation. *J. Org. Chem.* **2021**, *86* (1), 770–781. https://doi.org/10.1021/acs.joc.0c02343.

(4) He, X.; Borau-Garcia, J.; Woo, A. Y. Y.; Trudel, S.; Baumgartner, T. Dithieno[3,2-*c*:2′,3′-*e*]-2,7-diketophosphepin: A Unique Building Block for Multifunctional π-Conjugated Materials. *J. Am. Chem. Soc.* **2013**, *135* (3), 1137–1147. https://doi.org/10.1021/ja310680x.

(5) Grenz, D. C.; Schmidt, M.; Kratzert, D.; Esser, B. Dibenzo[*a*,*e*]pentalenes with Low-Lying LUMO Energy Levels as Potential n-Type Materials. *J. Org. Chem.* **2018**, *83* (2), 656–663. https://doi.org/10.1021/acs.joc.7b02250.

(6) Asok, N.; Gaffen, J. R.; Baumgartner, T. Unique Phosphorus-Based Avenues for the Tuning of Functional Materials. *Acc. Chem. Res.* **2023**, *56* (5), 536–547. https://doi.org/10.1021/acs.accounts.2c00707.

(7) Regulska, E.; Romero-Nieto, C. Highlights on π-Systems Based on Six-Membered Phosphorus Heterocycles. *Dalton Trans.* **2018**, *47* (31), 10344–10359. https://doi.org/10.1039/C8DT01485J.

(8) Ren, Y.; Dienes, Y.; Hettel, S.; Parvez, M.; Hoge, B.; Baumgartner, T. Highly Fluorinated Dithieno[3,2-*b*:2′,3′-*d*]phospholes with Stabilized LUMO Levels. *Organometallics.* **2009**, *28* (3), 734–740. https://doi.org/10.1021/om800874d.

(9) Romero-Nieto, C.; Baumgartner, T. Dithieno[3,2-*b*:2′,3′-*d*]phospholes: A Look Back at the First Decade. *Synlett.* **2013**, *24* (08), 920–937. https://doi.org/10.1055/s-0032-1317804.

(10) Dienes, Y.; Eggenstein, M.; Kárpáti, T.; Sutherland, T. C.; Nyulászi, L.; Baumgartner, T. Phosphorus-Based Heteropentacenes: Efficiently Tunable Materials for Organic n-Type Semiconductors. *Chem. Eur. J.* **2008**, *14* (32), 9878–9889. https://doi.org/10.1002/chem.200801549.

(11) Baumgartner, T.; Réau, R. Organophosphorus π-Conjugated Materials. *Chem. Rev.* **2006**, *106* (11), 4681–4727. https://doi.org/10.1021/cr040179m.

(12) Baumgartner, T.; Neumann, T.; Wirges, B. The Dithieno[3,2- *b*:2′,3′-*d*]phosphole System: A Novel Building Block for Highly Luminescent π-Conjugated Materials. *Angew. Chem. Int. Ed.* **2004**, *43* (45), 6197–6201. https://doi.org/10.1002/anie.200461301.

(13) Dienes, Y.; Durben, S.; Kárpáti, T.; Neumann, T.; Englert, U.; Nyulászi, L.; Baumgartner, T. Selective Tuning of the Band Gap of π-Conjugated Dithieno[3,2-*b*:2′,3′-*d*]phospholes toward Different Emission Colors. *Chem.Eur. J.* **2007**, *13* (26), 7487–7500. https://doi.org/10.1002/chem.200700399.

(14) Chua, C. J.; Ren, Y.; Baumgartner, T. Charge-Transfer Properties of Lateral Triphenylamine–Dithienophosphole Diads. *Org. Lett.* **2012**, *14* (6), 1588–1591. https://doi.org/10.1021/ol300331f.

(15) Dienes, Y.; Eggenstein, M.; Neumann, T.; Englert, U.; Baumgartner, T. Synthesis and Optoelectronic Properties of Transition Metal Complexes Incorporating Dithieno[3,2-*b*:2′,3′-*d*]phosphole Ligands. *Dalton Trans.* **2006**, No. 11, 1424–1433. https://doi.org/10.1039/B509277A.

(16) Hussein, A.; Asok, N.; Béland, V. A.; Gaffen, J. R.; LeBlanc, J.; Baumgartner, T. Development of the *P* -Arylation of Dithieno[3,2-*b*:2′,3′-*d*]phosphole with Aryl Iodonium Salts. *ChemPlusChem.* **2023**, *88* (7), e202300133. https://doi.org/10.1002/cplu.202300133.

(17) Ren, Y.; Kan, W. H.; Thangadurai, V.; Baumgartner, T. Bio-Inspired Phosphole-Lipids: From Highly Fluorescent Organogels to Mechanically Responsive FRET. *Angew. Chem. Int. Ed.* **2012**, *51* (16), 3964–3968. https://doi.org/10.1002/anie.201109205.

(18) Durben, S.; Dienes, Y.; Baumgartner, T. Cationic Dithieno[3,2-*b*:2′,3′-*d*]phospholes: A New Building Block for Luminescent, Conjugated Polyelectrolytes. *Org. Lett.* **2006**, *8* (25), 5893–5896. https://doi.org/10.1021/ol062580w.

(19) Elgrishi, N.; Rountree, K. J.; McCarthy, B. D.; Rountree, E. S.; Eisenhart, T. T.; Dempsey, J. L. A Practical Beginner's Guide to Cyclic Voltammetry. *J. Chem. Educ.* **2018**, *95* (2), 197–206. https://doi.org/10.1021/acs.jchemed.7b00361.

(20) Ren, Y.; Baumgartner, T. A Structure-Property Study toward π-Extended Phosphole Chromophores with Ambipolar Redox Properties. *Can. J. Chem.* **2016**, *94* (4), 297–304. https://doi.org/10.1139/cjc-2015-0347.

(21) Demay-Drouhard, P.; Baumgartner, T. Highly Luminescent 4-Pyridyl-Extended Dithieno[3,2-*b*:2′,3′-*d*]phospholes. *J. Org. Chem.* **2020**, *85* (22), 14627–14633. https://doi.org/10.1021/acs.joc.0c01369.

(22) He, X.; Woo, A. Y. Y.; Borau-Garcia, J.; Baumgartner, T. Dithiazolo[5,4-*b*:4′,5′-*d*]-phosphole: A Highly Luminescent Electron-Accepting Building Block. *Chem. Eur. J.* **2013**, *19* (23), 7620–7630. https://doi.org/10.1002/chem.201204375.

(23) Durben, S.; Baumgartner, T. 3,7-Diazadibenzophosphole Oxide: A Phosphorus-Bridged Viologen Analogue with Significantly Lowered Reduction Threshold. *Angew. Chem. Int. Ed.* **2011**, *50* (34), 7948–7952. https://doi.org/10.1002/anie.201102453.

(24) Stolar, M.; Borau-Garcia, J.; Toonen, M.; Baumgartner, T. Synthesis and Tunability of Highly Electron-Accepting, N-Benzylated "Phosphaviologens." *J. Am. Chem. Soc.* **2015**, *137* (9), 3366–3371. https://doi.org/10.1021/ja513258j.

(25) Bridges, C. R.; Borys, A. M.; Béland, V. A.; Gaffen, J. R.; Baumgartner, T. Phosphoryl- and Phosphonium-Bridged Viologens as Stable Two- and Three-Electron Acceptors for Organic Electrodes. *Chem. Sci.* **2020**, *11* (38), 10483–10487. https://doi.org/10.1039/D0SC04183A.

(26) He, X.; Baumgartner, T. Synthesis and Properties of a Dicationic π-Extended Dithieno[3,2-*c*:2′,3′-*e*]-2,7-Diketophosphepin.*Organometallics.***2013**, *32* (24), 7625–7628. https://doi.org/10.1021/om400991a.

(27) He, X.; Lin, J.; Kan, W. H.; Baumgartner, T. Phosphinine Lipids: A Successful Marriage between Electron-Acceptor and Self-Assembly Features. *Angew. Chem. Int. Ed.* **2013**, *52* (34), 8990–8994. https://doi.org/10.1002/anie.201303729.

(28) Wu, S.; Yan, Y.; Hou, H.; Huang, Z.; Li, D.; Zhang, X.; Xiao, Y. Polarity-Sensitive and Membrane-Specific Probe Quantitatively Monitoring Ferroptosis through Fluorescence Lifetime Imaging. *Anal. Chem.* **2022**, *94* (32), 11238–11247. https://doi.org/10.1021/acs.analchem.2c01737.

(29) Hindenberg, P.; Romero-Nieto, C. Phosphaphenalenes: An Evolution of the Phosphorus Heterocycles. *Synlett.* **2016**, *27* (16), 2293–2300. https://doi.org/10.1055/s-0035-1562506.

(30) Huy, N. H. T.; Donnadieu, B.; Mathey, F. Dithienophosphinine. *Organometallics.* **2007**, *26* (25), 6497–6500. https://doi.org/10.1021/om7006997.

(31) Huy, N. H. T.; Donnadieu, B.; Mathey, F. The Phosphaalkene-like Reactivity of Dithienophosphinines. *Organometallics.* **2008**, *27* (15), 4005–4008. https://doi.org/10.1021/om8003256.

(32) Schaub, T. A.; Brülls, S. M.; Dral, P. O.; Hampel, F.; Maid, H.; Kivala, M. Organic Electron Acceptors Comprising a Dicyanomethylene-Bridged Acridophosphine Scaffold: The Impact of the Heteroatom. *Chem. Eur. J.* **2017**, *23* (29), 6988–6992. https://doi.org/10.1002/chem.201701412.

Chapter 2: Phosphorus Modifications on the Dithieno[2,3-*b*:3',2'-*e*]-4-keto-1,4-dihydrophosphinine

Acknowledgements

The synthesis and characterization of a few compounds in this chapter were done with the assistance of Cheryl Cai Hui Tan, an undergraduate visiting student from Nanyang Technological University, Singapore. The XRD analyses were performed by Jesse Leblanc from the Le group and Casey Lenart from the Caputo group, both at York University, Toronto, Canada. Their contributions are greatly appreciated.

2.1 Introduction

A captivating feature of trivalent-phosphorus incorporation into π-conjugated scaffolds is the ability to post-functionalize the phosphorus lone pair to alter the properties of the system. As mentioned in the previous chapter, the pyramidal geometry of the phosphorus atom creates a unique σ*-π* (negative) hyperconjugation.[1] The degree of negative hyperconjugation can be modulated based on the nature of the substituent being attached to the phosphorus and in turn, has a direct effect on the HOMO-LUMO gap. Many functionalizations such as oxidation, sulfidation, metalation, alkylation, arylation, and as a consequence of the basicity of the lone pair, Lewis acid coordination, as well as their corresponding impact on the properties of phosphorus-based systems have been reported.[2,3] However, reports on phosphorus functionalization thus far predominately focus on five-membered, phosphole-based heterocycles and very few examples exist of fused-phosphinines, i.e., six-membered ring systems.[1] In the case of phosphinine, much work has focused

on its coordination chemistry as an ambidentate ligand, and its usefulness in catalysis but only few examples exist of it being functionalized whilst part of a fused system.[4] Some representative fused phosphinine-containing systems have been reported by the Baumgartner, Kivala, and Romero-Nieto groups in recent years (Figure 2-1).

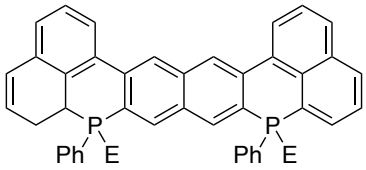

2-1 E = lone pair

2-1O E = O

2-1Me E = CH_3^+

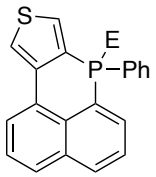

2-2 E = lone pair

2-2O E = O

2-2Me E = CH_3^+

2-2Au E = AuCl

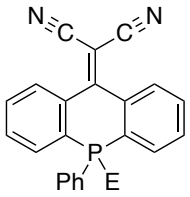

1-37 E = lone pair

1-37O E = O

1-37Me E = CH_3^+

Figure 2-1. Diphosphahexaarenes with various phosphorus modifications (left);[5] phosphaphenalenes with fused thiophene and multiple phosphorus functionalizations (middle);[6] dicyanomethylene functionalized acridophosphine with various phosphorus functionalities (right).[3]

Evidence of significant property changes by simple phosphorus functionalization in large phosphinine-containing systems was reported by Romero-Nieto and coworkers on a diphosphahexaarene motif (Figure 2-1).[5] The two phosphorus centres in compound **2-1** were oxidized (**2-1O**) and methylated (**2-1Me**) to then understand the property enhancements/changes that can be brought upon the entire system. When the compound is oxidized, a small decrease in the HOMO-LUMO gap compared to the trivalent species is noted, whereas methylation leads to a larger energy decrease.[5] These changes are also confirmed by the electrochemical properties of the system, wherein **2-1** has two reductions at -1.63 V and -1.87 V, **2-1O** has lower reductions at -1.43 V and -1.71 V and even lower reductions were seen with **2-1Me** with -1.1 V, -1.26 V and -1.6 V

(all vs. SCE), respectively, which not only introduces another redox step but also displays lower reduction potentials through quaternization. It was noted that quaternization leads **2-1Me** to be water soluble in addition to being the most red-shifted emitter. Overall, the Romero-Nieto group reported that by changing the substituent at the phosphorus centre the electronic properties change noticeably among the three species.

Another example, also reported by the Romero-Nieto group, involves ring-fused phosphaphenalenes.[6] Although many different architectures of these compounds were addressed in the study, phosphaphenalenes with a thiophene fused at the periphery is most closely related to our system (Figure 2-1, compound **2-2**). P-functionalization of the system included oxidation (**2-2O**), aurylation (**2-2Au**), and methylation (**2-2Me**). All compounds display fully reversible electrochemical reduction events with the exception of compound **2-2Au**.[6] The optical properties correlate with the optical gap of these systems, evident in a notable shift in the emission upon going from **2-2** to **2-2Me**. Using the electrochemical properties trivalent species **2-2** as a benchmark, which has one reversible reduction at -1.97 V, oxidation to **2-2O** leads to a decreased reduction potential of -1.74 V (vs. Fc/Fc^{+}). Thereafter, **2-2Au** has a lower threshold of reduction at -1.62 V, while lastly **2-2Me** exhibits the lowest reduction potential. Additionally, although not in the scope of this thesis, to highlight the various applications that can be accessed by simple phosphorus functionalization, compound **2-2Au** was recognized as a powerful candidate in use for brain cancer treatment in a follow-up study.[7]

The last series of relevant compounds for this thesis are the acridophosphines reported by the Kivala group.[3] This system is structurally most similar to our system as it contains a central phosphinine ring flanked by two benzo groups. There is also an electron-accepting dicyanomethylene moiety opposite to the phosphorus centre, which in our case is a keto group

(Figure 2-1, compounds with prefix **1-37**). To alter the properties of these systems, the phosphorus centre was oxidized (**1-37O**), methylated (**1-37Me**) and also kept in its trivalent state (**1-37**). Major differences in this system were dominantly seen in the cyclic voltammetry. As mentioned previously, the highest reduction potential is usually seen for the trivalent congeners, i.e., compound **1-37** with -1.49 V followed by **1-37O,** and lastly **1-37Me** that has the lowest reduction potential at -0.96 V (vs. Fc/Fc^{+}).[3]

The final example of pertinent fused phosphinines was reported in 2013 by our group, where we introduced the dithieno[2,3-*b*:3′,2′-*e*]-4-keto-1,4-dihydrophosphinine **2-3O** (Figure 2-2) and the corresponding benzylated species **2-3Bn** (Figure 2-2).[8] It was noted in the study that quaternization of the phosphorus toward **2-3Bn** leads to a decrease in the LUMO energy level unlocking a second reduction peak in the cyclic voltammogram. Additionally, the system displays unique self-assembly properties as a function of just a simple change at the phosphorus centre.[8]

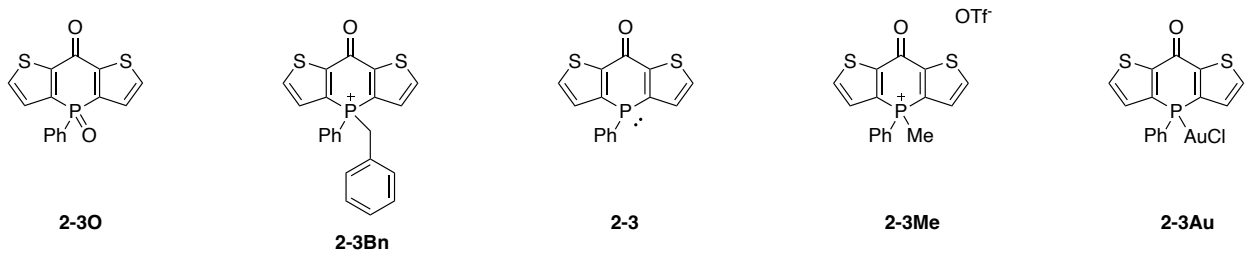

Figure 2-2. Previous dithieno[2,3-*b*:3,2-*e*]-4-keto-1,4-dihydrophosphinine systems reported by the Baumgartner group (**2-3O** and **2-3Bn**):[8] Proposed P-functionalization of the dithienoketophosphinine system as part of this thesis (**2-3**, **2-3Me**, **2-3Au**).

Based on the systems and their properties discussed above, derivatization of phosphorus-based systems by quaternization, oxidation, and aurylation to alter the properties is most representative. Moreover, not many P-functionalized fused phosphorus species exist to date. This led us to our

initial investigation on studying the impact of simple phosphorus-functionalization on the previously reported dithienoketophosphinine system **2-3O**. As a benchmark study, four derivatizations were studied: oxidation (**2-3O**), reduction (**2-3**), methylation (**2-3Me**), and aurylation (**2-3Au**). The corresponding syntheses and the ensuing changes in the electrochemical, optical and solid-state properties including some computational insights, are discussed in the following sections.

2.2 Results and Discussion

2.2.1 Synthesis of Precursor Compounds

The synthesis of the dithienoketophosphinine **2-3O** involves six steps.[8] Initially, 3-bromothiophene is lithiated at the 2-position using lithium diisopropylamide (LDA), which then reacts with methyl formate in *situ* to create the hydroxymethylene-bridged bis-3-bromothiophene **2-4** (Scheme 2-1). Thereafter, pyridinium chlorochromate is used to oxidize the alcohol to the corresponding ketone **2-5** that is then protected using ethylene glycol and p-toluenesulfonic acid to form **2-6**. The ketal protected trivalent phosphinine **2-7** (with a $^{31}P\{^{1}H\}$-NMR shift at -36 ppm) is formed in a two-step reaction, where the brominated positions on the thiophene are first lithiated to form intermediate **2-6int** (Scheme 2-1), followed by the addition of dichlorophenylphosphine through a salt metathesis. Oxidation of the phosphorus centre to form **2-7O** is performed using hydrogen peroxide with a $^{31}P\{^{1}H\}$-NMR peak at 2.4 ppm, while the deprotection is achieved by trifluoracetic acid leading to the final keto-species **2-3O** ($^{31}P\{^{1}H\}$-NMR: 1.4 ppm).

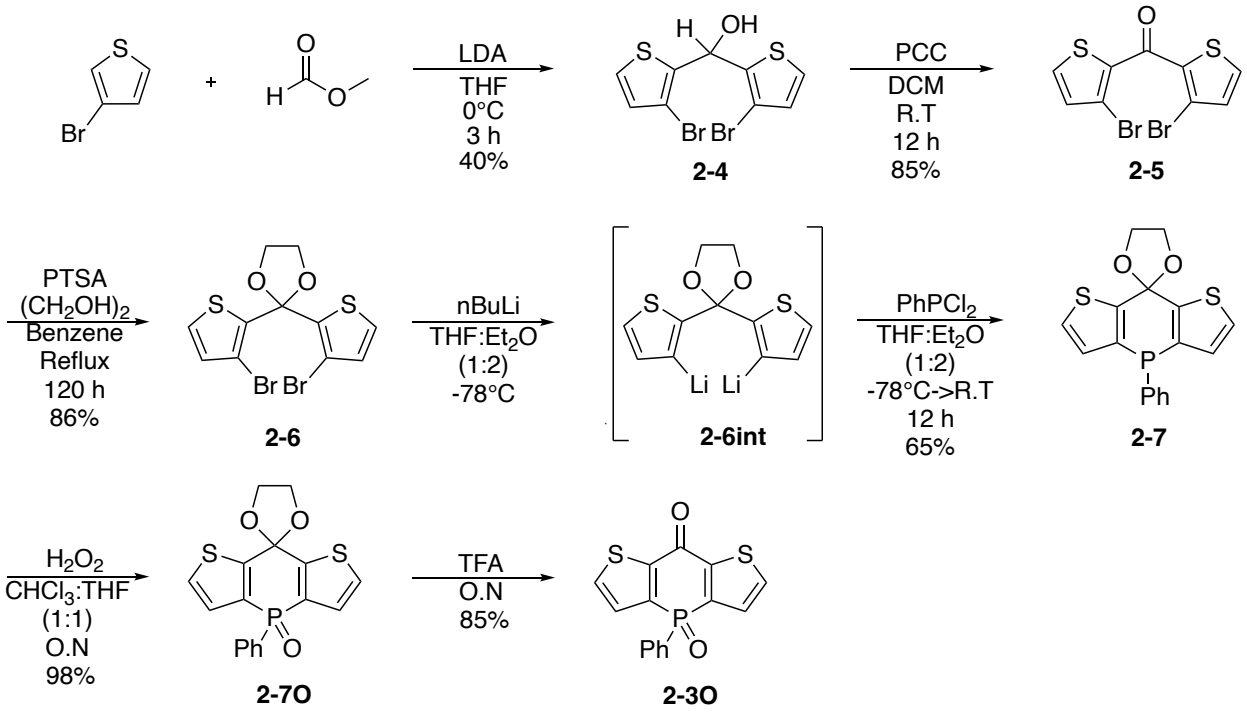

Scheme 2-1. Synthetic pathway to form dithieno[2,3-*b*:3′,2′-*e*]-4-keto-1,4-dihydrophosphinine oxide **2-3O**.

2.2.2 Further Phosphorus-Functionalization

Since the oxidation of **2-7** already leads to a considerable amount of P-oxidized compound **2-7O**, our initial attempts toward methylation and aurylation of the phosphorus centre involved the protected species **2-7**, as it precludes the need to first reduce the phosphorus centre before functionalization (Scheme 2-2A,B).

The successful formation of both the methylated and gold species **2-8Me** and **2-8Au** was confirmed by $^{31}P\{^{1}H\}$-NMR resonances at -6.5 ppm and -5.7 ppm, respectively. However, the pathway to deprotect the compounds involved triflic acid (Scheme 2-2B) in order to maintain the triflate counterion in the final product, so that the methylated and gold species can be effectively compared.

Unfortunately, the deprotection of **2-8Au** using triflic acid to form **2-3Au** led to many phosphorus-containing compounds confirmed by $^{31}P\{^{1}H\}$ NMR spectroscopy (See Supporting Information; Figure S2-32) and was thus deemed unsuitable.

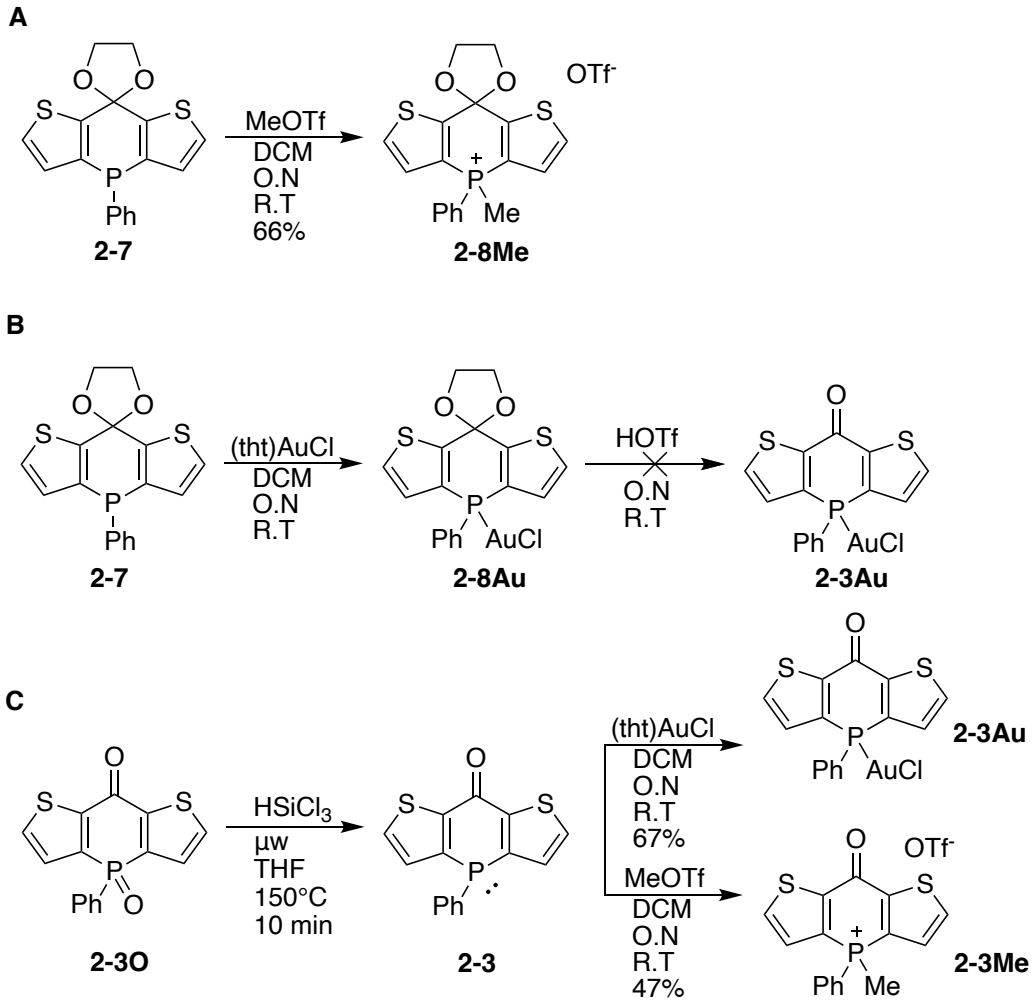

Scheme 2-2. Methylation of protected phosphinine (A); aurylation of protected phosphinine and failed deprotection attempt (B); reduction followed by successful aurylation and methylation of dithienoketophosphinine (C).

The alternative path was to reduce the ketophosphinine **2-3O** and then perform P-functionalization. Our group has previously shown that using the borane dimethylsulfide complex followed by exposure to triethylamine, a phosphole oxide can effectively be reduced to the corresponding trivalent species.[9] This method, however, depends on the quality of the borane and is quite time consuming. Thus, another literature-reported method using trichlorosilane under microwave conditions for 10 minutes (Scheme 2-2C).[5] This synthetic methodology led to the successful formation of **2-3** as confirmed by $^{31}P\{^{1}H\}$-NMR spectroscopy with a peak at -28 ppm. Thereafter, methyl triflate was used to form the methylated species **2-3Me** in an isolated yield of 47% and confirmed via a $^{31}P\{^{1}H\}$-NMR resonance at -4.2 ppm. Similarly, the gold complex **2-3Au**, with a $^{31}P\{^{1}H\}$-NMR resonance at -3.8 ppm, was formed in 67% isolated yield by treating **2-3** with tetrahydrothiophene gold(I)chloride. More details can be found in the Experimental Section and the Supporting Information.

2.2.3 Solid-State Structures of Select Compounds

Single crystals of compounds **2-3Me** and **2-3Au** as well as that of the oxidized species **2-3O**, which was not reported in the original 2013 publication, were obtained from slow evaporation in acetone for **2-3Me** and **2-3Au** and slow evaporation from acetonitrile for **2-3O** at room temperature.[8]

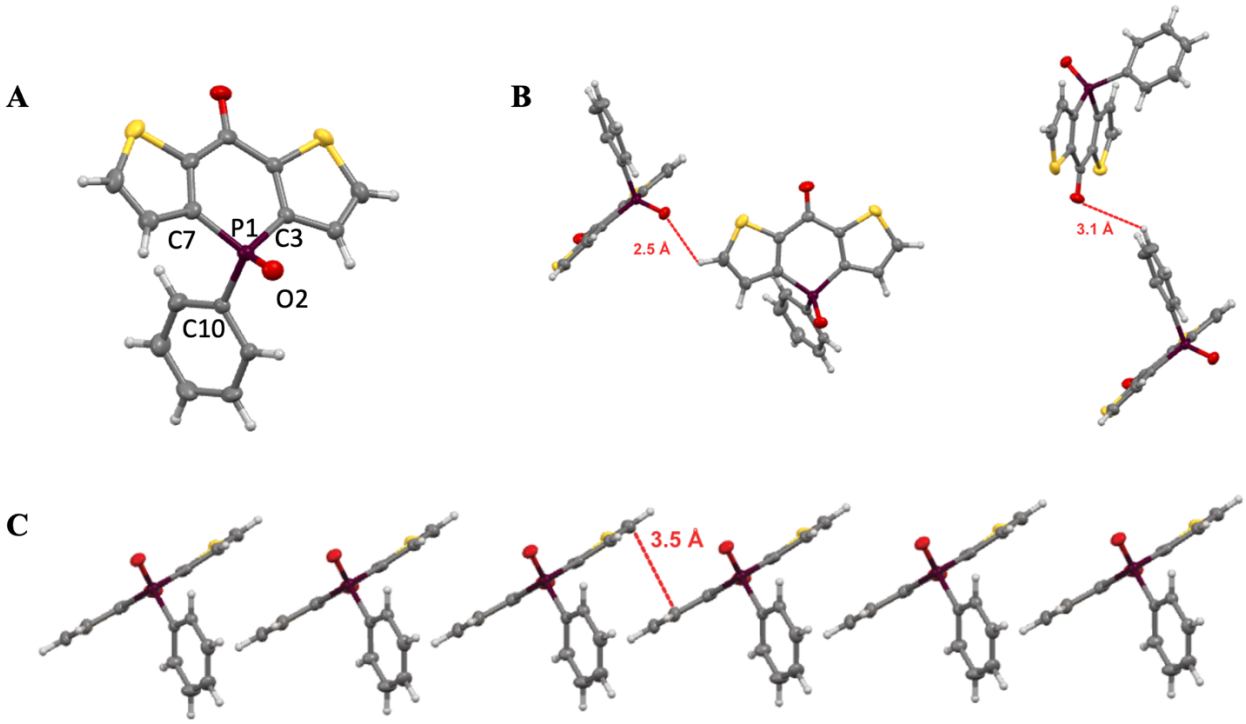

Figure 2-3. (A) Solid-state structure of single molecule of **2-3O** (thermal ellipsoids at 50% probability); (B) intermolecular hydrogen bonding interactions of **2-3O**; (C) packing of **2-3O** with evident π-stacking between adjacent compounds.

The solid-state structure of compound **2-3O** (Figure 2-3A), exhibits endocylic bonds lengths of 1.798(2) Å (P1-C3) and 1.797(3) Å (P1-C7) that are shorter than those of the related dithienophosphole oxide, indicating an increased involvement of the phosphorus with the π-system.[10] The exocyclic phenyl bond (P1-C10) at 1.797(2) Å is also shorter. The P1-O2 bond is the shortest of the bonds at the phosphorus at 1.485(2) Å, which is expected as there is strong back bonding from the oxygen to the phosphorus centre.[11] The phosphorus centre in the dithienoketophosphinine maintains an overall tetrahedral but slightly skewed geometry as the largest angle is 115.8(1)° with the smallest angle being 106.6(1)°. The main backbone of the scaffold maintains planarity, with the keto group in the same plane as the rest of the conjugated

system. The supramolecular organization of the molecule involves hydrogen bonding between the phosphine oxide and an adjacent α-hydrogen on the thieno group, and additional hydrogen-bonding interactions between a *para*-hydrogen atom on the exocyclic phenyl ring with a keto group on an adjacent molecule (Figure 2-3B). Lastly, there are π-stacking interactions at a typical distance of 3.5 Å between neighbouring molecules (Figure 2-3C).

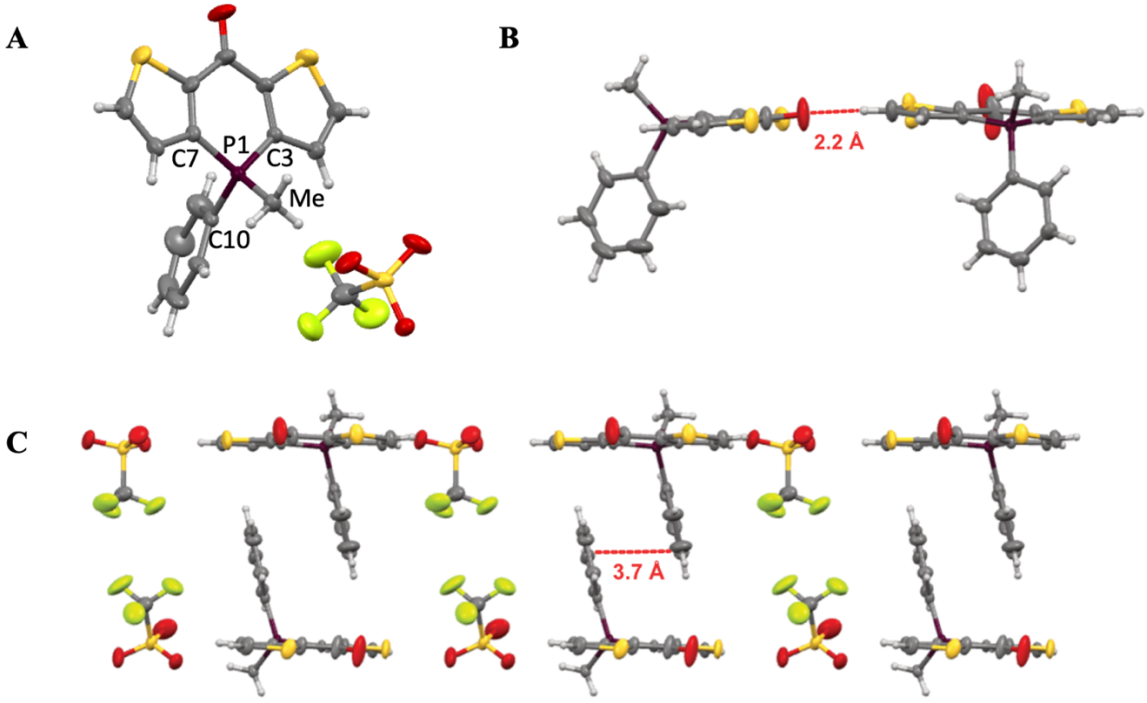

Figure 2-4. (A) Solid-state structure of single molecule of **2-3Me** (thermal ellipsoids at 50% probability); (B) intermolecular hydrogen bonding interactions in **2-3Me**; (C) packing of **2-3Me** with evident π-stacking between adjacent compounds and interpenetrating triflate counter anions.

For the methylated species **2-3Me** (Figure 2-4A), the only difference in the solid-state structure to the related oxide **2-3O** is the expectedly longer P-methyl bond length at 1.784(2) Å; all other angles are quite similar. There is also hydrogen bonding at a distance of 2.2 Å between the α-hydrogen atoms on the thiophenes and the keto-group on adjacent molecules (Figure 2-4B). Differences can be seen in the supramolecular organization wherein the exocyclic phenyl groups π-stack at a

distance of 3.7 Å and neighbouring molecules are separated by the triflate anion. The packing is also stabilized by S-O---H bonding between the α and β hydrogen atoms on the thiophene with distances of 2.4-2.5 Å and additional hydrogen bonding interactions between the methyl hydrogen atoms at 2.5 Å (Figure 2-4C). In comparison to the related methylated dithienophosphole, the bonding around the phosphorus centre is relatively similar, however, the internal C3-P-C7 angle in **2-3Me** is 104.17(9)° and the phosphole 93.94(19)° as a function of the six-membered vs. the five-membered ring in the phosphole-relative.[12]

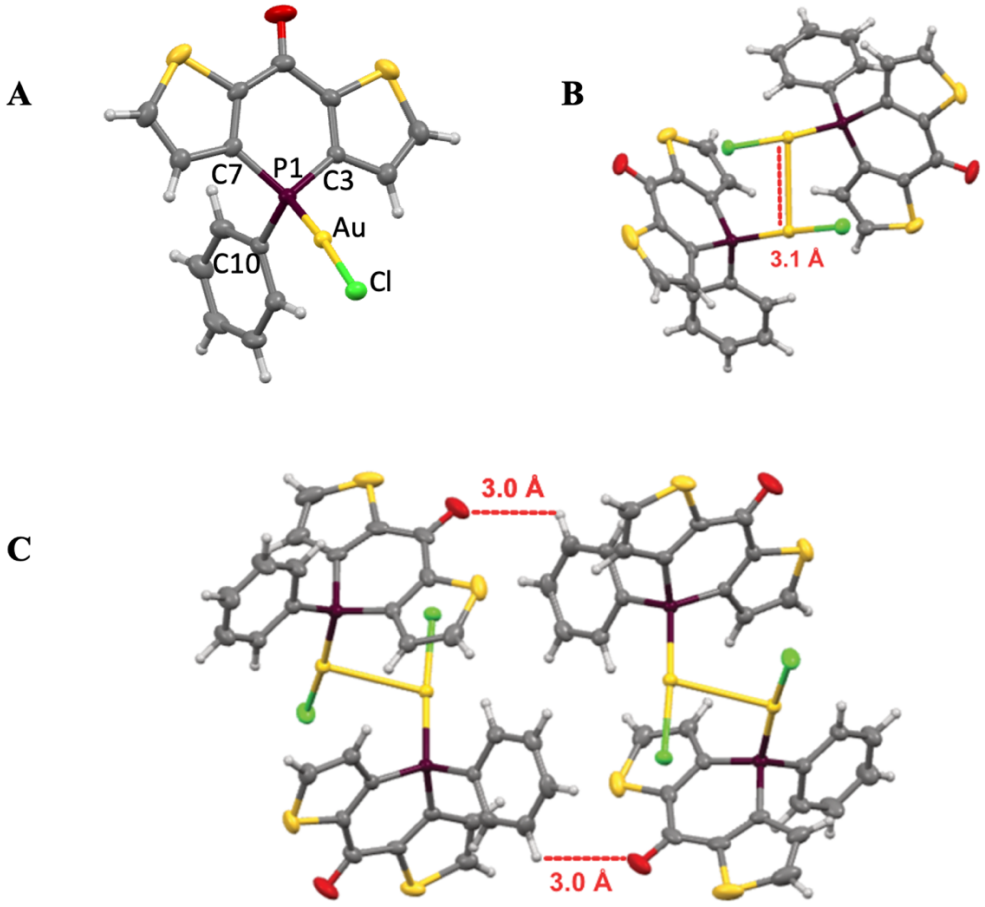

Figure 2-5. (A) Solid-state structure of single molecule of **2-3Au** (thermal ellipsoids at 50% probability); (B) aurophilic interaction between adjacent molecules of **2-3Au**; (C) packing of **2-3Au** with hydrogen-bonding interactions between adjacent compounds.

Lastly, the solid-state structure of **2-3Au** (Figure 2-5A), exhibits quite comparable bond lengths for both the endocyclic and the exocyclic P-C bonds with the other species in this series (**2-3O** and **2-3Me**). The P-Au bond at 2.2279(9) Å is relatively longer than the corresponding P=O and P-Me bonds but consistent with other phosphorus gold bonds previously studied in the related dithienophosphole-based systems.[13] The supramolecular organization of **2-3Au** involves the formation of dimers, enabled by aurophilic interactions at 3.0820(4) Å, relatively stronger than those of similar six-membered systems presented in literature (Figure 2-5B).[6] The last feature enabled by the keto-group is hydrogen bonding interactions between adjacent dimers wherein the *meta*-hydrogen atom on the exocyclic phenyl ring interacts with the keto group (Figure 2-5C).

2.2.4 Optical Properties

The observed trends in the absorption properties of the compounds matched our anticipation, but none of the compounds were emissive. It is known that the introduction of carbonyl groups does inhibit the emission pathways, as it could lead to non-radiative processes due to the enhancement of intersystem crossing.[14]

The complete absorption data are shown in Table 2-1. When comparing the absorption spectra across the different phosphorus functionalizations (Figure 2-6), the most closely related spectra are those of compounds **2-3O** and **2-3Me**, both of which have three absorption peaks, a high-energy maximum at 273 nm with relatively similar molar extinction coefficients, lower-energy maxima at 315 nm and 304 nm, respectively, and finally the lowest energy absorption at 343 nm for **2-3O** and 350 nm for **2-3Me**, consistent with a lower LUMO energy for the latter due to its cationic nature. Compound **2-3Au** contains only two peaks in its absorption spectrum (293 nm,

331 nm), and the trivalent species **2-3** being the most different among the species, with only one large absorption peak at 362 nm with a higher energy shoulder as well.

Table 2-1. (a) Absorption wavelengths and (b) molar extinction coefficients of all P-functionalized species in CH_2Cl_2 at $5x10^{-5}$ M. (c) Reduction potentials obtained from cyclic voltammetry experiments (vs. Fc/Fc^+) with NBu_4PF_6 as supporting electrolyte in CH_3CN. (d) Computational values of frontier molecular orbitals B3LYP/6-31G+(d) basis set and a LANL2MB for **2-3Au** using PCM solvation model in CH_2Cl_2. (e) Optical bandgap (HOMO-LUMO).

Compound	**λ_{Max} (nm)[a]**	**Ɛ ($M^{-1}cm^{-1}$)[b]**	**E_{red} (V)[c]**	**HOMO (eV)[d]**	**LUMO (eV)[d]**	**$\Delta_{HOMO-LUMO}$ (eV)[e]**
2-3O	273 315 343	15,760 10,480 10,510	-1.46	-7.10	-3.07	4.03
2-3	362	17,720	-1.90	-6.58	-2.56	4.02
2-3Me	273 304 350	15,780 5940 9380	-1.19, -1.84	-7.75	-3.70	4.05
2-3Au	293 331	12,490 9300	-1.55, -2.05	-7.21	-3.07	4.14

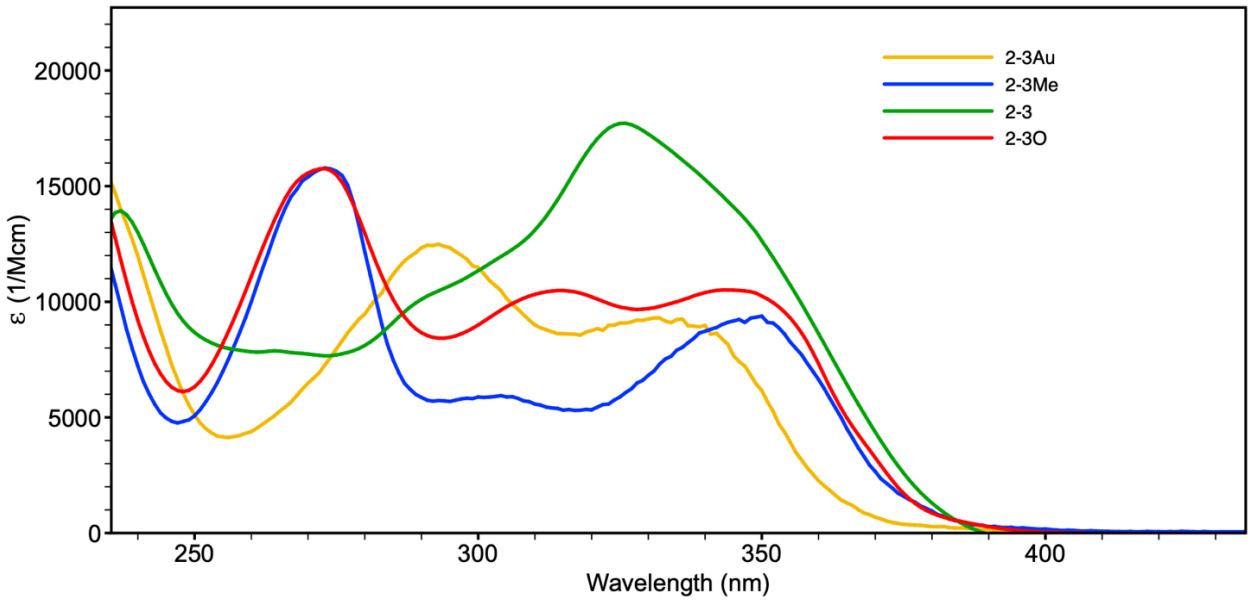

Figure 2-6. Absorption spectra of the phosphorus-functionalized species (CH_2Cl_2; c = $5x10^{-5}$ M).

2.2.5 Density Functional Theory Calculations

To gain a deeper understanding of the electronics of the system, density functional theory (DFT) calculations were performed (Figure 2-7). The HOMO of all compounds largely corresponds to the carbon-based π system, with the exception of **2-3** that also has a large contribution from the phosphorus, sulfur, and oxygen lone pairs. Compound **2-3Au** also has some additional delocalization of the HOMO onto the exocyclic AuCl unit. The LUMO of each compound largely corresponds to the π* system and one (**2-3**) or two (**2-3O**, **2-3Me**, **2-3Au**) σ*-π* interactions with the exocyclic substituents are evident in all species as well. With respect to the calculated energies of the molecular orbitals, the trivalent species **2-3** has the highest LUMO and HOMO energies of all species at -2.56 eV and -6.58 eV, respectively. Compound **2-3O** has a slightly lower LUMO level at -3.07 eV compared to **2-3**, as anticipated by the presence of an electron-accepting phosphoryl (P=O) group. Coincidentally, the gold species **2-3Au** exhibits the same LUMO energy

as **2-3O** but has a slightly lower HOMO level at -7.21 eV. The most significant change in energies for the frontier molecular orbitals is seen in **2-3Me** with a -0.67 eV lower LUMO energy than **2-3O** making it the strongest acceptor in the series.

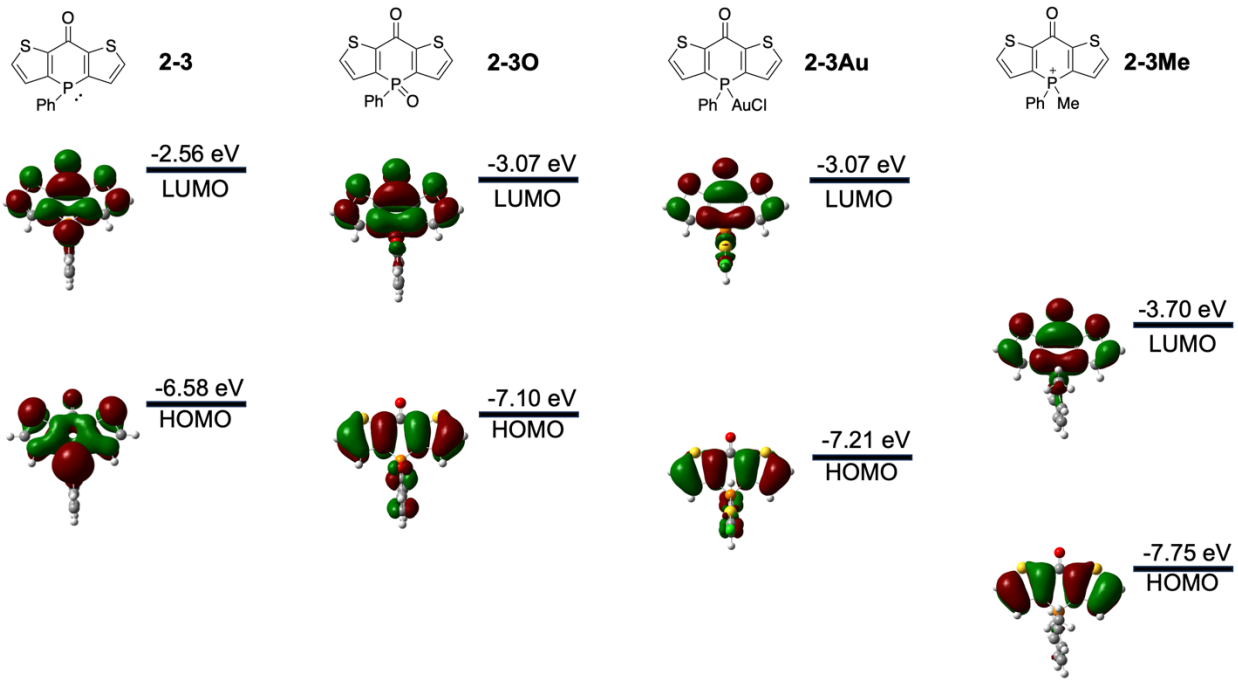

Figure 2-7. Frontier molecular orbitals of **2-3**, **2-3O**, **2-3Me**, and **2-3Au** with respective HOMO and LUMO energies (eV). B3LYP6-31G+(d) with LanL2MB level of theory for **2-3Au** using a PCM solvation model in CH_2Cl_2.

2.2.6 Time-dependent Density Functional Theory (TDDFT) Calculations

To further enhance our understanding on the absorption properties of the compounds, time-dependent density functional theory (TDDFT) calculations at the TD-SCF/CAM-B3LYP/6-31G+(d) level of theory using the polarizable continuum model (PCM solvation model) were performed. The molecular orbital transitions along with the calculated contribution (in percent) of

each transition are summarized in Table 2-2 and the corresponding molecular orbitals are shown in Figure 2-8. It is important to note that for the previously reported dithienophosphole systems, the absorption maxima generally correspond to π- π* transitions.[9]

Table 2-2. Time-dependent density functional theory calculation results for phosphorus-functionalized species using TD-SCF CAM-B3LYP/6-31G+(d) using PCM solvation model in CH_2Cl_2. (a) Oscillator strengths used to determine (b) dominant transitions.

	2-3O	**2-3**	**2-3Me**	**2-3Au**
λ/nm (*f*)[a]	328 (0.14)	312 (0.32)	325 (0.22)	317 (0.24)
Transitions[b]	H → L (67%)	H → L (96%)	H → L (95%)	H → L (94%)
	H-6 → L (25%)			
λ/nm (*f*)[a]	286 (0.16)		278 (0.11)	289 (0.16)
Transitions[b]	H-1 → L (68%)		H-1 → L (31%)	H-1 → L (83%)
	H-4 → L (23%)		H-5 → L (26%)	H-3 → L (12%)
λ/nm (*f*)[a]	256 (0.37)		256 (0.43)	
Transitions[b]	H-5 → L (91%)		H-4 → L (92%)	
	H-3 → L (3%)			

All four compounds have a dominant HOMO to LUMO π–π* transition with an additional n–π* contribution in **2-3** based on the molecular orbital delocalization discussed above. There is however, an additional contribution from a HOMO-6 to LUMO in **2-3O** (Figure 2-8). The second absorption process exhibited by **2-3O**, **2-3Me** and **2-3Au** is dominated by HOMO-1 to LUMO transitions, which, for **2-3O** and **2-3Me**, are π–π* transitions as the HOMO-1 constitutes the π system of the thieno-backbone as well the exocyclic phenyl π system. In the case of **2-3Au**, the HOMO-1 is dominated by the sulfur lone pairs as well as the gold chloride moiety, making it more

of a n–π* transition, with additional delocalization on the σ bonds of the thiophene as well as the exocyclic P-C σ bond (σ–π*). For this absorption there are also minor contributions from the HOMO-4, HOMO-5 and HOMO-3. The highest energy absorption that is only present in **2-3O** and **2-3Me** is dominated by a π –π* HOMO-5 to LUMO transition for **2-3O**. Compound **2-3O** also has minor contributions from HOMO-3 to LUMO. In the case of **2-3Me** the absorption is dominated by a n–π* HOMO-4 to LUMO transition (Figure 2-8).

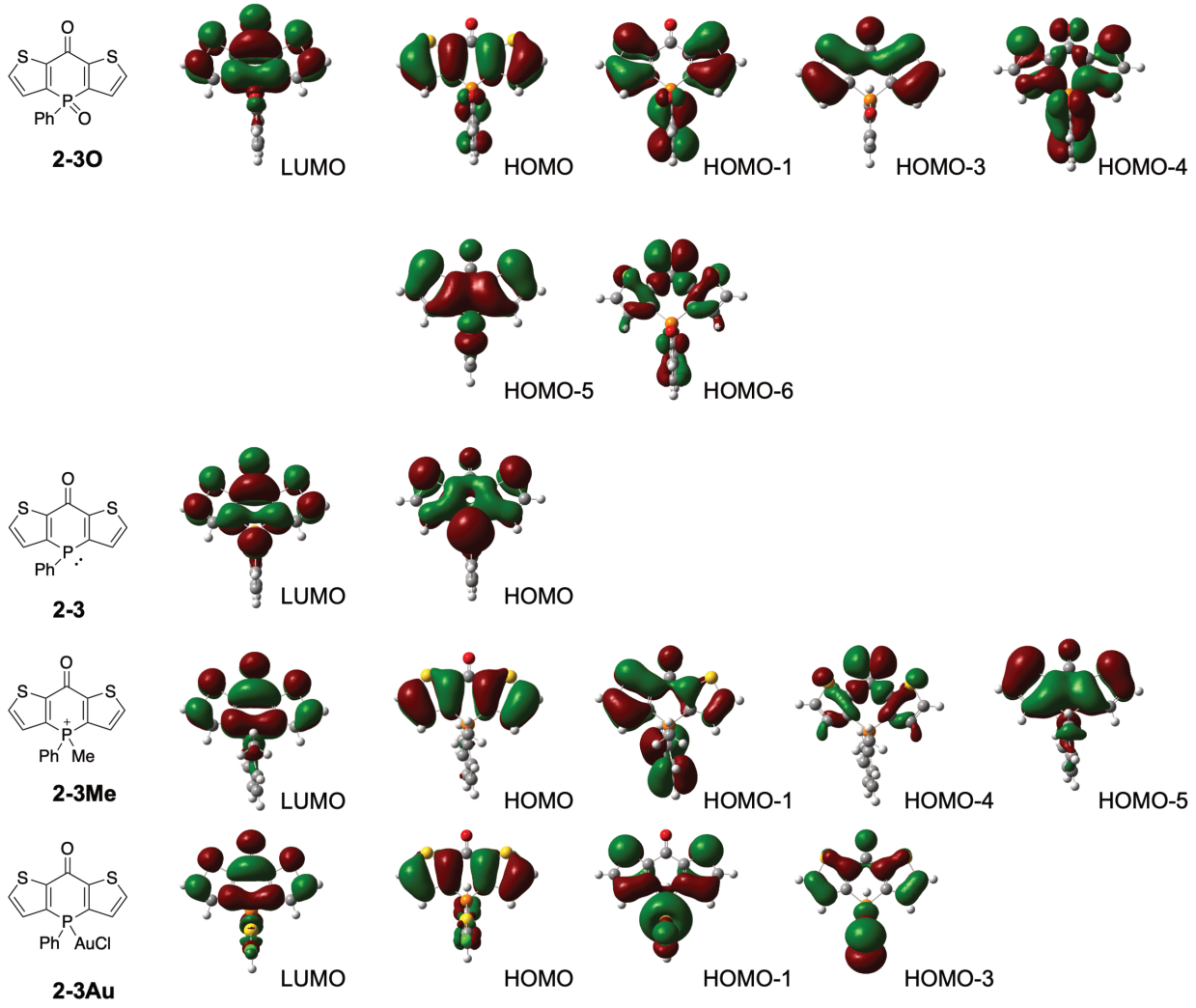

Figure 2-8. Select molecular orbitals for phosphorus functionalized species.

2.2.7 Cyclic Voltammetry

The fundamental development of inherently rare organic n-type species materials focuses on the ability of the compounds to accept electrons. This feature can effectively be verified via cyclic voltammetry. All of the new compounds in this series show mostly reversible reduction events in their cyclic voltammograms (Figure 2-9). The oxidation events, on the other hand, are largely irreversible, as is typical for P-containing conjugated materials, and can be found in the Supporting Information (Figure S2-49).

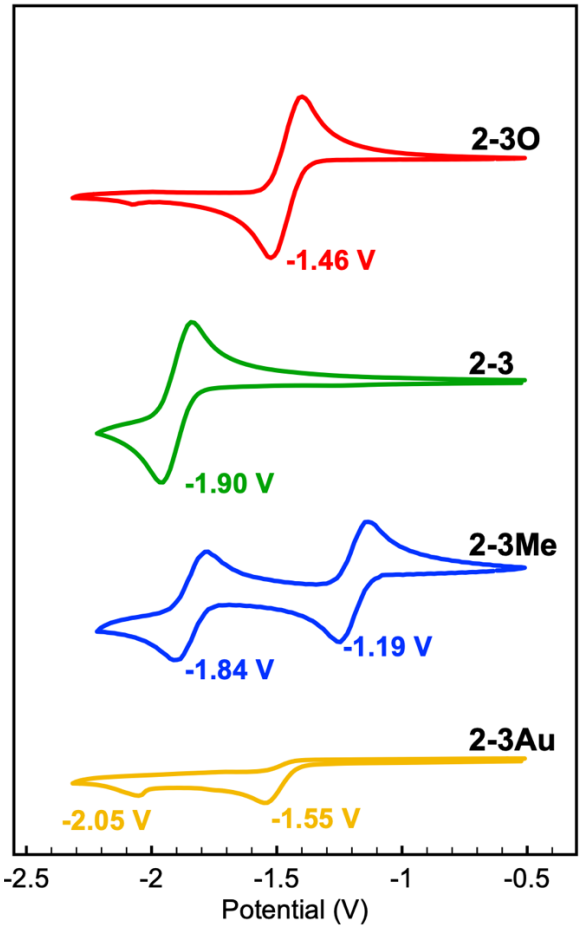

Figure 2-9. Cyclic voltammograms of **2-3O** (red), **2-3** (green), **2-3Me** (blue) and **2-3Au** (yellow). Potentials are referenced to Fc/Fc^{+}. Scan rate 100 mV/s with NBu_4PF_6 as supporting electrolyte. All experiments performed in dry CH_3CN under argon.

To establish the impact of phosphorus functionalization on the dithienoketophosphinine system, we use the trivalent species **2-3**, with one reversible reduction at -1.90 V (vs. Fc/Fc^+) as a reference point (Figure 2-9). Simple oxidation toward **2-3O** affords a lower reduction event at -1.46 V that maintains full reversibility. Oxidation of the P-centre **2-3O** to its pentavalent state is an effective strategy to enhance its electron-acceptor character also shown by the lower LUMO at -3.07 eV compared to the LUMO of **2-3** at -2.56 eV.[11] The quaternized species **2-3Me** exhibits a second reversible reduction event at -1.84 V with a lower-threshold first reduction event at -1.19 V. The second reduction can be assigned to the cationic nature of the phosphorus centre and the lower reduction potential results from the lowest LUMO energy of -3.70 eV among all new compounds. Lastly, **2-3Au** has two irreversible reductions at -1.55 V and -2.05 V and this change in reversibility is similar to a related aurylated dithienodiketophosphepin species with central seven-membered heterocycle.[15]

2.3 Conclusion and Outlook

In conclusion we were able to successfully synthesize various phosphorus-functionalized dithienoketophosphinines with the goal of understanding the impact of these changes on the optical, electrochemical and solid state-organization of these molecules. To this end, we have demonstrated that the optical and electrochemical properties of the dithienoketophosphinine can be effectively altered by the substituent on the phosphorus centre, aligning well with the features of related dithienophosphole species. With a view toward potential application as effective n-type materials, **2-3**, **2-3O**, and **2-3Me** proved to be promising electron acceptors with low lying LUMOs and mostly reversible reduction events providing a useful benchmark for further modifications.

2.4 Experimental Section

2.4.1 General Methods

Most reactions were performed under an inert argon atmosphere using standard Schlenk techniques. Solvents were dried using an MBraun SPS solvent purification system. The reagents used were purchased from Sigma Aldrich, Fischer, or Oakwood Chemicals and used as received. Compound **2-3O** was synthesized according to the literature procedure.[8] The NMR data were obtained on Bruker NEO 300, 400 or 600 MHz spectrometers. All microwave reactions were performed in an Anton Paar Monowave 2000. Single crystal X-ray crystallographic data were obtained on a Bruker D8 Quest Eco diffractometer. The optical studies were carried out with an Agilent Cary 5000 UV-vis spectrophotometer using standard quartz cuvettes. Cyclic voltammetry was performed using a Metrohm Autolab Potentiostat with NOVA software in dry acetonitrile with tetrabutylammonium hexafluorophosphate as the electrolyte. Theoretical calculations were done using Gaussian on clusters provided by the Digital Research Alliance of Canada.

2.4.2 Synthesis and Characterization

Synthesis of **2-3O**:

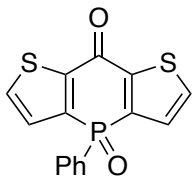

Compound **2-7O** (0.95 g, 2.7 mmol) was dissolved in 10 mL TFA and stirred at room temperature for 12 h. The reaction mixture was then added to 100 mL of water, quenched with sodium bicarbonate, and extracted with dichloromethane. The organic layer was dried with magnesium sulfate, then gravity filtered, and the solvent was subsequently removed to give tan solids (yield: 0.72 g, 87%). $^{31}P\{^{1}H\}$ NMR (162 MHz, $CDCl_3$) δ = 1.4 ppm. ^{1}H NMR (400 MHz, $CDCl_3$) δ = 7.82 (dd, J_{HH} = 8.0, J_{HP} = 4 Hz, 2H), 7.68 – 7.62 (m,

2H), 7.54-7.49 (m, 1H), 7.45-7.40 (m, 4H). ^{13}C NMR (100.6 MHz, $CDCl_3$) δ = 172.5 (d, J_{CP} = 5 Hz), 146.2 (d, J_{CP} = 9 Hz), 140.3 (d, J_{CP} = 102.6 Hz), 135.8 (d, J_{CP} = 16.1 Hz), 132.8 (d, J_{CP} = 3 Hz), 131.1 (d, J_{CP} = 113.7 Hz), 130.9 (d, J_{CP} = 11 Hz), 130.3 (d, J_{CP} = 11.1 Hz), 129.2 (d, J_{CP} = 14.1 Hz).The NMR data match the literature-reported values.[8]

Synthesis of **2-8Me:**

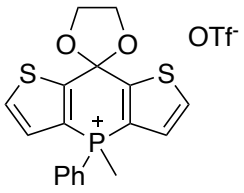

Compound **2-7** (0.12 g, 0.4 mmol) was dissolved in 1 mL of dichloromethane. Methyl triflate (0.59 g, 3.6 mmol) was added before allowing the reaction to stir for 12 h. The solvent was removed in *vacuo* and the compound was crashed out in acetone to give white solids (yield: 0.07 g, 40%).^{31}P{^{1}H} NMR (162 MHz, MeOD) δ = -6.5 ppm. ^{1}H NMR (400 MHz, MeOD) δ = 8.01 (dd, *J* = 5.2, 3.3 Hz, 2H), 7.90 – 7.79 (m, 3H), 7.70 (td, *J* = 8.1, 3.7 Hz, 2H), 7.64 (dd, *J* = 5.3, 4.3 Hz, 2H), 4.57 – 4.39 (m, 4H), 2.91 (d, *J* = 14.9 Hz, 3H). ^{13}C NMR (100.6 MHz, MeOD) δ = 157.1 (d, J_{CP} = 9.1 Hz), 134.9 (d, J_{CP} = 3 Hz), 131.7 (d, J_{CP} = 12.2 Hz), 131.2 (d, J_{CP} = 18.1 Hz), 130.1 (d, J_{CP} = 14.1 Hz), 127.5 (d, J_{CP} = 15.1 Hz), 121.9 (q, J_{CF} = 317.9 Hz), 117.5 (d, J_{CP} = 93.6 Hz), 76.5 (d, J_{CP} = 517.1 Hz), 67.6 (s), 66.0 (s), 7.72 (d, J_{CP} = 58.3 Hz). Theoretical mass 359.42 g/mol. HRMS (ESI): m/z = 359.0328 $[M]^+$ (calcd. 359.0328).

Synthesis of **2-8Au:**

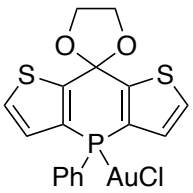

Compound **2-7** (0.14 g, 0.4 mmol) was dissolved in 8 mL of dichloromethane to which tetrahydrothiophene gold(I)chloride (0.17 g, 0.5 mmol), dissolved in 2 mL dichloromethane was added. The reaction was stirred for 12 h and the solvent was removed in *vacuo*. The product was precipitated from acetone to give white solids (yield: 0.15

g, 66%). $^{31}P\{^{1}H\}$ NMR (162 MHz, $CDCl_3$) δ = -5.4 ppm. ^{1}H NMR (400 MHz, $CDCl_3$) δ = 7.75 (m, 2H), 7.51 ppm (m, 3H), 7.43 ppm (m, 2H), 7.17 ppm (m, 2H), 4.45 (m, 4H). ^{13}C NMR (100.6 MHz, $CDCl_3$) δ = 149.8 (d, J_{CP} = 3.0 Hz), 134.1 (d, J_{CP} = 16.1 Hz), 132.4 (d, J_{CP} = 3.0 Hz), 129.9 (d, J_{CP} = 21.1 Hz), 129.7 (d, J_{CP} = 63.4 Hz), 129.4 (d, J_{CP} = 13.1 Hz), 127.9 (d, J_{CP} = 17.1 Hz), 126.7 (d, J_{CP} = 65.4 Hz), 102.1 (d, J_{CP} = 4 Hz), 67.2 (s), 65.8 (s). HRMS (ESI): m/z = 576.9522 $[M+H]^+$ (calcd. 576.9527).

Synthesis of **2-3:**

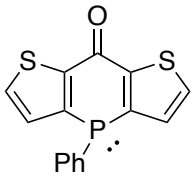

Compound **2-3O** (0.23 g, 0.7 mmol), trichlorosilane (2.95 g, 21.7 mmol), and dry tetrahydrofuran (15 mL) were added into a microwave vial to microwave the mixture for 10 min. at 150 °C. The solvent was removed under *vacuo* to provide **2-3** as tan solids (yield: 0.17 g, 80%). $^{31}P\{^{1}H\}$ NMR (162 MHz, $CDCl_3$) δ= -28.5 ppm. ^{1}H NMR (400 MHz, $CDCl_3$) δ= 7.76 (dd, J=8.0, J=4 Hz, 2H), 7.41-7.30 (m, 5H), 7.19 (dd, J=8 J=4, 2H).$^{13}C\{^{1}H\}$ NMR (100.6 MHz, $CDCl_3$): δ= 174.3 (d, J_{CP} = 3 Hz), 146.1 (d, J_{CP} = 11 Hz), 141.7 (s), 134.3 (d, J_{CP} = 2 Hz), 134.1 (d, J_{CP} = 11 Hz), 133.5 (d, J_{CP} = 16 Hz), 131.3 (d, J_{CP} = 27 Hz), 130.7 (s), 129.4 (d, J_{CP} = 8 Hz). HRMS (ESI): m/z = 300.99094 $[M+H]^+$ (calcd. 300.9910).

Synthesis of **2-3Au:**

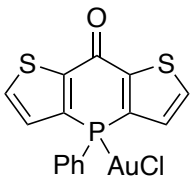

Compound **2-3** (0.17 g, 0.6 mmol) and tetrahydrothiophene gold(I)chloride (0.24 g, 0.8 mmol) were dissolved in 8 mL of dichloromethane and let stir overnight. Subsequently, the solvent was removed in *vacuo* to afford **2-4Au** as grey solids (yield: 0.21 g, 67%). $^{31}P\{^{1}H\}$ NMR (162 MHz, $CDCl_3$) = -3.8 ppm. ^{1}H NMR (400 MHz, CDCl3) δ = 7.94 (dd, J_{HH} = 8.0 Hz, J_{HP} = 4 Hz, 2H), 7.65-7.56 (m, 3H), 7.49-7.46 (m, 2H), 7.39 (t, J_{HH} = 4Hz, J_{HP} = 3 Hz, 2H). ^{13}C NMR (151 MHz, $CDCl_3$) δ = 172 (d, J_{CP} = 4.6 Hz), 144.4

(d, J_{CP} = 3.8 Hz), 135.7 (d, J_{CP} = 17 Hz), 134.6 (d, J_{CP} = 60.8 Hz), 133.9 (d, J_{CP} = 16.3 Hz), 133.2 (d, J_{CP} = 2.3 Hz), 131.3 (d, J_{CP} = 20 Hz), 129.9 (d, J_{CP} = 13 Hz), 127.2 (d, J_{CP} = 63.5 Hz). HRMS (ESI): m/z = 549.95250 $[M+H]^+$ (calcd. 532.9264).

Synthesis of **2-3Me**:

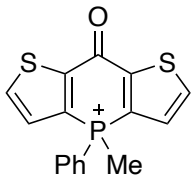

Compound **2-3** (0.10 g, 0.3 mmol) was dissolved in 8 mL of dry dichloromethane. Methyl triflate (2 mL, 18.3 mmol) was added to the mixture at 0 °C. The mixture was stirred for 12 h and the solvent was then removed in *vacuo*. The product was reprecipitated from acetone at 0 °C to give white solids (yield: 0.07 g, 47%). $^{31}P\{^1H\}$ NMR (162 MHz, $(CD_3)_2CO$): δ = -4.2 ppm. ^1H NMR (400 MHz, $(CD_3)_2CO$): δ = 8.54 ppm (dd, J_{HH} = 5.0 Hz, J_{HP} = 3.3 Hz, 2H), 8.11 (m, 4H), 7.89 (m, 1H), 7.75 (m, 2H), 3.25 (d, J_{HP} = 15.2 Hz, 3H, -Me). $^{13}C^1H\}$ NMR (100.6 MHz, $(CD_3)_2CO$): δ = 171.9 ppm (d, J_{CP} = 6.2 Hz), 150.4 (d, J_{CP} = 8.7 Hz), 139.7 (d, J_{CP} = 18.2Hz), 136.6 (d, J_{CP} = 2.9 Hz), 133.7 (d, J_{CP}= 12.3 Hz), 131.8 (d, J_{CP} = 14.7 Hz), 131.4 (d, J_{CP} = 13.9 Hz), 125.5 (d, J_{CP} = 91.5 Hz), 122.5 (q, J_{CF} = 321.9 Hz), 120.0 (d, J_{CP} = 91 Hz), 9.1 (d, J_{CP} = 55.6 Hz). HRMS (ESI): m/z = 315.0070 $[M]^+$ (calcd. 315.0062).

2.5 References

(1) De Cózar, A.; Romero-Nieto, C. Boundaries of the Hyperconjugation from π-Extended Six-Membered Phosphorus Heterocycles. *Inorg. Chem.* **2023**, *62* (10), 4097–4105. https://doi.org/10.1021/acs.inorgchem.2c03884.

(2) Romero-Nieto, C.; Baumgartner, T. Dithieno[3,2-*b*:2′,3′-*d*]phospholes: A Look Back at the First Decade. *Synlett.* **2013**, *24* (08), 920–937. https://doi.org/10.1055/s-0032-1317804.

(3) Schaub, T. A.; Brülls, S. M.; Dral, P. O.; Hampel, F.; Maid, H.; Kivala, M. Organic Electron Acceptors Comprising a Dicyanomethylene-Bridged Acridophosphine Scaffold: The Impact of the Heteroatom. *Chem. Eur. J.* **2017**, *23* (29), 6988–6992. https://doi.org/10.1002/chem.201701412.

(4) Müller, C.; Broeckx, L. E. E.; De Krom, I.; Weemers, J. J. M. Developments in the Coordination Chemistry of Phosphinines. *Eur. J. Inorg. Chem.* **2013**, *2013* (2), 187–202. https://doi.org/10.1002/ejic.201200912.

(5) Hindenberg, P.; Rominger, F.; Romero-Nieto, C. Phosphorus Post-Functionalization of Diphosphahexaarenes. *Chem. Eur. J.* **2019**, *25* (57), 13146–13151. https://doi.org/10.1002/chem.201901837.

(6) Hindenberg, P.; López-Andarias, A.; Rominger, F.; de Cózar, A.; Romero-Nieto, C. A Guide for the Design of Functional Polyaromatic Organophosphorus Materials. *Chem. Eur. J.* **2017**, *23* (56), 13919–13928. https://doi.org/10.1002/chem.201701649.

(7) Roesch, S.; Fermi, V.; Rominger, F.; Herold-Mende, C.; Romero-Nieto, C. Gold(I) Complexes Based on Six-Membered Phosphorus Heterocycles as Bio-Active Molecules against Brain Cancer. *Chem. Commun.* **2020**, *56* (93), 14593–14596. https://doi.org/10.1039/D0CC05761D.

(8) He, X.; Lin, J.; Kan, W. H.; Baumgartner, T. Phosphinine Lipids: A Successful Marriage between Electron-Acceptor and Self-Assembly Features. *Angew. Chem. Int. Ed.* **2013**, *52* (34), 8990–8994. https://doi.org/10.1002/anie.201303729.

(9) Dienes, Y.; Durben, S.; Kárpáti, T.; Neumann, T.; Englert, U.; Nyulászi, L.; Baumgartner, T. Selective Tuning of the Band Gap of π-Conjugated Dithieno[3,2-*b*:2′,3′-*d*]phospholes toward Different Emission Colors. *Chem. Eur. J.* **2007**, *13* (26), 7487–7500. https://doi.org/10.1002/chem.200700399.

(10) Baumgartner, T.; Neumann, T.; Wirges, B. The Dithieno[3,2-*b*:2′,3′-*d*]phosphole System: A Novel Building Block for Highly Luminescent π-Conjugated Materials. *Angew. Chem. Int. Ed.* **2004**, *43* (45), 6197–6201. https://doi.org/10.1002/anie.200461301.

(11) Baumgartner, T. Insights on the Design and Electron-Acceptor Properties of Conjugated Organophosphorus Materials. *Acc. Chem. Res.* **2014**, *47* (5), 1613–1622. https://doi.org/10.1021/ar500084b.

(12) Hussein, A.; Asok, N.; Béland, V. A.; Gaffen, J. R.; LeBlanc, J.; Baumgartner, T. Development of the *P* -Arylation of Dithieno[3,2-*b*:2′,3′-*d*]phosphole with Aryl Iodonium Salts. *ChemPlusChem.* **2023**, *88* (7), e202300133. https://doi.org/10.1002/cplu.202300133.

(13) Dienes, Y.; Eggenstein, M.; Neumann, T.; Englert, U.; Baumgartner, T. Synthesis and Optoelectronic Properties of Transition Metal Complexes Incorporating Dithieno[3,2-*b*:2′,3′-*d*]-phosphole Ligands. *Dalton Trans.* **2006**, No. 11, 1424–1433. https://doi.org/10.1039/B509277A.

(14) Šámal, M.; Sturm, L.; Banasiewicz, M.; Deperasinska, I.; Kozankiewicz, B.; Morawski, O.; Nagata, Y.; Dechambenoit, P.; Bock, H.; Rossel, A.; Buděšínský, M.; Boudier, A.; Jančařík, A. Carbonyl Mediated Fluorescence in Aceno[*n*]Helicenones and Fluoreno[*n*]Helicenes. *Chem. Sci.* **2024**, *15* (25), 9842–9850. https://doi.org/10.1039/D4SC00892H.

(15) He, X.; Borau-Garcia, J.; Woo, A. Y. Y.; Trudel, S.; Baumgartner, T. Dithieno[3,2-*c*:2′,3′-*e*]-2,7-diketophosphepin: A Unique Building Block for Multifunctional π-Conjugated Materials. *J. Am. Chem. Soc.* **2013**, *135* (3), 1137–1147. https://doi.org/10.1021/ja310680x.

Chapter 3: Ketone Modifications of the Dithieno[2,3-b; 3',2'-e]-4-keto-1,4-dihydrophosphinine Toward Stronger Electron Acceptors

Acknowledgements

Some of the compounds in this chapter were synthesized and characterized with the assistance of Cheryl Cai Hui Tan, a visiting undergraduate student from Nanyang Technical University in Singapore. Additional NMR studies were performed with the assistance of Dr. Howard Hunter from York University Canada. XRD analysis was done by Jesse LeBlanc from the Le group at York University. Their contributions to the research are greatly appreciated.

3.1 Introduction

Among the many electron-accepting compounds studied for use as n-type materials is the well-studied 7,7,8,8-tetracyano-p-quinodimethane (TCNQ), introduced in the 1960s (Figure 3-1).[1] This species was reported to form stable radical anions and unique charge-transfer complexes with donor compounds, enabling a variety of semiconducting applications.[1,2] After the initial introduction of TCNQ, many different modifications have been made to its π-system to study the resulting properties. One such modification was benzoannulation (Figure 3-1), to create 11,11,12,12-tetracyano-9,10-anthraquinodimethane (TCAQ) with the idea that this extension would create for more accepting electrochemical properties. However, cyclic voltammetry experiments on TCAQ showed that it has, in fact, a more negative reduction potential with one reversible peak at -0.24 V (vs SCE) involving to a two-electron process. Due to the steric repulsion of the dicyanomethylene groups with the hydrogen atoms on the aryl system, TCAQ has an unfavourable butterfly like geometry, as achieving planarity for the scaffold would require the

formation of an unstable diradical species.[3] By contrast, the central core aryl system is planar whereas the CN groups are out of plane in TCNQ. Although it is not as strong of an acceptor as TCNQ, TCAQ is nonetheless studied for its utility in materials applications such as organic battery materials, photoinduced electron-transfer, luminescent materials and catalysis.[2,3]

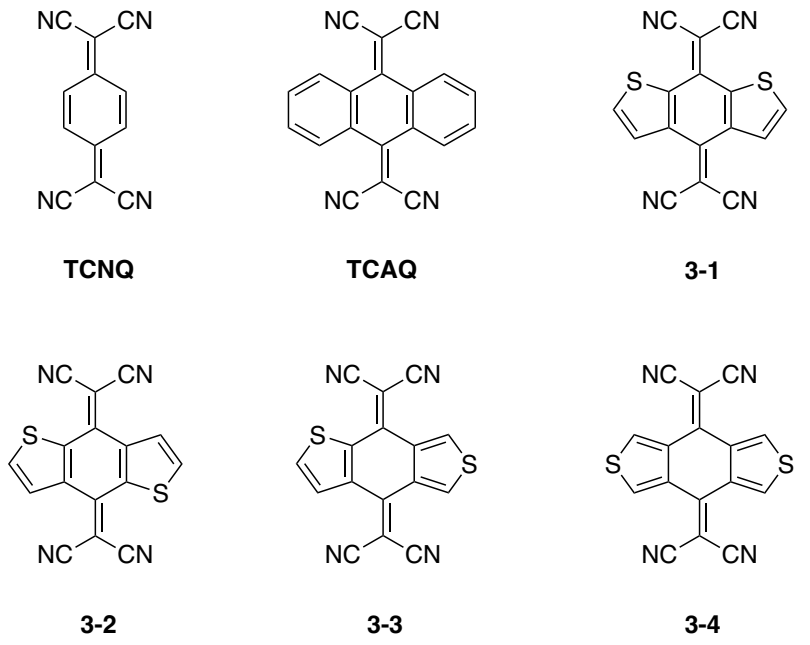

Figure 3-1. Select scaffolds based on 7,7,8,8-tetracyano-*p*-quinodimethane. Compounds **3-1** to **3-4** reported by Kobayashi et al.[4]

Aside from purely benzo-fused annulated TCNQ species, Kobayashi et al. reported a series of thiophene-fused TCNQ compounds in 1986,[4] wherein thiophenes are annulated in different positions to form compounds **3-1** to **3-4** (Figure 3-1) to investigate the impact of the different binding modes on the electrochemical properties. Compounds **3-1** and **3-2** exhibit two reversible one-electron reduction events and values similar to those of TCNQ, whereas the latter two are weak acceptors.[4] Interestingly incorporation of the thiophenes leads to more structural planarity when compared to the benzo-annulated system.[3] In addition to the extension of the π-system, other

intriguing TCNQ-inspired structures, reported in recent years, involve main-group-element incorporation. A prime example are the dicyanomethylene functionalized acridophosphines **1-37a,b,c** (Figure 3-2) by the Kivala group (*vide supra*), which have a similar butterfly-shaped structure to TCAQ but with a phosphorus centre in place of one of the dicyanomethylene groups. The compounds, as previously mentioned, have great electron-accepting properties with reduction potentials as low as -0.9 V (vs. Fc/Fc^+) for the P-methylated species.[5]

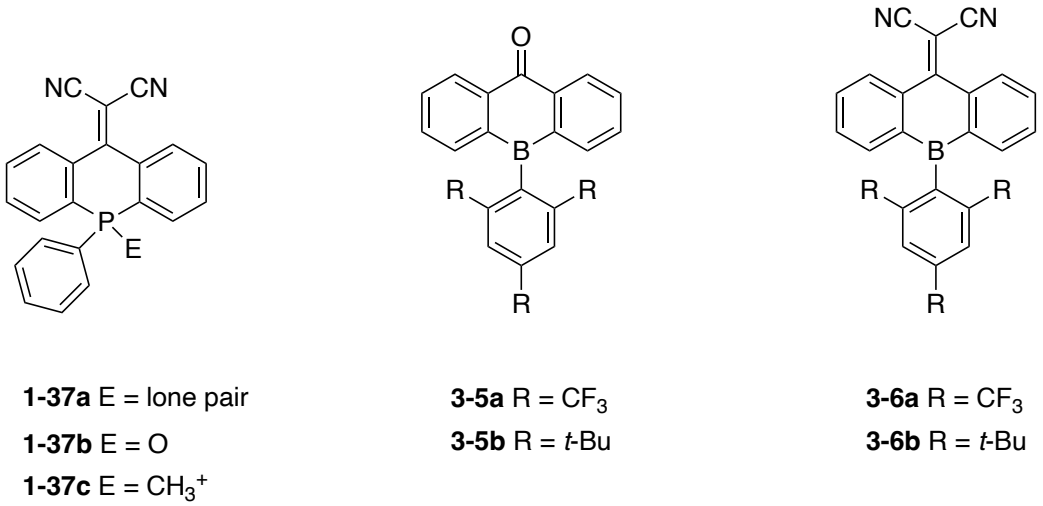

1-37a E = lone pair
1-37b E = O
1-37c E = CH_3^+

3-5a R = CF_3
3-5b R = *t*-Bu

3-6a R = CF_3
3-6b R = *t*-Bu

Figure 3-2. Dicyanomethylene functionalized acridophosphines (left)[5] and arylborane-based systems reported by Yin et al. (middle, right)[6].

Another example of a main-group-element based TCAQ-like structure was reported by Yin et al. for the synthesis of electron-accepting borinine systems **3-5** and **3-6** (Figure 3-2).[6] The intended purpose for these compounds was to merge the Lewis acidic properties of triarylboranes, useful in catalysis, anion sensing, and other organic materials applications, with the redox properties of TCAQ. The carbonyl-based compounds **3-5** were transformed via a Knovenagel reaction to afford the dicyanomethylene functionalized species **3-6** (Figure 3-2).[6] Compared to the carbonyl-functionalized species **3-5**, the air-stable dicyanomethylene derivatives **3-6** have a more red-shifted

absorption as well as the known butterfly shape. The redox properties of the compounds expectedly show that the dicyanomethylene species exhibits a lowered LUMO and corresponding reduction potentials (**3-5a**: -1.46 V, **3-5b**: -1.73 V; **3-6a**: -1.14 V, **3-6b**: -1.28 V; vs. Fc/Fc^{+}).[6] Due to the full electrochemical reversibility, the species were also subjected to chemical reduction by either $CoCp_2^*$ (Cp*=1,2,3,4,5-pentamethylcyclopentadienyl) or KC_8 to obtain planar mono- and di-reduced species that lose the butterfly shape of the neutral species.[6] Based on the intriguing results reported by the Kivala and Yin groups, we envisioned that the properties of the dithienoketo-phosphinine species could be similarly improved. To this end we targeted the synthesis of the thieno-fused species **3-7O**, **3-7**, and **3-7Me** as shown in Figure 3-3. The expectation for the properties of this series is that these modifications would create even stronger electron-accepting species with lower reduction potentials than that of the dithienoketophosphinine.

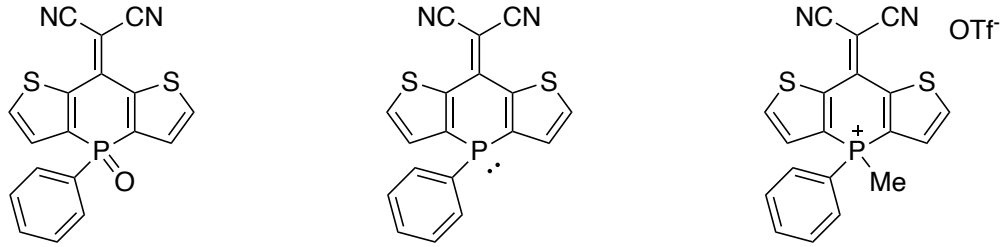

3-7O **3-7** **3-7Me**

Figure 3-3. Dicyanomethylene functionalized dithienophosphinines.

3.2 Results and Discussion

3.2.1 Synthesis

The first target species **3-7O** is accessible directly from the previously mentioned dithienoketophosphinine **2-3O** by Knoevenagel condensation with malononitrile, pyridine, and titanium tetrachloride in dry chlorobenzene (Scheme 3-1A).[7]

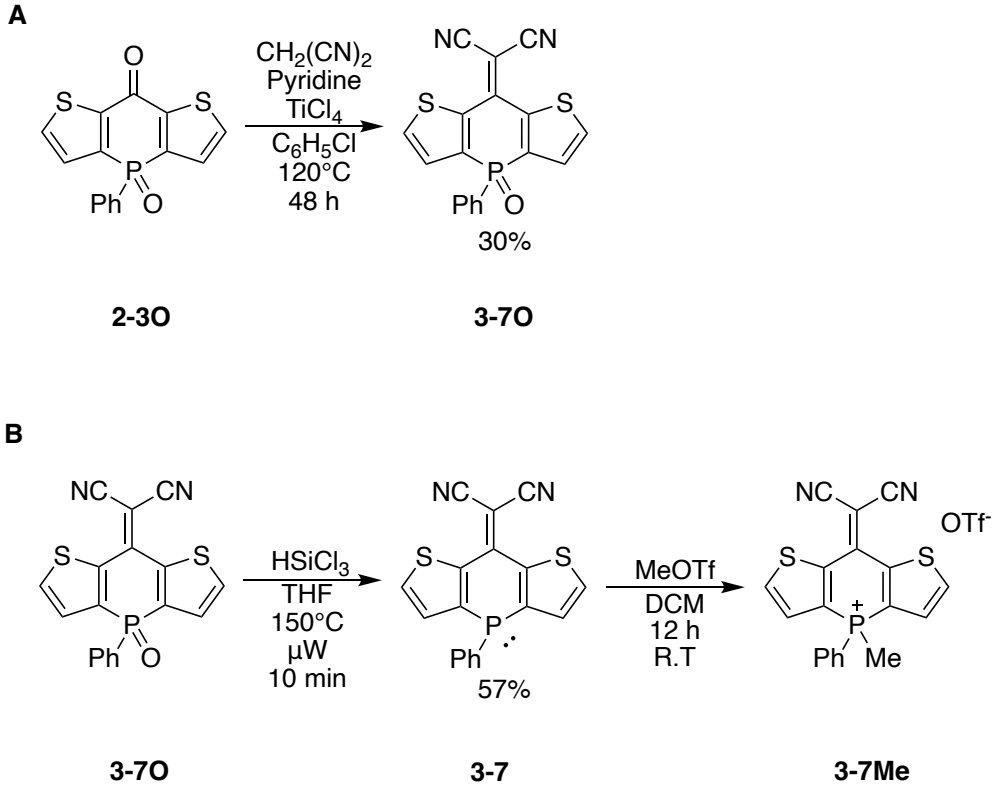

Scheme 3-1. (A) Synthesis of **3-7O** from dithienoketophosphinine precursor **2-3O** (B) reduction of **3-7O** to form **3-7** and methylation to form **3-7Me**.

The successful formation of **3-7O** was confirmed by a $^{31}P\{^{1}H\}$ NMR resonance at 0.1 ppm. To access the other two targets, the phosphorus centre in **3-7O** was reduced according to a literature procedure using $HSiCl_3$ under the microwave conditions (Scheme 3-1B)[8] providing the trivalent species **3-7** ($\delta^{31}P\{^{1}H\}$: -20 ppm). Lastly, the methylated compound **3-7Me** was isolated after

treatment of **3-7** with an excess of MeOTf ($\delta^{31}P\{^1H\}$: -5.5 ppm).[9] More detailed information on the purification can be found in the experimental section.

3.2.2 Solid-state structures

Suitable single crystals for x-ray diffraction were obtained via slow evaporation from acetonitrile for **3-7O** and from chloroform for **3-7Me**, respectively. Compared to the solid-state structures described by Kivala and coworkers, the new species exhibit a similar "butterfly-shape" that is, however, less pronounced than in the Kivala system due to the reduced steric repulsion between the cyano groups and the fused thieno units.[4,5] On the other hand, other pertinent structural parameters of the new species align well with those reported by Kivala et al.[5]

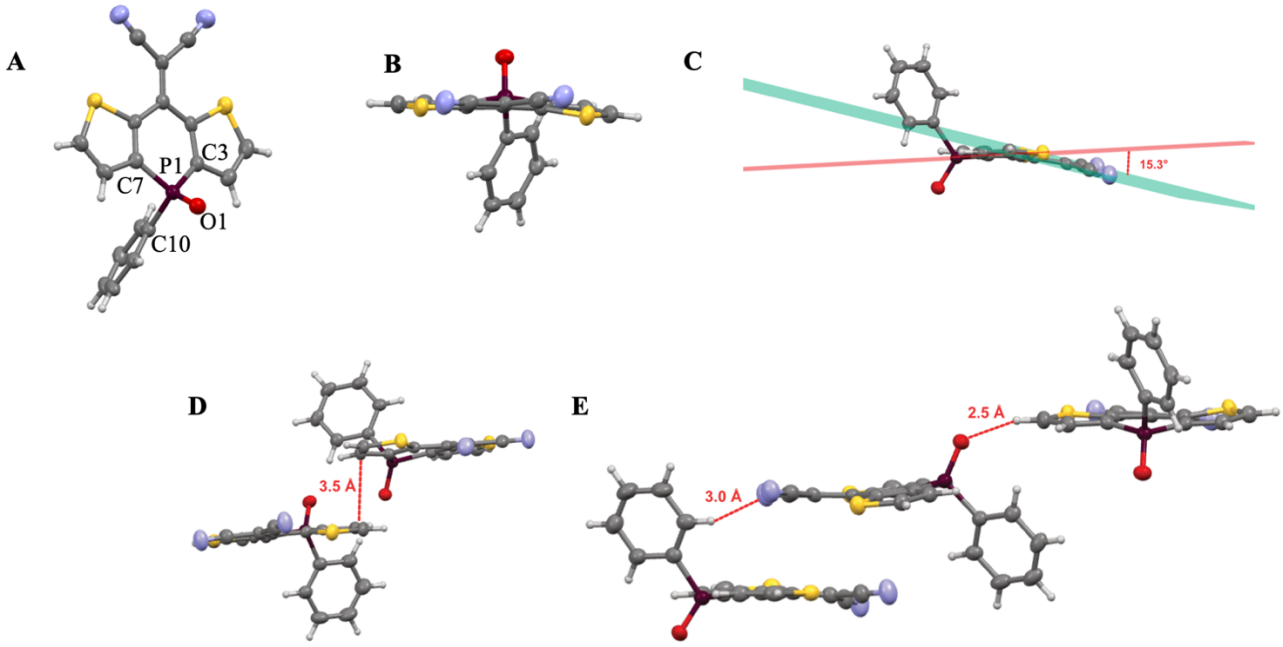

Figure 3-4. A) Solid-state structure of **3-7O** (thermal ellipsoids 50% probability); B) front-image depicting non-planarity of dicyanomethylene; C) dihedral angle; D) intermolecular π-stacking; E) O-H and N-H hydrogen-bonding interactions.

Moreover, the overall bond lengths and angles in **3-7O** (Figure 3-4A) are smaller than those of the keto-species **2-3O** described in the previous chapter. For **3-7O**, the endocyclic P-C bonds (P1-C3: 1.773(5) Å; P1-C7: 1.789(5) Å) are a bit shorter than those in **2-3O** (1.798(2) Å and 1.797(3) Å), indicative of a stronger electronic involvement of the phosphorus centre within the conjugated framework of the dicyanomethylene species (Figure 3-4A).[10] However, the exocyclic P-C bond length in **3-7O** is 1.798(5) Å, nearly identical to that in **2-3O** (1.797(2) Å). Lastly, the shorter P=O bond with a length of 1.481(3) Å (cf.: **2-3O** (1.485(2) Å), indicates stronger back donation from the oxygen in **3-7O**.[11] The internal C7-P1-C3 angle of **3-7O** is nearly identical to that of the keto species **2-3O** at 101.2(2)° and it also has a skewed tetrahedral geometry, with angles ranging from 114.4(2)° to 104.6(2)° and both smaller than those of the keto species **2-3O**.

Compared to the keto species **2-3O** with planar backbone, the main-backbone of **3-7O** is slightly curved and the dicyanomethylene group is out of plane (Figure 3-4B). Based on intersecting planes visualized in the solid-state structure (Figure 3-4C) the dihedral angle is approximately 15°. The compound also displays π-stacking between the carbon atoms on the thieno-backbone at 3.5 Å between adjacent molecules (Figure 3-4D). Finally, intermolecular hydrogen bonding interaction is also observed. The two sites are shown in Figure 3-4E, one involving N-H interaction between the CN group and an adjacent ortho-hydrogen on the exocyclic phenyl group, and the second an O-H interaction between the phosphine oxide and the α-hydrogen on a thieno ring.

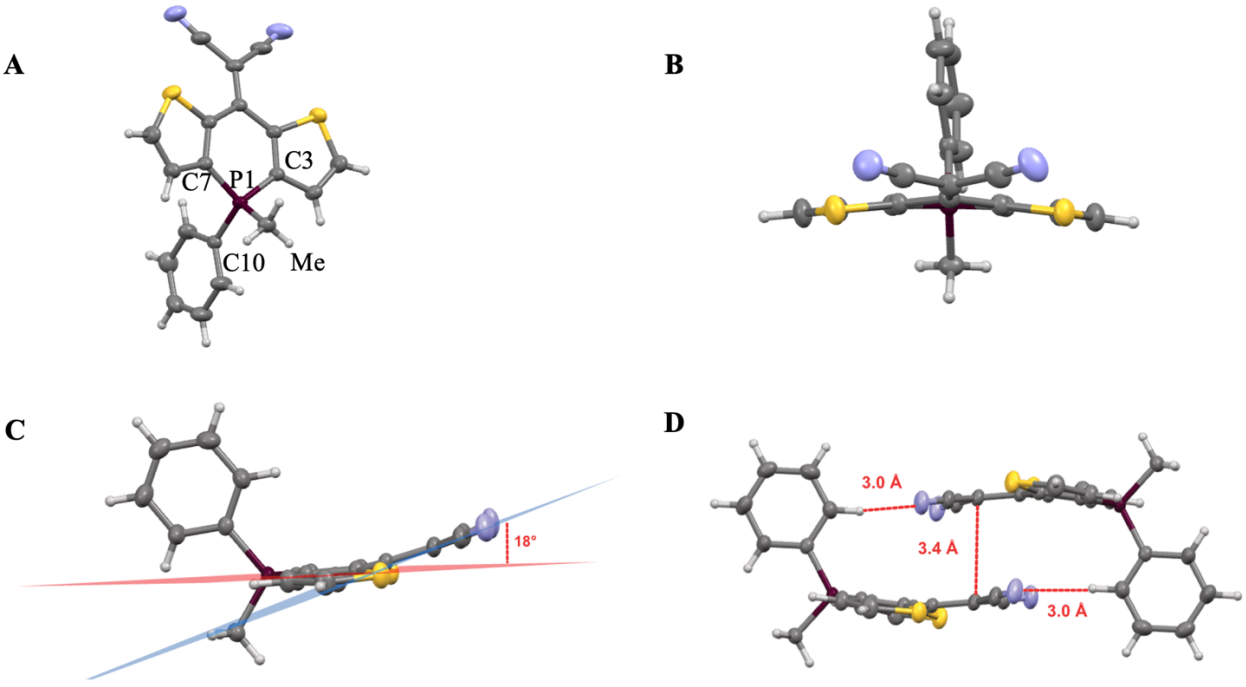

Figure 3-5. A) Solid-state structure of **3-7Me** (thermal ellipsoids 50% probability); B) image depicting non planarity of dicyanomethylene and dithieno-backbone; C) dihedral angle; D) intermolecular π-stacking and NH hydrogen-bonding interactions.

For the methylated species **3-7Me** (Figure 3-5A), there are only small variances for the endo- and exocyclic bonds compared to the keto-congener in the previous chapter. Compound **3-7Me** exhibits endocyclic bond lengths of 1.768(2) Å and 1.765(2) Å for P1-C3 and P1-C7 that are 1.766(2) Å and 1.779(2) Å for the keto species **2-3Me**. The exocyclic bonds for **3-7Me** of 1.784(2) Å and 1.790(2) Å for the P-methyl and P-C10 similar to the keto-species **2-3Me** mentioned in Chapter 2. Compound **3-7Me** has a more curved backbone compared to its keto-congener (Figure 3-5B). The dicyanomethylene group in **3-7Me** is also more significantly bent out of plane with respect to the conjugated framework (18°; Figure 3-5B,C). The supramolecular organization of this system has two notable features (Figure 3-5D): π-stacking at about 3.4 Å that involves part of the core and the CN groups on adjacent molecules and hydrogen bonding interactions between a

CN nitrogen atom and the *meta*-hydrogen atom on the exocyclic phenyl group on the phosphorus centre.

3.2.3 Optical Properties

Similar to the dithienoketophosphinine system reported in the previous chapter, the compounds in this series are also not emissive. However, all dicyanomethylene functionalized compounds display similar three-maxima absorption patterns (Figure 3-6).

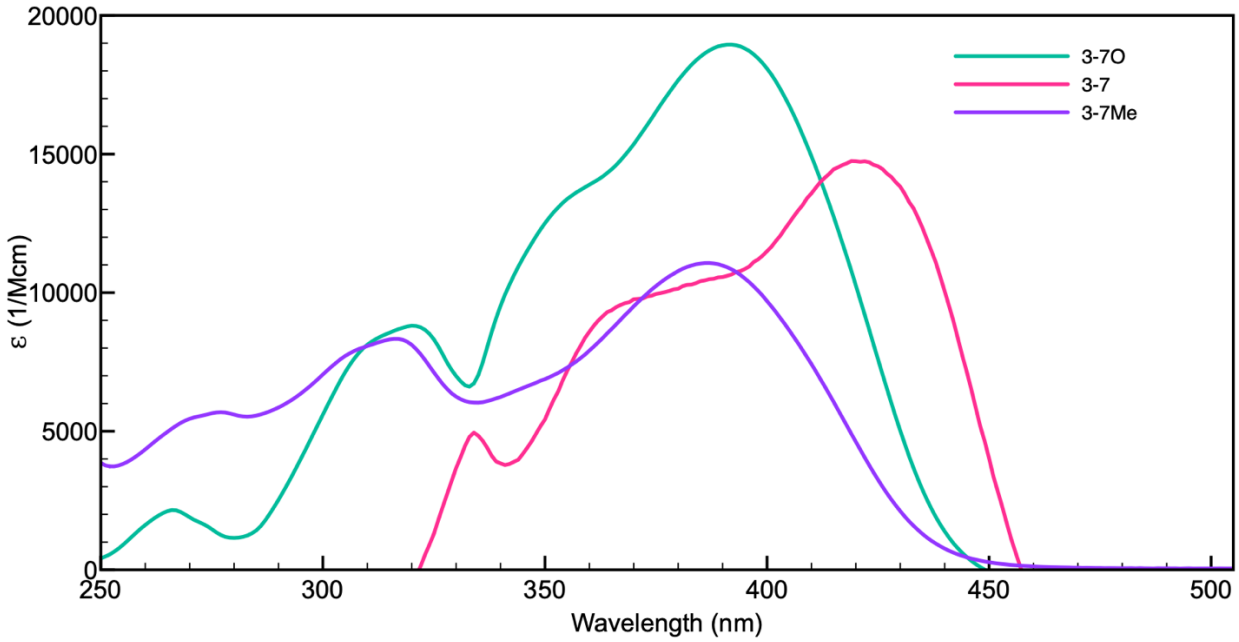

Figure 3-6. Absorption spectra of the dicyanomethylene species (CH_2Cl_2; c = $5x10^{-5}$ M)

The absorption maxima for the highest energy absorptions are between 266 nm to 334 nm for all three species and the low energy absorptions are from 387 nm to 419 nm. The most red-shifted

species is **3-7**, while **3-7Me** is the most blue-shifted in this series. The molar extinction coefficients also increase from the highest to lowest energy absorption and are summarized in Table 3-1.

Table 3-1. (a) Absorption wavelengths and (b) molar extinction coefficients of all species in CH_2Cl_2 at $5x10^{-5}$ M. (c) Reduction potentials obtained from cyclic voltammetry experiments (vs Fc/Fc^+) with NBu_4PF_6 as supporting electrolyte in CH_3CN. (d) Computational values of frontier molecular orbitals B3LYP/6-31G+(d) basis set using the PCM solvation model in CH_2Cl_2. (e) Optical bandgap (HOMO-LUMO).

Compound	**λ_{max} (nm)[a]**	**ε ($M^{-1}cm^{-1}$)[b]**	**E_{red} (V)[c]**	**HOMO (eV)[d]**	**LUMO (eV)[d]**	**$\Delta_{HOMO-LUMO}$ (eV)[e]**
3-7O	266 320 390	2200 8800 19,000	-0.87, -1.31	-7.04	-3.65	3.39
3-7	334 419	4900 14,700	-1.16, -1.79	-6.45	-3.20	3.25
3-7Me	277 316 387	5700 8300 11,100	-0.65, -1.0	-7.55	-4.21	3.34

3.2.4 Density Functional Theory Calculations

To understand the electronics of the system density functional theory calculations were performed for **3-7O**, **3-7Me** and **3-7** using the B3LYP 6-31G+(d) level of theory with PCM model for solvation in dichloromethane (Figure 3-7). The theoretical data support the experimentally determined photophysical properties. As shown in Table 3-1, **3-7** has a LUMO of -3.20 eV and a HOMO of -6.45 eV. Upon P-functionalization, the LUMO energy decreases to -3.65 eV in **3-7O**

and more substantially to -4.21 eV in **3-7Me**. In comparison to the keto species discussed in the previous chapter, the LUMO energies for all three dicyanomethylene species are lower, supporting their enhanced acceptor character. The HOMO in all species is delocalized over the entire π-system, including the core and the dicyanovinylene groups, however, without contribution from the phosphorus centre in **3-7O** and **3-7Me** and the LUMO for all species is represented by the π* system (Figure 3-7). All species also show σ*-π* interactions at the phosphorus centre in the LUMO. The HOMO-LUMO are reported in table 3-1 and the smallest gap is **3-7** which is corelated to it being the most red shifted, a similar report by Kivala et al.[5]

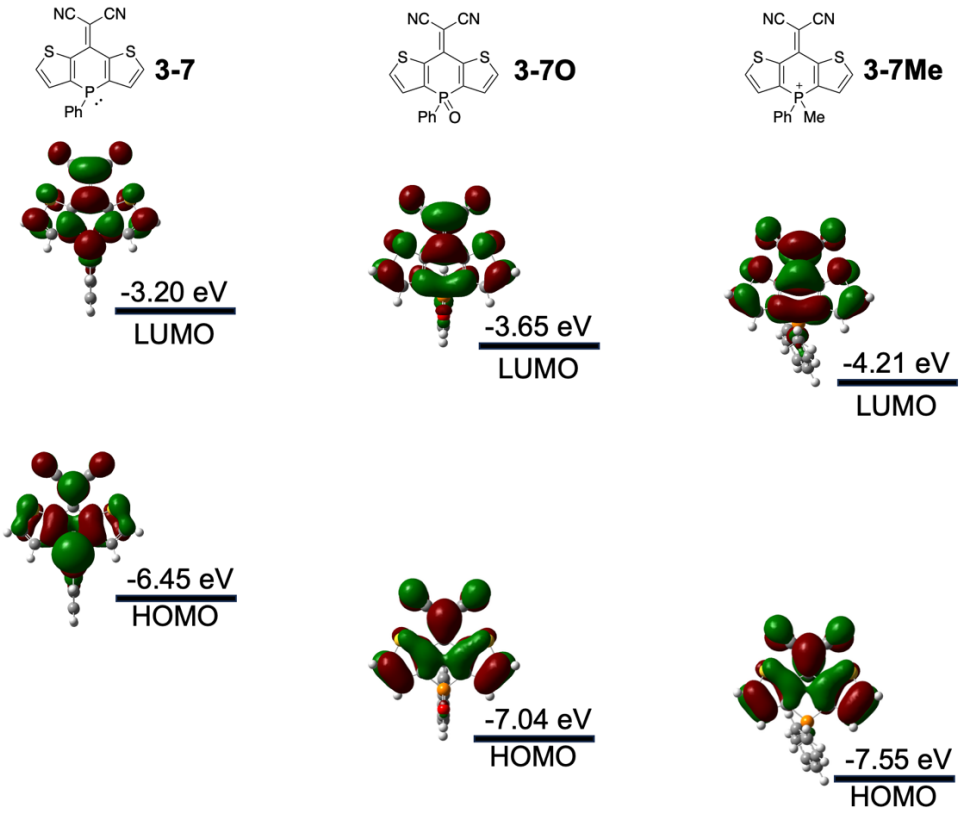

Figure 3-7. Frontier molecular orbitals of **3-7**, **3-7O** and **3-7Me** with respective HOMO and LUMO energies (eV). B3LYP 6-31G+(d) using a PCM solvation model in CH_2Cl_2.

3.2.5 Time-dependent Density Functional Theory (TDDFT) Calculations

Table 3-2. Time-dependent density functional theory calculation results for the dicyanomethylene-functionalized species using TD-SCF CAM-B3LYP 6-31G+(d) using PCM solvation model in CH_2Cl_2. (a) Oscillator strengths used to determine dominant transitions(b).

	3-7O	**3-7**	**3-7Me**
λ/nm (*f*)[a]	369 (0.18)	383 (0.70)	370 (0.43)
Transitions[b]	H-1 → L (89%) H-2 → L (5%)	H → L (98%)	H → L (95%)
λ/nm (*f*)[a]	316 (0.11)	344 (0.24)	306 (0.09)
Transitions[b]	H-2 → L (64%) H-5 → L (27%)	H-2 → L (96%)	H-3 → L (61%) H-5 → L (33%)
λ/nm (*f*)[a]	294 (0.23)		289 (0.26)
Transitions[b]	H-4 → L (96%)		H-4 → L (91%) H-2 → L (4%)

To gain a better understanding of the absorption data, time-dependent density functional theory calculations in dichloromethane were performed (Table 3-2 and Figure 3-8). Compounds **3-7** and **3-7Me** have the same dominant π–π* transition (HOMO to LUMO) similar to that of the dithienoketophosphinine mentioned in the previous chapter and similar to that of the compounds reported by the Kivala group.[5] The outlier is **3-7O** with a dominant contribution from the HOMO-1 to LUMO and a minor transition from HOMO-2 to LUMO that, however, also constitute a π- π*

transition (Figure 3-8) . The second absorption that is higher in energy is dominated by the same frontier molecular orbital transitions for **3-7O** and **3-7** which is a HOMO-2 to LUMO (π–π*) transition. For **3-7Me** this is dominated by a HOMO-3 to LUMO also π–π*. Lastly with respect to the lowest energy absorptions only applicable to **3-7O** and **3-7Me**, there is a large contribution from a n–π* transition (HOMO-4 to LUMO).

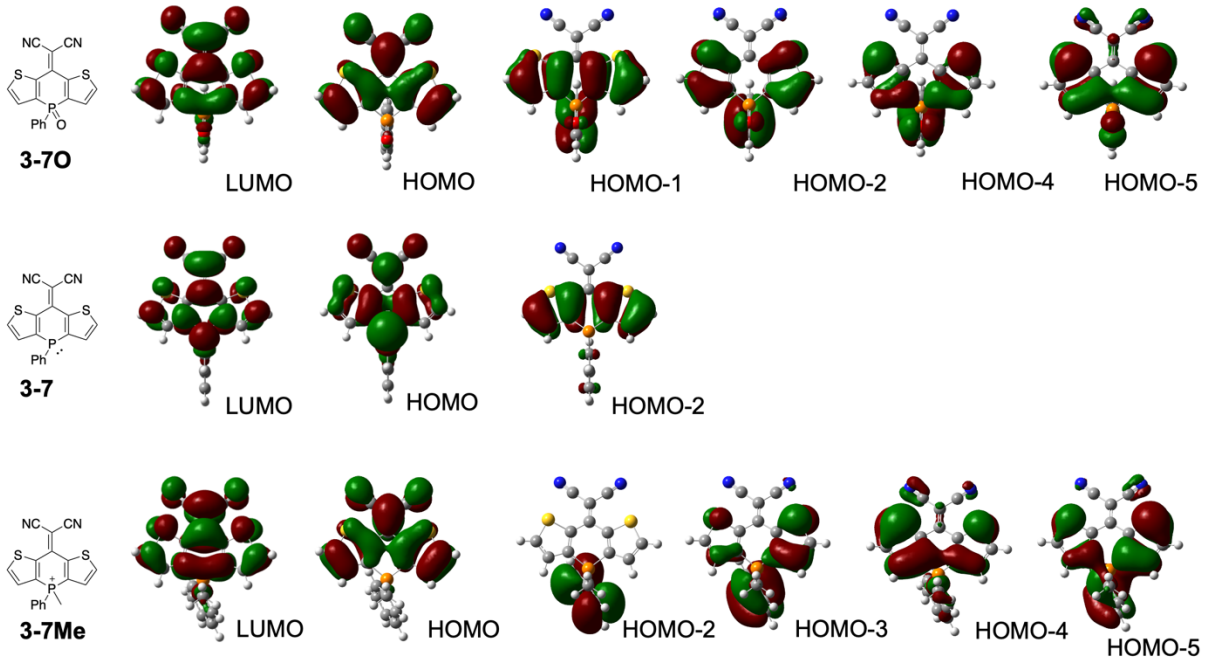

Figure 3-8. Select molecular orbitals for the dicyanomethylene functionalized species.

3.2.6 Cyclic Voltammetry

The electrochemical properties of the dicyanomethylene series were verified by cyclic voltammetry. As a reference point, these species are compared to the previously mentioned dithienoketophosphinines and those reported by the Kivala group.[5] The trivalent species **3-7** with the highest LUMO energy (*vide supra*), also exhibits the highest reduction potential in the series (Figure 3-9). Two reversible reduction events occur at -1.16 V and -1.79 (vs. Fc/Fc^+), respectively, confirming a higher reduction threshold than for **1-37a** at -1.14 V and -1.49 V (vs. Fc/Fc^+) reported by the Kivala group. However, compared to its trivalent dithienoketophosphinine congener **2-3**, that only has a single reduction event at -1.90 V (vs. Fc/Fc^+), both reductions have a lower reduction threshold.

It is important to note that the introduction of the dicyanomethylene unit introduces a second reduction event otherwise not seen in the trivalent dithienoketophosphinine. Upon oxidation the reduction potentials for species **3-7O** decrease to -0.87 V and -1.31 V (vs. Fc/Fc^+) that are also lower compared than those of **1-37b** (-1.26 V and -1.44 V).[5] Compared to the dithienoketo-phosphinine oxide **2-3O** with a reduction potential of -1.46 V, **3-7O** is clearly more electron-accepting. The methylated species **3-7Me** has the lowest LUMO and consequentially the lowest reduction potentials of all methylated species reported thus far.[5] The two reversible reductions events occur at -0.65 V and -1.0 V, respectively (c.f., **2-3Me:** -1.19 V and -1.84; **1-37c**: -1.14 V and -1.49 V; vs. Fc/Fc^+).[5] The oxidation CV spectra that are all irreversible, can be found in the supporting information (Figure S3-21).

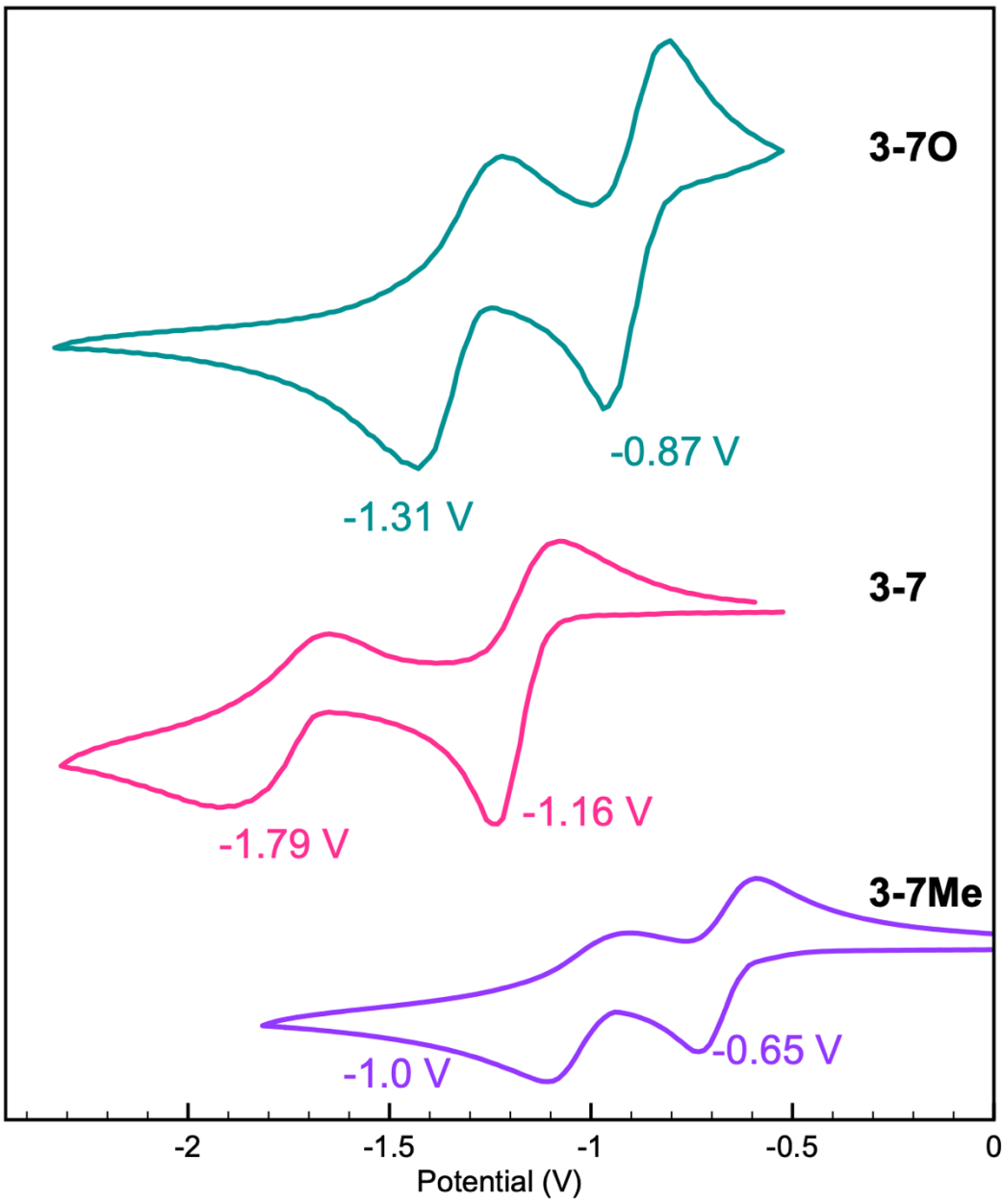

Figure 3-9. Cyclic voltammograms displaying the reduction regime for **3-7O**, **3-7**, and **3-7Me**. Potentials are references to Fc/Fc^{+}. Scan rate is 100 mV/s with NBu_4PF_6 as supporting electrolyte. All experiments performed in dry CH_3CN.

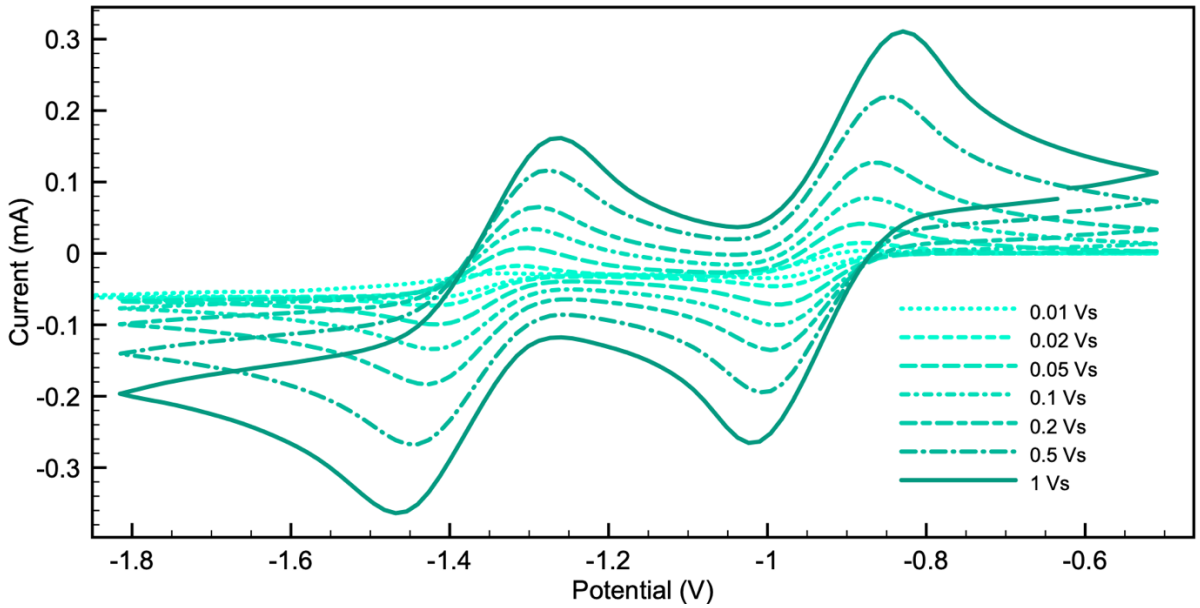

Figure 3-10. Cyclic voltammogram of **3-7O** with varying scan rates from 0.01 V/s to 1 V/s/ Potentials are references to Fc/Fc^{+} with NBu_4PF_6 as supporting electrolyte; all experiments performed in dry CH_3CN under argon.

To confirm the reversibility of the reduction events, **3-7O** was representatively exposed to various scan rates from 0.01 V/s to 1 V/s, similar to previous work on phosphaviologens (Figure 3-10).[12] To our satisfaction, reversibility is maintained as the scan rate increases there is an almost linear increase in the magnitude of the current generated, supporting the outstanding electron-acceptor features for this compound.

3.3 Conclusion and Future Outlook

Overall, we have reported the successful synthesis and characterization of a small series of dicyanomethylene functionalized dithienophosphinines. By implementing the knowledge gained from the previous chapter on phosphorus modifications, we were able to create a series that not only has improved acceptor qualities but is tunable by specific modifications at the phosphorus

centre. The highly desirable, improved qualities of our system, particularly compared to the dithienoketophosphinine and the dicyanomethylene functionalized acridophosphines, establishes this core as a promising building block for the development of next-generation electroactive conjugated materials.

3.4 Experimental Section

3.4.1 General Methods

Most reactions in this section were performed under an inert argon atmosphere using standard Schlenk techniques. Solvents were dried using an MBraun SPS solvent purification system. Chemical reagents were purchased from Sigma Aldrich, Fischer, or Oakwood Chemicals and used as received. The NMR data were obtained on a Bruker NEO 300, 400 or 600 MHz spectrometer. All microwave reactions were performed in an Anton Paar Monowave 2000. Single crystal X-ray crystallographic data were obtained on a Bruker D8 Quest Eco diffractometer. The optical studies were carried out with an Agilent Cary 5000 UV-vis spectrophotometer using standard quartz cuvettes. Cyclic voltammetry was performed using a Metrohm Autolab Potentiostat with NOVA software in dry acetonitrile or dichloromethane with tetrabutylammonium hexafluorophosphate as the electrolyte. Theoretical calculations were done using Gaussian on clusters provided by the Digital Research Alliance of Canada.

3.4.2 Synthetic procedures

Compound 3-7O

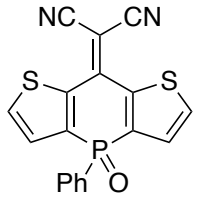

Compound **2-3O** (0.52 g, 1.6 mmol) and malononitrile (0.55 g, 8.3 mmol) were added to 120 mL dry chlorobenzene. Pyridine (1.64 g, 21 mmol) and $TiCl_4$ (2.83 g, 15 mmol) were added to this solution. The mixture was stirred at 120 °C for 48 hours. After cooling the solvent was removed in *vacuo*. Chloroform was added to the crude solids heated to reflux and then passed through a filter paper. The mixture was then extracted with water and ammonium chloride. After drying with magnesium sulfate and gravity filtering the solvent was removed. The product was purified by column chromatography (EtOAc:hexane 3:1) affording a yellow solid after evaporation of the solvent (Yield: 0.18 g, 30%). $^{31}P\{^1H\}$ NMR (162 MHz, $CDCl_3$) δ= 0.1 ppm. ^1H NMR (400 MHz, $CDCl_3$) δ = 7.84 (dd, *J* = 5.2, 2.1 Hz, 2H), 7.66 – 7.51 (m, 5H), 7.47 (td, *J* = 7.7, 4.3 Hz, 2H). ^{13}C NMR (100.6 MHz, $CDCl_3$): δ= 147.4 (d, J_{CP} = 6 Hz), 140.40 (d, J_{CP} = 101 Hz), 140.1 (d, J_{CP} = 8 Hz), 136.0 (d, J_{CP} = 17 Hz), 134.3 (d, J_{CP} = 16 Hz), 133.1 (d, J_{CP} = 3 Hz), 132.8 (d, J_{CP} = 2 Hz), 131.0 (d, J_{CP} = 7 Hz), 130.7 (d, J_{CP} = 11 Hz), 129.4 (d, J_{CP} = 14 Hz), 114.8 (s, CN). HRMS (ESI): m/z = 364.9970 $[M+H]^+$ (calcd. 364.9972).

Compound 3-7

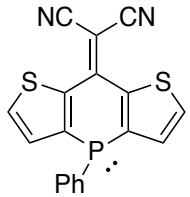

Compound **3-7O** (0.11 g, 0.3 mmol), trichlorosilane (2.1 g, 15 mmol) and dry tetrahydrofuran (15 mL) were combined in a microwave vial and microwaved for 10 minutes at 150 °C. The solvent was removed under *vacuo* to provide the product as yellow solid (Yield: 0.06 g, 58%). $^{31}P\{^1H\}$ NMR (162 MHz, $CDCl_3$) δ= -20.2. ^1H NMR (400 MHz, $CDCl_3$) δ = 7.73 (dd, J_{HH} = 5.2, J_{HP} = 2.3 Hz, 2H), 7.48 – 7.43 (m, 1H), 7.40 – 7.31 (m, 5H), 7.11 (dd, J_{HH} = 5.2, J_{HP} = 3.1 Hz, 2H). ^{13}C NMR (100.6 MHz, $CDCl_3$) δ = 149.4 (d, J_{CP} = 1

Hz), 147.5 (d, J_{CP} = 11.1 Hz), 134.8 (d, J_{CP} = 23.1 Hz), 133.8 (s), 133.3 (d, J_{CP} = 17.1 Hz), 132.6 (d, J_{CP} = 9.1 Hz), 131.2 (s), 130.6 (d, J_{CP} = 24.1 Hz), 129.5 (d, J_{CP} = 9.1 Hz), 116.55 (d, J_{CP} = 4.0 Hz). HRMS (ESI): m/z = 349.00263 $[M+H]^+$ (calcd. 349.0023).

Compound 3-7Me

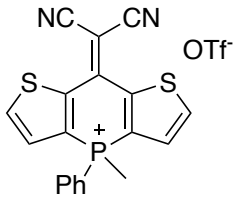

Compound **3-7** (0.1 g, 0.3 mmol) was dissolved in dry dichloromethane under argon. Methyl triflate (2.4 g, 14 mmol) was added to the solution at 0 °C and stirred for 5 minutes. Upon removing the cold bath, the mixture was allowed to stir at room temperature for 12 hours after which the solvent was removed in *vacuo*. The compound was reprecipitated from diethyl ether to afford the product as light green solid (yield: 0.03 g, 16%). $^{31}P\{^1H\}$ NMR (162 MHz, MeOD) δ = -5.3 ppm. ^1H NMR (400 MHz, MeOD) δ = 8.43 (dd, *J* = 5.3, 2.9 Hz, 2H), 7.94 – 7.82 (m, 5H), 7.77 – 7.70 (m, 2H), 3.02 (d, *J* = 15.2 Hz, 3H). ^{13}C NMR (100.6 MHz, MeOD) δ = 144.8 (d, J_{CP} = 8.0 Hz), 144.1 (d, J_{CP} = 8.0 Hz), 136.4 (d, J_{CP} = 18.1 Hz), 135.5 (d, J_{CP} = 3.0 Hz), 132.2 (d, J_{CP} = 12.1 Hz), 130.4 (d, J_{CP} = 8.0 Hz), 130.2 (d, J_{CP} = 15.1 Hz), 124.7 (s), 123.0 (d, J_{CP} = 91.5 Hz), 119.8 (d, J_{CP} = 91.5 Hz), 119.43 (s), 7.99 (d, J_{CP} = 56.3 Hz). HRMS (ESI): m/z = 363.0181 $[M]^+$ (calcd. 364.0252).

3.5 References

(1) Ortí, E.; Viruela, R.; Viruela, P. M. Influence of Benzoannulation on the Molecular and Electronic Structures of Tetracyanoquinodimethanes. *J. Phys. Chem.* **1996**, *100* (15), 6138–6146. https://doi.org/10.1021/jp952820h.

(2) Gómez, R.; Seoane, C.; Segura, J. L. The First Two Decades of a Versatile Electron Acceptor Building Block: 11,11,12,12-Tetracyano-9,10-Anthraquinodimethane (TCAQ). *Chem. Soc. Rev.* **2007**, *36* (8), 1305. https://doi.org/10.1039/b605735g.

(3) Warrington, S.; Montanaro, S.; Elsegood, M. R. J.; Nichol, G. S.; Wright, I. A. Structure-Property Relationships for Potential Inversion From Electron Acceptors Based on Thiophene-Fused Triptycene Quinones, 1,4-Diketones and Their Malononitrile Adducts. *Chem. Eur. J.* **2024**, *30* (30), e202400782. https://doi.org/10.1002/chem.202400782.

(4) Kobayashi, K.; Gajurel, C. L. Thiophene-Fused Tetracyanoquinodimethanes as Electron Acceptors for Conducting Charge-Transfer Salts. *J. Chem. Soc. Chem. Commun.* **1986**, No. 24, 1779. https://doi.org/10.1039/c39860001779.

(5) Schaub, T. A.; Brülls, S. M.; Dral, P. O.; Hampel, F.; Maid, H.; Kivala, M. Organic Electron Acceptors Comprising a Dicyanomethylene-Bridged Acridophosphine Scaffold: The Impact of the Heteroatom. *Chem. Eur. J.* **2017**, *23* (29), 6988–6992. https://doi.org/10.1002/chem.201701412.

(6) Liao, G.; Chen, X.; Qiao, Y.; Liu, K.; Wang, N.; Chen, P.; Yin, X. Highly Electron-Deficient Dicyanomethylene-Functionalized Triarylboranes with Low-Lying LUMO and Strong Lewis Acidity. *Org. Lett.* **2021**, *23* (15), 5836–5841. https://doi.org/10.1021/acs.orglett.1c01983.

(7) Ye, Q.; Chang, J.; Huang, K.-W.; Dai, G.; Zhang, J.; Chen, Z.-K.; Wu, J.; Chi, C. Incorporating TCNQ into Thiophene-Fused Heptacene for n-Channel Field Effect Transistor. *Org. Lett.* **2012**, *14* (11), 2786–2789. https://doi.org/10.1021/ol301014d.

(8) Hindenberg, P.; Rominger, F.; Romero-Nieto, C. Phosphorus Post-Functionalization of Diphosphahexaarenes. *Chem. Eur. J.* **2019**, *25* (57), 13146–13151. https://doi.org/10.1002/chem.201901837.

(9) Durben, S.; Dienes, Y.; Baumgartner, T. Cationic Dithieno[3,2-*b*:2′,3′-*d*]phospholes: A New Building Block for Luminescent, Conjugated Polyelectrolytes. *Org. Lett.* **2006**, *8* (25), 5893–5896. https://doi.org/10.1021/ol062580w.

(10) Baumgartner, T.; Neumann, T.; Wirges, B. The Dithieno[3,2-*b*:2′,3′-*d*]phosphole System: A Novel Building Block for Highly Luminescent π-Conjugated Materials. *Angew. Chem. Int. Ed.* **2004**, *43* (45), 6197–6201. https://doi.org/10.1002/anie.200461301.

(11) Baumgartner, T. Insights on the Design and Electron-Acceptor Properties of Conjugated Organophosphorus Materials. *Acc. Chem. Res.* **2014**, *47* (5), 1613–1622. https://doi.org/10.1021/ar500084b.

(12) Durben, S.; Baumgartner, T. 3,7-Diazadibenzophosphole Oxide: A Phosphorus-Bridged Viologen Analogue with Significantly Lowered Reduction Threshold. *Angew. Chem. Int. Ed.* **2011**, *50* (34), 7948–7952. https://doi.org/10.1002/anie.201102453.

Chapter Four: Extending the Conjugation of the Dithieno[2,3-b;3',2'-e]-4-keto-1,4-dihydrophosphinine Core

Acknowledgements

I would like to thank Cheryl Cai Hui Tan, a visiting undergraduate student from Nanyang technical university, Singapore, for assistance with some of the experiments in this chapter. I would also like to thank Dr. Howard Hunter from York University for his contributions to the NMR elucidation of these systems, as well as Jesse Leblanc from the Le group at York University for the XRD analysis.

4.1 Introduction

The development of π-conjugated systems in the past few decades has been greatly driven by their usefulness in many materials applications such as organic optoelectronic devices, catalysis, and bioimaging.[1] Tailoring the properties by modulating the π-system is of great importance for specific applications.[2] In the previous chapters it was shown that the optical, electrochemical, and solid-state properties of such systems are controlled by chemical structure and conjugation.[3] Up until now, our group and others have shown that incorporation of main group elements (B, Si, P, N etc.) provides an additional way to modulate the properties, however, in the case of phosphorus chemistry, the scope of phosphorus modifications has a natural limit.[1] For this reason, a well-studied method to further enhancing the properties of phosphorus-containing species is extending the π-conjugation of the systems.[2] This method has been employed by our group on several families revolving around the dithieno[3,2-*b*:2′,3′-*d*]phosphole system, as highlighted in Chapter 1 of this thesis. As a result of the convenient α-halogenation of the dithienophosphole **4-1** to form

4-2 (Figure 4-1A), various cross-coupling reactions (Suzuki, Stille, and Sonogashira) to form various π-extended systems have been accomplished throughout the years.[2,4] The extension of the π system allows for further decreasing the HOMO-LUMO gap and obtaining emissions from blue all the way to the red region of the visible light spectrum, as a function of the groups attached to the dithienophosphole core.[2,4] A few notable examples are species with pyridyl **1-14**, phenyl **1-10**, and dimethylamino phenyl **4-3** termini (Figure 4-1B), as they are representatives for acceptor-, neutral-, and donor-terminated extended species, respectively.[2,4,5]

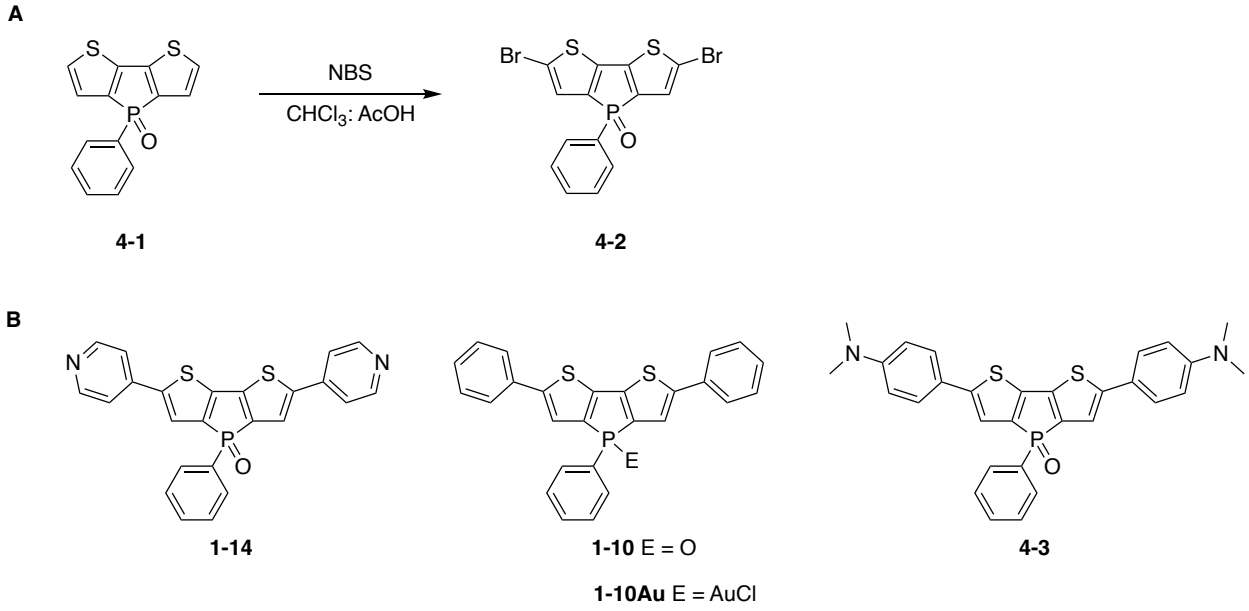

Figure 4-1. A) α-Bromination of the dithieno[3,2-*b*:2,3′-*d*]phosphole;[2] (B) various cross-coupled dithieno[3,2-*b*:2′,3′-*d*]phospholes.[2,4,5]

The resulting acceptor-acceptor (A-A-A) or donor-acceptor (D-A-D) type infrastructure in these species allows for fine tuning of the frontier orbital energies, i.e., the absorption/emission features, but also intramolecular charge-transfer features of the system.[6] For the dithienophosphole system, the emissions vary across the series, with compound **1-14** emitting at 507 nm, **1-10** at 520 nm, and

4-3 at 602 nm.[2,4,5] Other features, such as **1-14** having redox properties not seen in the parent system **4-1**, compound **1-10** being ambipolar and **4-3** being acid-sensitive with its emission changing from orange to green upon protonation of the nitrogen centres, are evident (see Chapter 1 for more information).

By contrast, not many examples exist for six-membered systems where the π system is extended in this manner. Although the Romero-Nieto group has reported many ring-fused systems,[7,8] the only example of extending the π system of the dithienoketophosphinine core was recently reported by Xiao et al. (Figure 4-2).[9] As a result of the charge-transfer character in these species, **1-29** and **1-30** display a range of emission wavelengths from 453 nm to 503 nm in various solvents. The systems were primarily used as fluorescent labels to monitor ferroptosis using fluorescence lifetime imaging.[9]

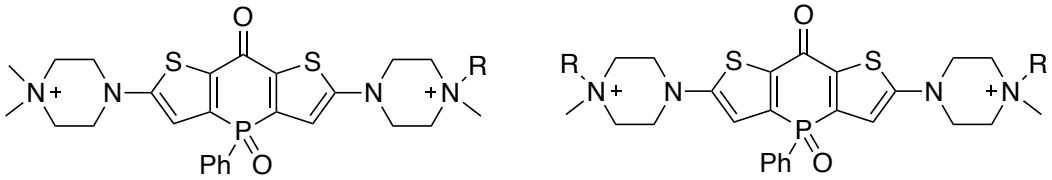

1-29 **1-30**

Figure 4-2. Fluorescent probes based on the dithienoketophosphinine reported by Xiao et al.[9]

Along similar lines, Dr. Xiaoming He, a postdoctoral researcher in our group, attempted the bromination of the dithienoketophosphinine already in 2013, in order to replicate that which has been done on the dithienophospholes. His initial, and most intuitive approach to brominating the dithienoketophosphinine **2-3O,** was to replicate the conditions of the dithienophosphole using *N*-bromosuccinimide (NBS) in chloroform and acetic acid to obtain compound **4-4** (Scheme 4-1A).[210] However, these conditions were not successful. Dr. He reported conditions using NBS with a

mixture of trifluoroacetic acid and sulfuric acid as the solvent system, a method commonly employed in halogenation type reactions for electron-poor systems (Scheme 4-1B).[10] With the new conditions employed, a new species with a ^{31}P NMR resonance at -1.6 ppm was formed. However, X-ray crystallography revealed that the new species was in fact not the dibrominated species **4-4**, but the tetrabrominated compound **4-5** (see Scheme 4-1C) that has lain dormant since.

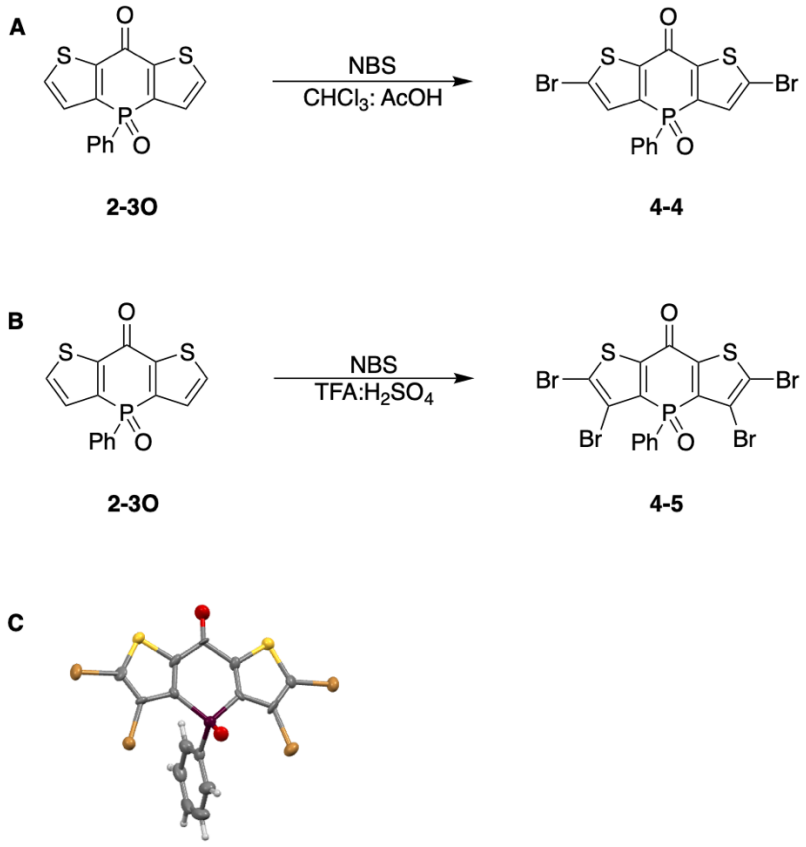

Scheme 4-1. (A) Attempted bromination of the dithienoketophosphinine using conditions previously employed on the dithienophosphole; (B) New conditions for the bromination of the dithienoketophosphinine; (C) Molecular structure of **4-5** in the solid state, thermal ellipsoids at 50% probability.

The previous two chapters highlighted the profound impact of phosphorus and keto modification on the dithienoketophosphinine scaffold. While not originally targeted, the successful

tetrabromination of the dithienoketophosphinine opens an intriguing third site for modification on the dithienoketophosphinine scaffold, with even greater potential for diversification by extending the π-conjugation of the system in potentially cross-conjugated fashion. Drawing inspiration from our previous research on the conjugated dithienophosphole systems, the synthesis and properties of a small family of cross-coupled species (**4-6** to **4-9**), with four aryl termini differing in their electron accepting/donating character, were investigated in the context of this thesis (Figure 4-3).

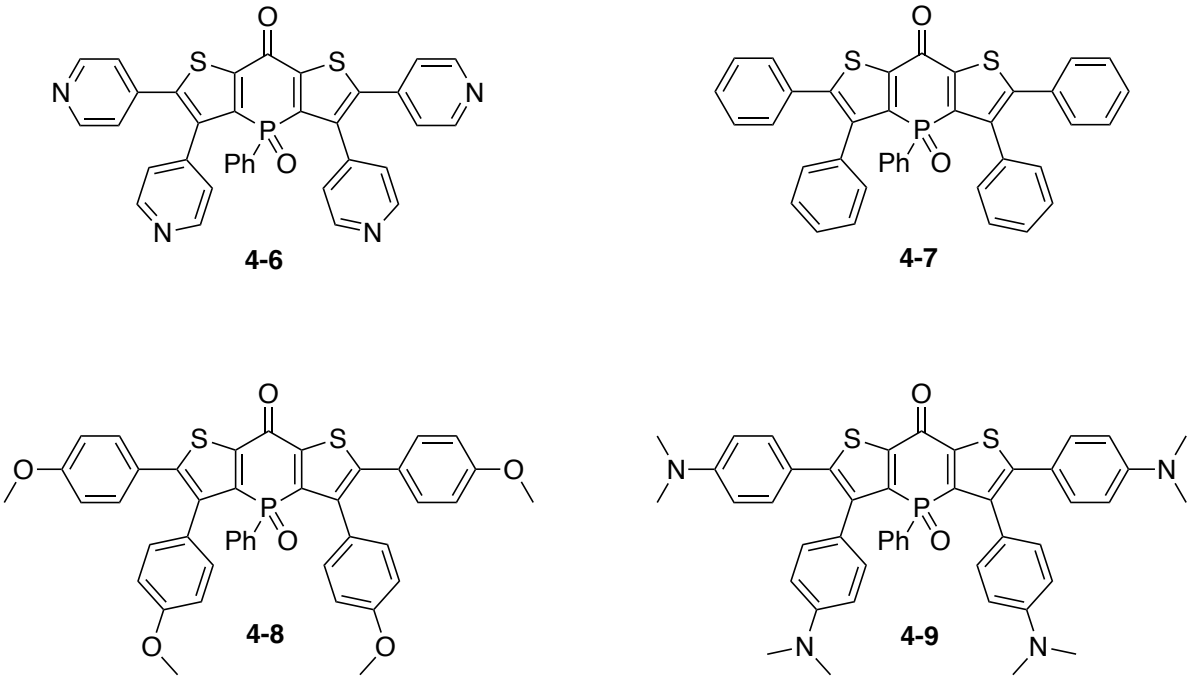

Figure 4-3. Targeted tetra-substituted dithienoketophosphinines with various donor/acceptor termini.

4.2 Results and Discussion

4.2.1 Synthesis

Although the initial tetrabromination of the core by Dr. He established a general methodology to synthesize compound **4-5**, further optimization was deemed necessary to increase the yield as using the conditions employed by Dr. He generally results in multiple phosphorus species as confirmed by $^{31}P\{^{1}H\}$ NMR of the crude mixture. For this reason, variables such as time, temperature, acid, and brominating reagent were studied by Cheryl Cai Hui Tan and reported in her undergraduate thesis.[11] For this MSc thesis, a few different approaches to increase yield and potentially obtain a better conversion rates are highlighted (Scheme 4-2).

Various attempts to tetrabrominated the dithienoketophosphinine were made (Scheme 4-2), including conditions reported for deactivated aromatic species (Scheme 4-2A) and dithienopyrazine systems (Scheme 4-2B), however, none were successful as confirmed by $^{31}P\{^{1}H\}$ NMR spectroscopy (see Figures S4-1 and S4-2).[11,12]

In the end, the conditions that were the most reproducible were those originally employed by Dr. He, involving four equivalents of NBS with a 1:3 ratio of sulfuric acid to trifluoroacetic acid (Scheme 4-2C). It is important to note that **4-5** can only be isolated in 85% purity at a low yield of 7% and the next steps are carried out with this level of purity.

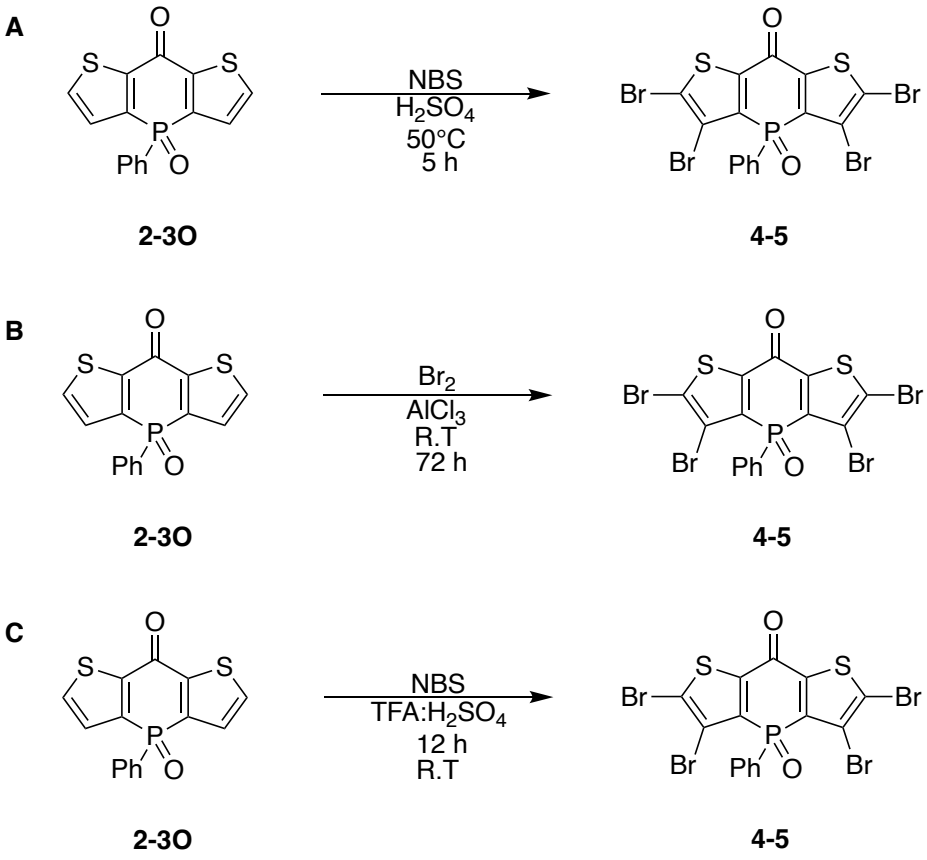

Scheme 4-2. Attempted tetra-bromination using various literature methods.

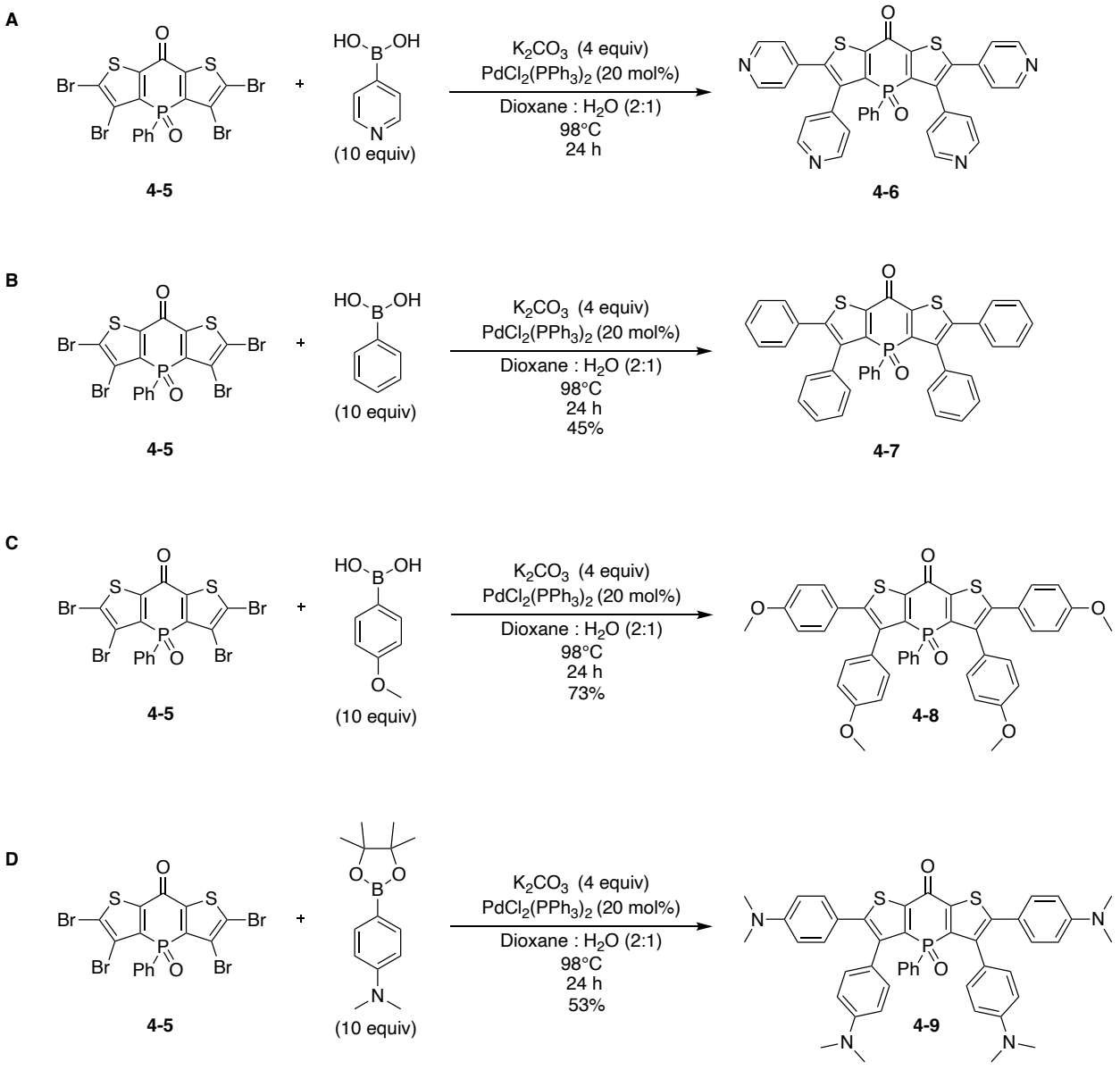

Scheme 4-3. Synthesis and reaction conditions toward cross-coupled species **4-6** – **4-9**.

The cross-coupling reactions to form the tetra-arylated compounds **4-6**, **4-7**, **4-8**, **4-9** (Scheme 4-3A-D) employed conditions reported by Le et al.,[13] using 10 equivalents of the respective boronic acid/ester, four equivalents of potassium carbonate, and bis(triphenylphosphine)-palladium(II) dichloride (20% loading) in dioxane/water (2:1). Each reaction was heated at 98 °C for 24 hours

in air (for more details, see the experimental section). Compounds **4-7**, **4-8** and **4-9** were confirmed by $^{31}P\{^{1}H\}$ NMR resonances at 0.3 ppm, 0.0 ppm and 0.2 ppm with isolated yields of 45%, 73%, and 53%, respectively. For the pyridyl species **4-6** complete purification has not been done as of yet; thus, it is not reported in-depth in this thesis.

4.2.2 Solid State Structures

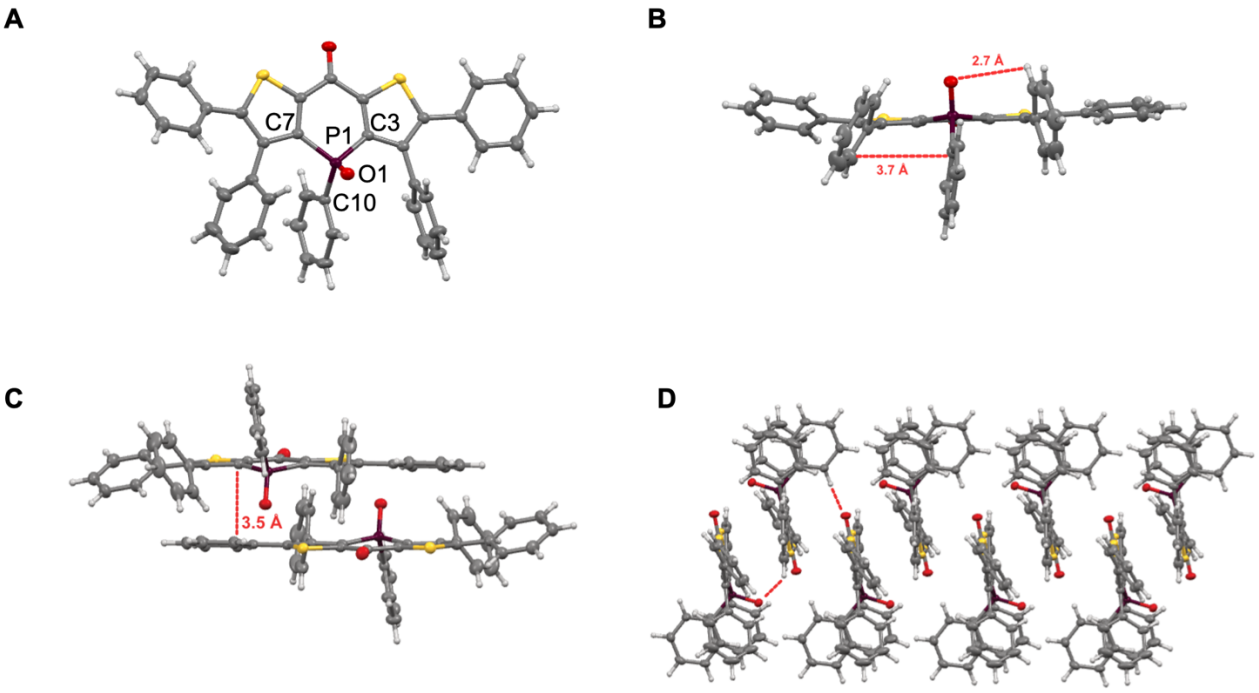

Figure 4-4. (A) Structure of **4-7** in the solid state, thermal ellipsoids at 50% probability; (B) intramolecular π-stacking and hydrogen bonding interactions; (C) intermolecular π-stacking; (D) bulk packing with some intermolecular hydrogen-bonding interactions shown as red dashes.

Single crystals suitable for the characterization of the molecular structures of all four species in the solid state by XRD were obtained from different conditions, as described in the experimental section. Compound **4-7**, obtained through slow evaporation in acetone, is representatively discussed here. The simple terminal phenyl groups make it more comparable to the parent keto-

system **2-3O** (presented in Chapter 2) as well as the previously synthesized phenyl-extended dithienophosphole **1-10Au** with a gold chloride at the phosphorus centre; the structure of the oxide **1-10** has not been reported to date.[2] The X-ray crystallographic data and molecular structures of all other tetra-cross coupled species can be found in the Supporting Information (Figure S4-32/33). The overall bond lengths and angles in **4-7** are quite similar to those of compound **2-3O**, which was introduced in Chapter 2 (Figure 4-4A). The exocyclic phosphorus bond lengths for both systems (**4-7** vs. **2-3O**) are similar with P-O bond lengths of 1.49 Å and P-C bond lengths of 1.80 Å in each of the species. A bigger difference is seen in the endocyclic bond lengths with **4-7** having internal P1-C3 and P1-C7 bond lengths of 1.808(2) Å and 1.807(1) Å, slightly longer than those of **2-3O** (1.798(2) Å and 1.797(3) Å). The internal C3-P1-C7 angles observed in both **2-3O** and **4-7** are nearly identical at 101.68(7)° and 101.8(1)°. The phosphorus centre in **4-7** is nearly tetrahedral with the smallest angle around it being 107.45(7)° and the largest 112.64(7)°, whereas **2-3O** is more skewed toward a larger range of 106.6(1)° and 115.8(1)°. Another feature consistent for all derivatives is the phosphorus centre being notably out of plane, unlike in **2-3O**, the dithienoketophosphinine scaffold displays a slight curvature near the phosphorus centre, indicative of geometric strain (Figure 4-4B).[14]

In comparison to the dithienophosphole relative **1-10Au**,[2] a few similarities are evident. As a result of steric strain imposed by four phenyl groups on the backbone of **4-7**, the substituents twist out of the plane from the dithienoketophosphinine core (Figure 4-4A), and more so for the β-positions as a result of the additional steric issues arising from the exocyclic phenyl on the phosphorus centre. The torsion angles between the dithienophosphole core and the phenyl groups are 31.5° and 14.4° in **1-10Au** whereas the corresponding torsion angles are 7.2(2)° and 28.1(2)° in **4-7**. The torsion angles are expectedly more pronounced in the β-position for **4-7** at 63.7(2)° and 82.7(2)°

(Figure 4-4A).[2] Additionally, there are both intra- and intermolecular π-stacking interactions. The intramolecular π-stacking occurs between the exocyclic phenyl group at the phosphorus centre and the β-phenyl substituents at a distance of 3.8 Å (Figure 4-4B), whereas the intermolecular interactions are present at a few different points between neighbouring molecules with an average π-stacking distance of 3.5 Å (Figure 4-4C). The packing of the neighboring molecules is also stabilized by hydrogen bonding interactions that are also seen in the packing of **2-3O**. The molecules stack in a staggered conformation with neighbouring molecules in 'anti' configuration due to the core's dipole moment (consistent for all derivatives presented in this chapter; Figure 4-4D).

4.2.3 Optical properties

Table 4-1. (a) Absorption and emission maxima c = $5x10^{-6}$ M in CH_2Cl_2. (b) Molar extinction coefficient. (c) Stokes shift in wavenumbers. (d) Quantum yield in CH_2Cl_2 (e) cyclic voltammetry in CH_3CN, vs. Fc/Fc^+, NBu_4PF_6 as supporting electrolyte. (f) B3LYP/6-31G+(d) level of theory using the PCM solvation model in CH_2Cl_2. (g) optical gap HOMO-LUMO.

Compound	λ_{Abs}[a] nm	ε[b] [$M^{-1}cm^{-1}$]	λ_{Em}[a] [nm]	Stokes Shift[c] [cm^{-1}]	QY[d] [%]	E_{Red}[e] [V]	HOMO[f] [eV]	LUMO[f] [eV]	Δ_{H-L}[g] [eV]
4-7	235 414	31,100 16,700	491	3788	10	-1.43 -2.09	-6.40	-3.06	3.34
4-8	254 443	36,100 21,200	564	4843	23	-1.46 -2.11	-5.96	-2.97	2.99
4-9	277 523	40,900 24,100	726	5346	11	-1.54	-5.20	-2.80	2.40

All compounds reported in this series are emissive unlike the compounds reported in the previous two chapters. The absorption and emission values along with the quantum yield are reported in Table 4-1 and the corresponding absorption and emission spectra are shown in Figures 4-5 and 4-6.

Compounds **4-7**, **4-8** and **4-9** have two absorption maxima in dichloromethane, with an evident bathochromic shift when increasing the donor strength of the cross-coupled termini (Figure 4-5). The high-energy peak for **4-7** is at 235 nm, for **4-8** at 254 nm, and for **4-9** at 277 nm. The low-energy absorptions also red-shift from 414 nm to 523 nm for **4-7** to **4-9**. The molar extinction coefficients for all species are in the range of 31,000 $M^{-1}cm^{-1}$ to 41,000 $M^{-1}cm^{-1}$ for the high-energy absorption and 17,000 $M^{-1}cm^{-1}$ to 24,000 $M^{-1}cm^{-1}$ for the low-energy absorptions. In comparison to the dithienoketophosphinines from Chapter 2, with molar extinction coefficients from 10,500 $M^{-1}cm^{-1}$ to 18,500 $M^{-1}cm^{-1}$, the compounds in this series are clearly stronger absorbers, as extended from their extended π systems. The emission spectra are also reflective of the donor strength of the terminal groups with a red shift from 491 nm (**4-7**) to 726 nm (**4-9**) (Figure 4-6). Compared to the corresponding dithienophospholes **1-10** and **4-3** with emissions of 520 nm and 601 nm, the tetra-substituted species are more red-shifted in line with the strong acceptor character of the core. The Stokes shifts in the dithienophosphole and the dithieno-ketophosphinine systems have similar trends wherein **1-10** and **4-7** have Stokes shifts of 60 nm (2508 cm^{-1}) and 77 nm (3788 cm^{-1}). The more electron-donating dimethylaminophenyl-substituted species **4-3** and **4-9** have larger Stokes shifts of 128 nm (4,503 cm^{-1}) and 203 nm (5,346 cm^{-1}) reflective of their underlying inherent charge-transfer nature. The quantum yields for **4-7**, **4-8**, **4-9** ranging from 10-23% are inherently lower than those of the dithienophosphole relatives >50%,

which may be attributed to the quenching nature of the keto group at the core and additional rotational freedom for the β-aryl groups, promoting non-radiative relaxation processes.[12]

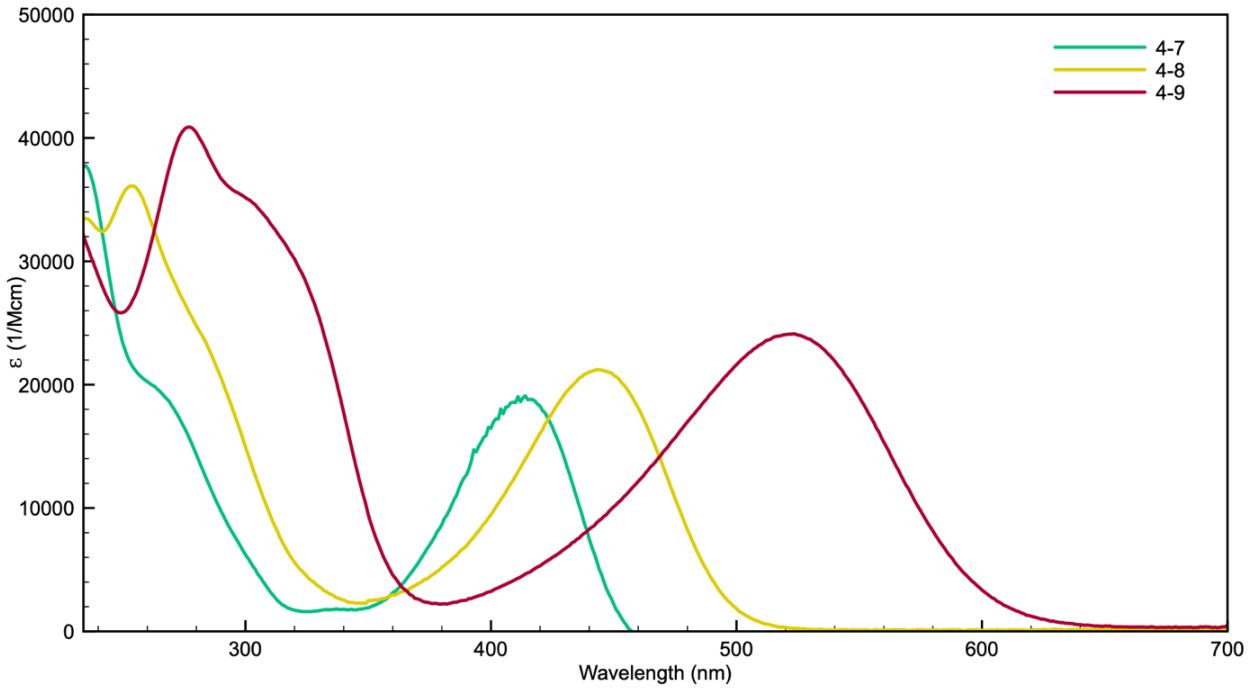

Figure 4-5. Absorption spectra of the tetra cross-coupled derivatives (CH_2Cl_2; $5x10^{-6}$ M)

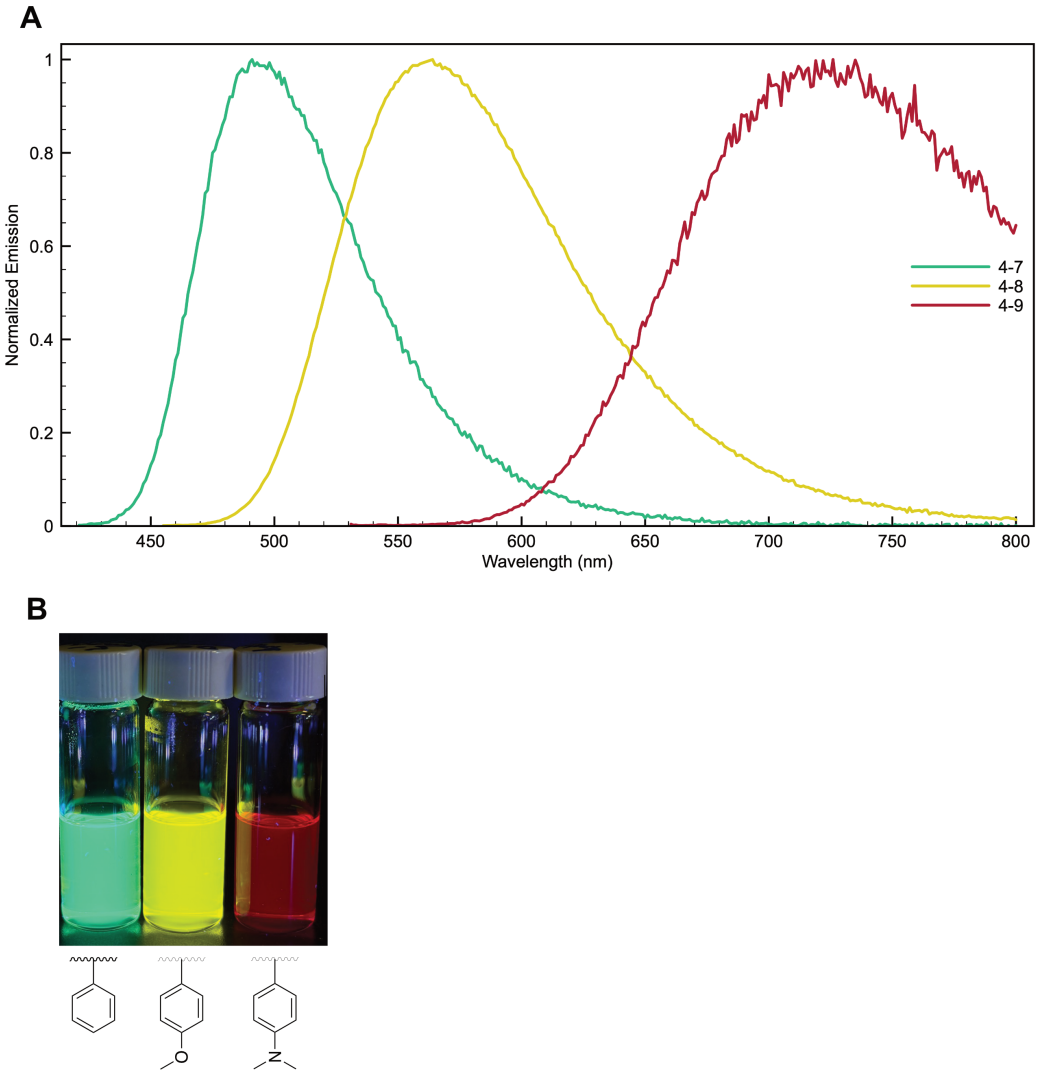

Figure 4-6. (A) Emission spectra of all derivatives (CH_2Cl_2; $5x10^{-6}$ M); (B) emission colours of all species in CH_2Cl_2.

4.2.4 Solvatochromism

Due to their inherent charge-transfer electronics, the tetra cross-coupled species also show positive solvatochromism.[15] This phenomenon arises from the solvation energy in the ground state and excited states of the molecules and is common in donor-acceptor type architectures due to internal

charge transfer.[16] Compounds **4-7** and **4-9** were studied in more detail because of their significant D-A-D character, which we expected to lead to the most pronounced responses.

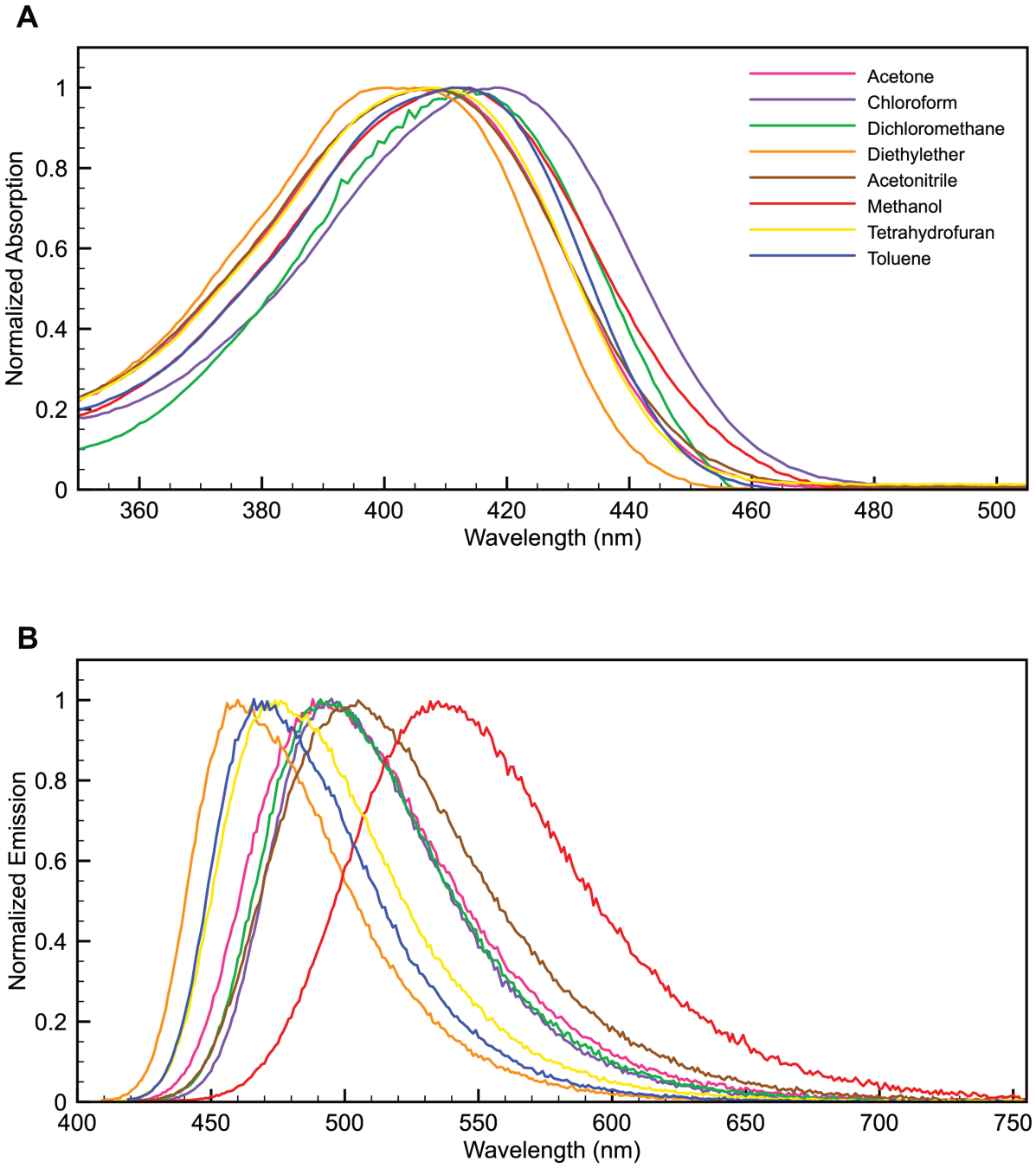

Figure 4-7. Normalized low-energy absorption (A) and emission (B) spectra of **4-7** in various solvents (c = $5x10^{-6}$ M)

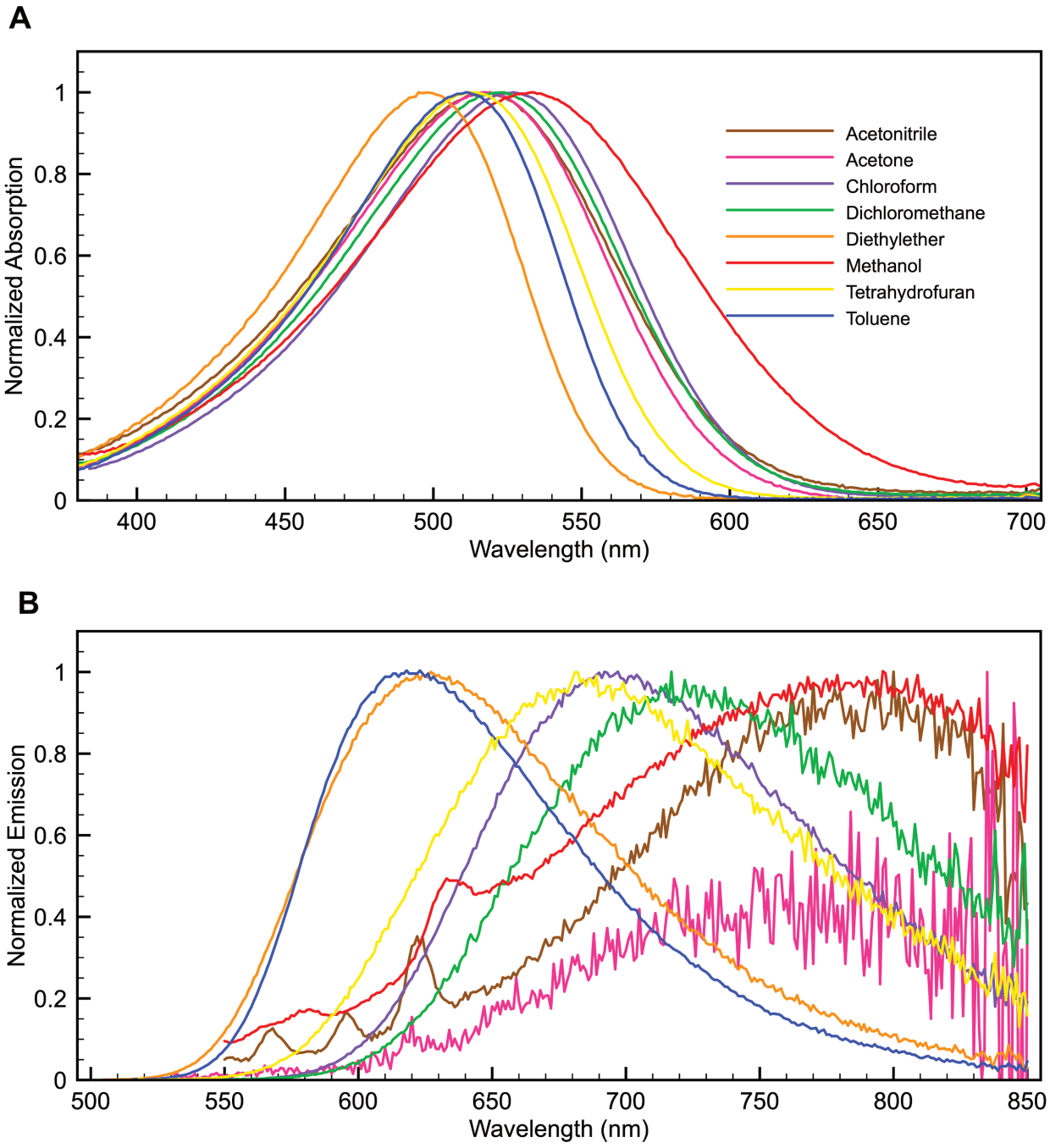

Figure 4-8. Normalized low-energy absorption (A) and emission (B) spectra of **4-9** in various solvents ($c = 5x10^{-6}$ M).

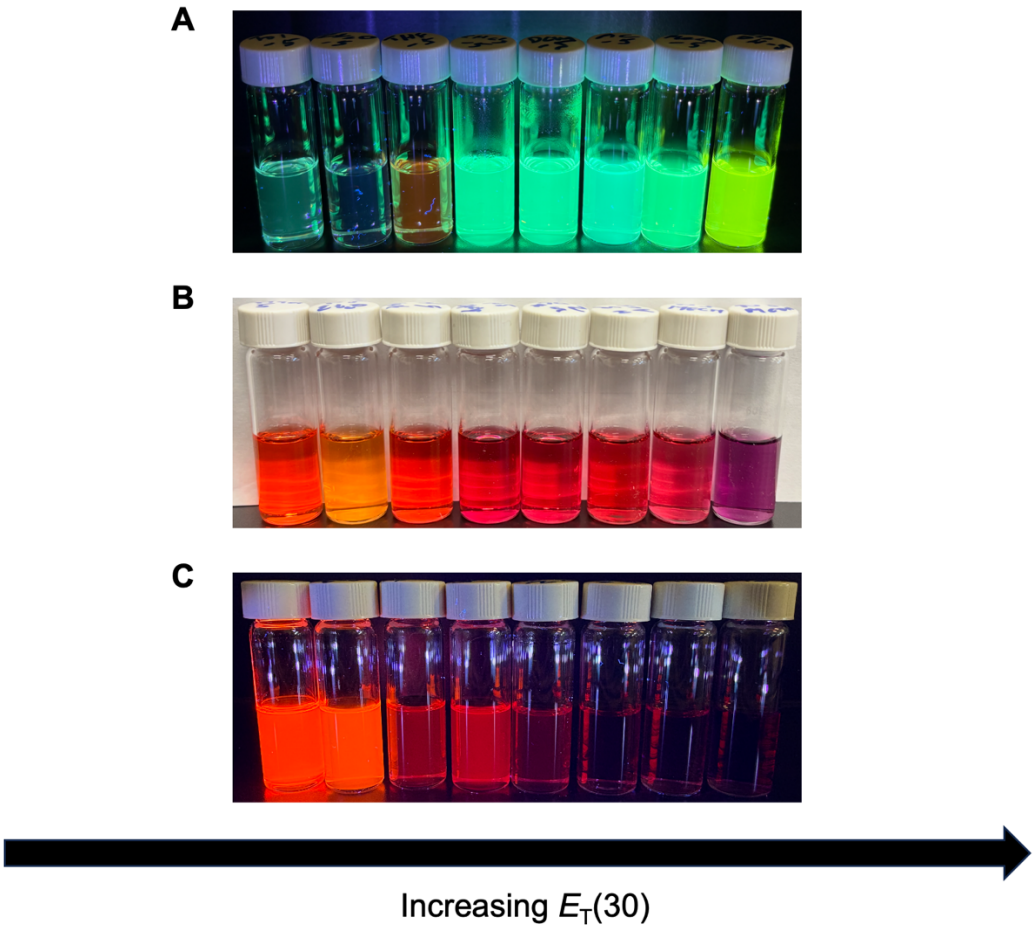

Figure 4-9. (A) Emission of **4-7** in various solvents under UV irradiation; (B) Different colours of **4-9** in various solutions non-irradiated; (C) Emission of **4-9** in various solvents under UV-irradiation. Solutions from left to right in order of increasing $E_T(30)$ value.

Eight different solvents with varying polarity and hydrogen bonding ability were tested. The increase in solvent polarity has minimal impact in the absorption spectra (Figure 4-7A and 4-8A). The absorption range for **4-7** is between 405 nm to 418 nm and for **4-9** it is 495 nm to 533 nm. The molar extinction coefficients also vary among the different solvents as summarized in Table 4-2.[16] A greater red-shift, indicative of charge transfer, is seen in the emission spectra for both species with increasing solvent polarity (Figures 4-7B and 4-8B). In the case of **4-7** the emission varies from 460 nm to 532 nm, while it is more dramatically impacted for **4-9** red-shifting from

623 nm to 835 nm. Note that the emission spectra for **4-9** approach the near infrared region and are close to the upper limit of the spectrometer thus appear to have significant noise. The solvent polarity with the observed emission maxima are plotted against the $E_T(30)$ value for each solvent (Figure 4-10).[17] For **4-7** the plot has a R^2 value of 0.9 indicating strong linearity in the solvent polarity increase and the red-shift in emission. However, for **4-9** the R^2 value is 0.62 indicative of outliers. Methanol and acetone are the outliers for **4-9** as when they are removed from the data set the R^2 value goes to 0.99 (see Supporting Information Figure S4-37). For the case of methanol, the deviation is related to its protic nature, which has been reported to disrupt the excited state conformations of a molecule and in turn alter the dynamics between the excited and local excited state due to formation of O-H bonds when compared to aprotic solvents.[18] Although acetone is known as a non-hydrogen bond donating solvent, there is reported spectroscopic and thermodynamic evidence that suggests it can be classified as hydrogen bond donating. This has been reported for its coordination with pyridine N-oxide.[19] In this chapter as well as the previous ones, we have shown that these dithienoketophosphinine systems participate in hydrogen bonding, thus for the case of **4-9** it could be hydrogen bonding with acetone leading to the deviation in the emission as a result of structural changes induced by the hydrogen bonds.

The overall trend for both species is that with increasing solvent polarity the emission wavelengths experience a red shift. Confirming the expected positive solvatochromism as a result of a more polar excited state than the ground state; thus higher polarity solvents are able to stabilize the highly polar excited state and produce the red shift.[15]

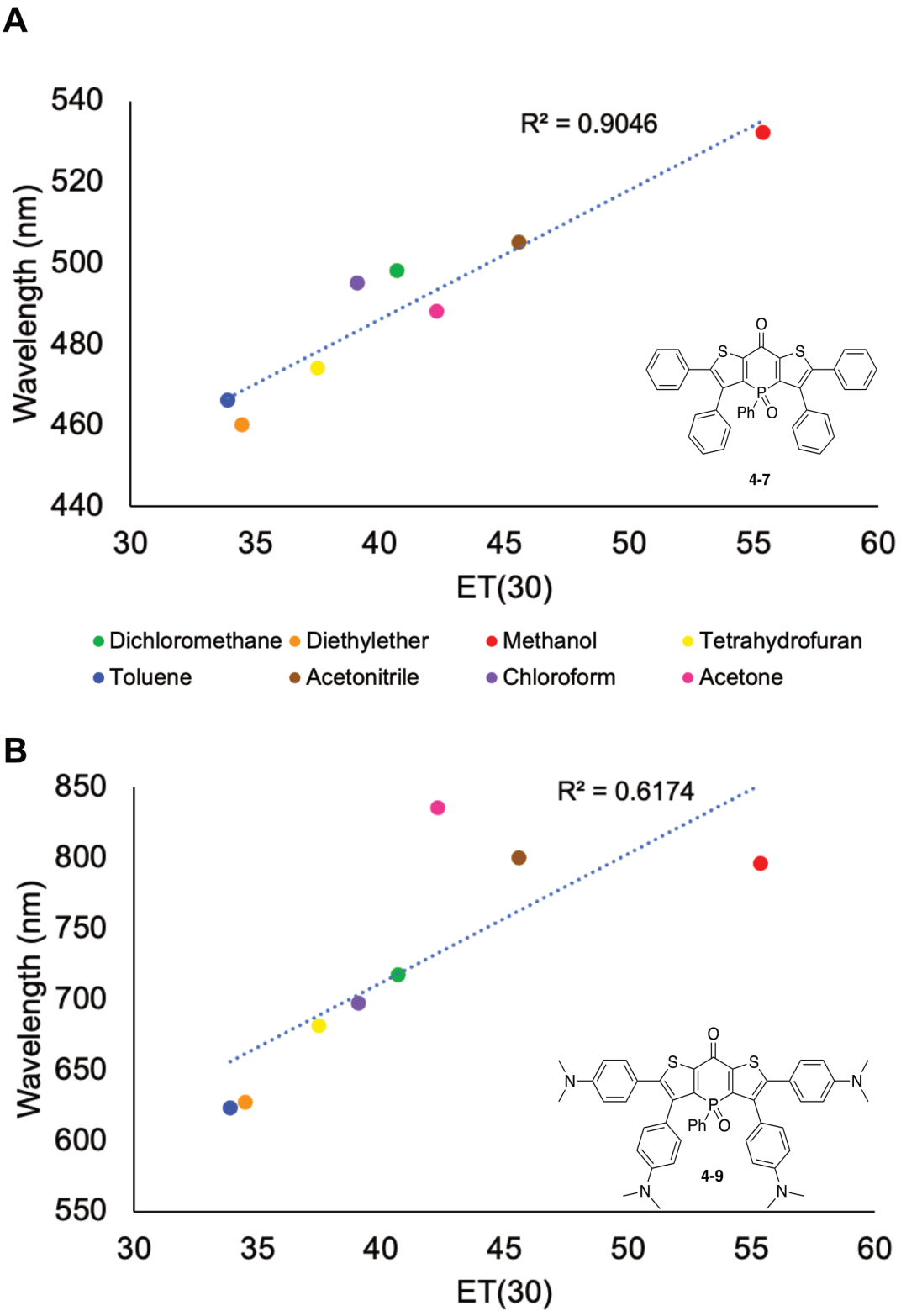

Figure 4-10. Emission maxima plotted against $E_T(30)$ value for **4-7** (A) and **4-9** (B).

Table 4-2. (a) Quantitative absorption, (b) molar extinction, and (c) emission values of **4-7** and **4-9** in various solvents ($5x10^{-6}$ M).

Compound	**Solvent**	**λ_{Abs} /nm[a]**	**Ɛ/$M^{-1}cm^{-1}$[b]**	**λ_{Em}/ nm[c]**
4-7	Toluene	411	24,500	466
	Diethyl ether	405	19,000	460
	Tetrahydrofuran	407	22,900	474
	Chloroform	418	18,600	495
	Dichloromethane	414	19,100	491
	Acetone	407	23,500	488
	Acetonitrile	407	21,400	505
	Methanol	412	17,100	532
4-9	Toluene	511	34,100	623
	Diethyl ether	495	14,600	627
	Tetrahydrofuran	514	28,100	681
	Chloroform	527	31,100	697
	Dichloromethane	523	24,100	717
	Acetone	517	23,500	835
	Acetonitrile	519	15,900	800
	Methanol	533	18,200	796

4.2.5 Density Functional Theory (DFT) Calculations

To obtain a deeper understanding of the observed photophysics of the extended dithieno-ketophosphinines, density functional theory calculations using a B3LYP/6-31G+(d) basis set solvated in dichloromethane using the PCM solvation model were performed (Figure 4-11).

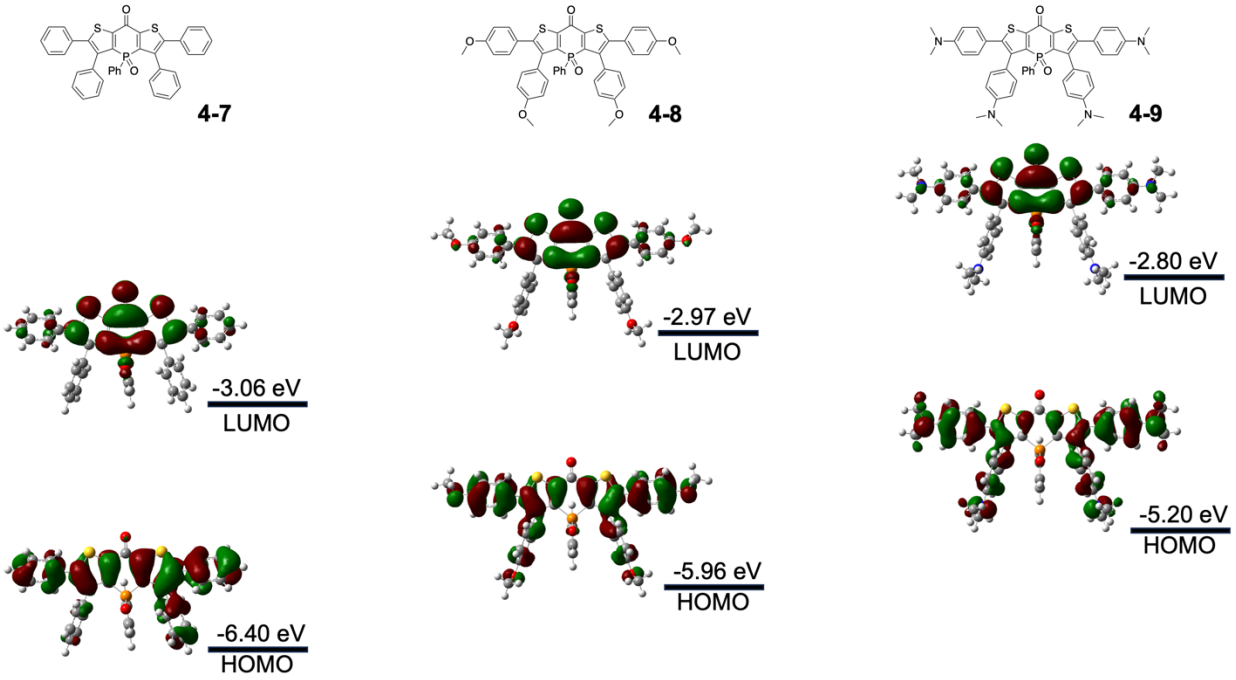

Figure 4-11. Frontier molecular orbitals of **4-7**, **4-8**, and **4-9** with respective HOMO and LUMO energies (eV). Level: B3LYP/6-31G+(d) using a PCM solvation model in CH_2Cl_2.

The HOMO of **4-7**, **4-8**, and **4-9** is largely situated across the extended dithienoketophosphinine π-system with some delocalization over the π system of the β-phenyl groups, however, without any contribution from the phosphorus centre. The delocalization becomes less concentrated on the core (based on orbital sizes) as the strength of the donor species increases from **4-7** to **4-9**. For **4-8** and **4-9**, there is additional contribution from the lone pairs of the heteroatom donor substituents in the HOMO. The LUMO for all three compounds is situated primarily on the π* system of the

dithienoketophosphinine core with only very small contributions from the extended aryl groups. Additionally, σ*-π* interactions at the phosphorus centre are also evident in the LUMO of all three species. The separation of the HOMO toward the terminal groups and the LUMO localized on the core supports their charge-transfer character. The HOMO energy increases as donor strength increases from **4-7** to **4-9** and goes from -6.40 eV to -5.20 eV, whereas the LUMO has a similar trend and goes from -3.06 eV to -2.80 eV. By comparison, the HOMO energy is -7.10 eV and the LUMO energy -3.07 eV for the dithienoketophosphinine core alone. The optical band gaps (Table 4-1) are a good representation of the absorption data, as the most hypsochromically shifted species **4-7** has the largest HOMO-LUMO gap of 3.3 eV and the most bathochromic species **4-9** has the smallest gap of 2.4 eV.

4.2.6 Time-dependent Density Functional Theory (TDDFT) Calculations

To gain even further insight on the transitions that occur at the high- and low- energy absorption maxima for each species TD-DFT calculations were carried out using the CAM-B3LYP/6-31G+(d) level of theory with PCM solvation in dichloromethane. The oscillator strength (f) was used to gauge the contribution for each excited state (Table 4-3).

Starting with the lowest energy absorption, the dominant transition responsible for all three compounds is primarily a HOMO to LUMO (π-π*) charge-transfer transition (Figure 4-12; Table 4-3). As for the higher energy absorptions, the major transition originates from different transitions that are all π-π* in nature. For **4-7** the highest contributor is a HOMO to LUMO+3 transition, for **4-8** this absorption is described by a transition from the HOMO-4 to LUMO, and for compound **4-9** the dominant transition is HOMO-1 to LUMO+1 (Figure 4-12). All species also have minor contributions from other transitions highlighted in Table 4-3.

Table 4-3. Time-dependent density functional theory calculation results for tetra cross-coupled species using TD-SCF CAM-B3LYP/6-31G+(d) using a PCM solvation model in CH_2Cl_2. (a) oscillator strengths used to determine dominant transitions (b)

	4-7	**4-8**	**4-9**
λ/nm (*f*)[a]	374.43 (0.67)	396.25 (0.79)	449.32 (0.99)
Transitions[b]	H → L (85%)	H → L (82%)	H → L (80%)
	H-11 → L (3%)	H-9 → L (4%)	H-4 → L (10%)
λ/nm (*f*)[a]	252.6 (0.27)	257.92 (0.08)	297.7 (0.08)
Transitions[b]	H → L+3 (14%)	H-4 → L (26%)	H-1 → L+1 (13%)
	H-1 → L+1 (11%)	H-12 → L (14%)	H → L+3 (12%)

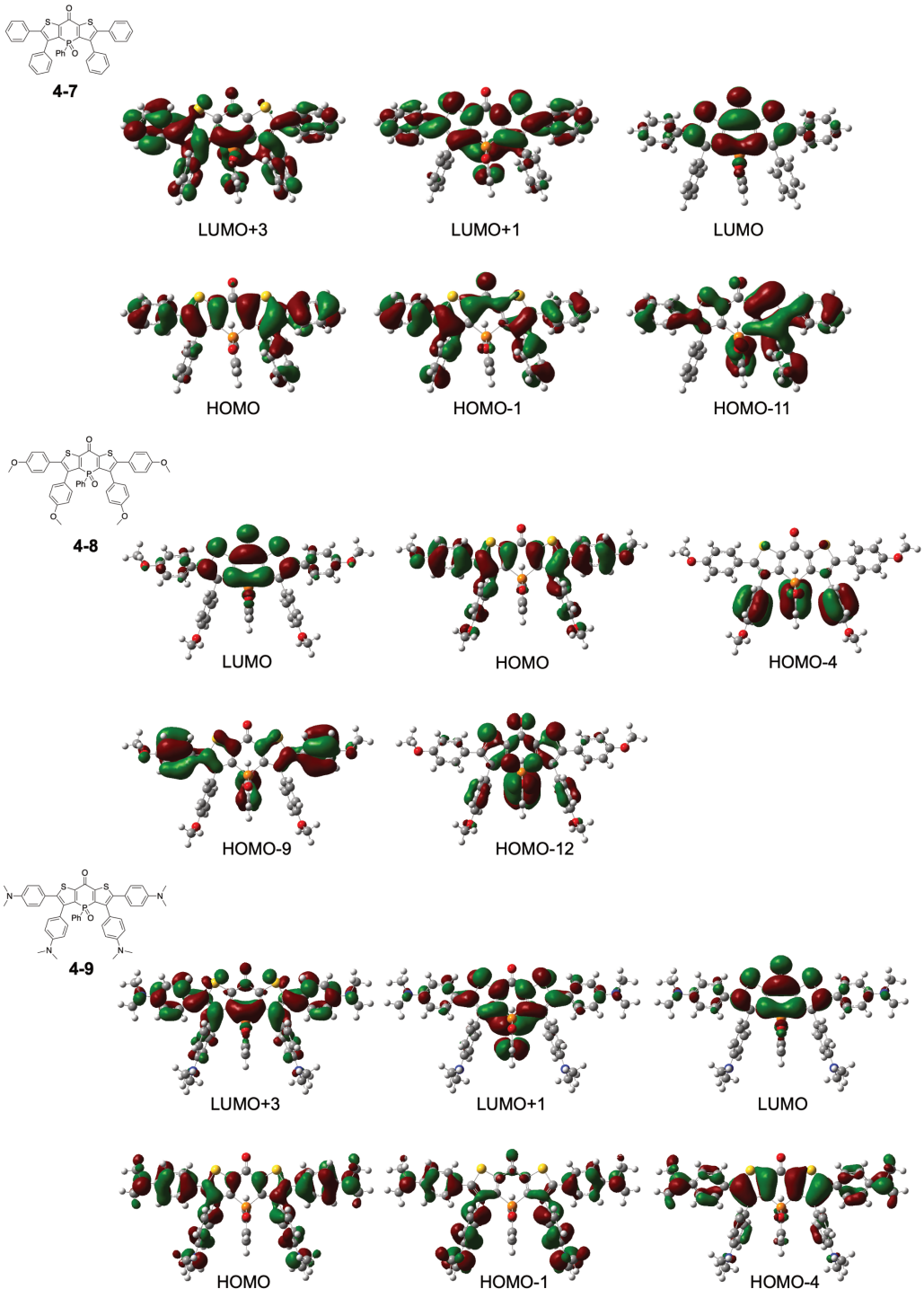

Figure 4-12. Select molecular orbitals for tetra cross-coupled species.

4.2.7 Cyclic Voltammetry

To establish the electronic impact of the different terminal groups on the overall redox features, the electrochemical properties of compounds **4-7**, **4-8**, and **4-9** were determined by cyclic voltammetry; the reduction values summarized in Table 4-1. The oxidations are in the Supporting Information (Figure S4-38).

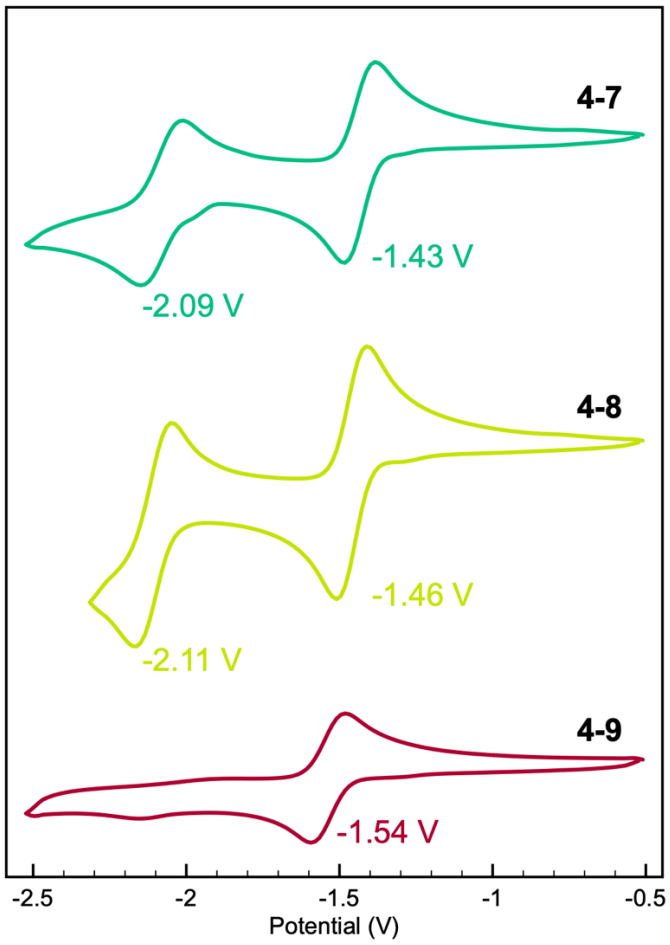

Figure 4-13. Cyclic voltammograms of **4-7**, **4-8** and **4-9**. Potentials are references to Fc/Fc^{+}. Scan rate 100 mV/s with $NBuPF_6$ as supporting electrolyte. All experiments performed in dry CH_3CN under argon.

Essentially all species show reversible reductions (Figure 4-13) and irreversible oxidations (oxidation sections of the CVs are found in the SI). Interestingly, **4-7** has two reduction events at

-1.43 V and -2.09 V (vs. Fc/Fc^+), notably the first reduction lower than that of the dithieno-ketophosphinine **2-3O**, which only has one reversible reduction at -1.46 V under similar conditions. The same phenomenon was reported for the dithienophosphole congener.[20] Compound **4-8** also exhibits two reversible reduction events, both of which at higher potentials of -1.46 V and -2.11 V when compared to **4-7** in line with its slightly higher LUMO energy (-2.97 eV vs. -3.06 eV). Finally, **4-9** only shows one reversible reduction at -1.54 V, reflective of this species having the highest LUMO energy of -2.80 eV of all species in this series (Figure 4-11). However, the second reduction may be occurring at a higher reduction potential past the solvent window, which will have to be studied further.

4.3 Conclusion and Future Outlook

Overall, we were able to successfully synthesize and characterize a series of π-extended dithienoketophosphinines via four-fold cross-coupling of the core, a feature not available in any of our previous studies to date. The new extended species differ in the nature of their terminal aryl groups with different degree of donor/acceptor character. To our satisfaction the extended species display visible light emissions, and solvatochromic behaviour due to their innate charge-transfer nature, none of which has been seen in the non-extended dithienoketophosphinine core. Moreover, the overall electron-acceptor qualities of the system are further tunable via this strategy through the different aryl groups. Future studies will involve full characterization of the tetrapyridyl species **4-6** and expanding the scope of applicable cross-coupling procedures (Sonogashira and Stille) to create a larger library of compounds with variable and highly tunable electronic and optical properties.

4.4 Experimental Section

4.4.1 General Methods

Most reactions in this section were performed under an inert argon atmosphere using standard Schlenk line techniques. Solvent was dried using an MBraun SPS solvent purification system. The reagents used were purchased from Sigma Aldrich, Fischer, or Oakwood Chemicals and used as received. The palladium catalyst was obtained from the Le group at York University. The NMR data were obtained from a NEO 300, 400 or 600 MHz spectrometer, respectively. Single crystal X-ray crystallographic data were obtained on a Bruker D8 Quest Eco diffractometer. The optical studies were carried out with an Agilent Cary 5000 UV-vis spectrophotometer and an Edinburg FS5 fluorescence spectrometer with an integration sphere for quantum yield measurements using standard quartz cuvettes. Cyclic voltammetry was performed using a Metrohm Autolab Potentiostat with NOVA software in dry acetonitrile or dichloromethane with NBu_4PF_6 as the electrolyte. Theoretical calculations were carried out using Gaussian on clusters provided by the Digital Research Alliance of Canada.

4.4.2 Synthetic Procedures

Synthesis of **4-5**

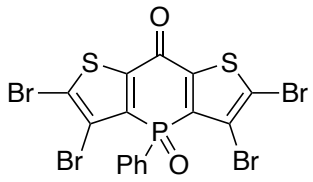

Compound **2-3O** (0.4 g, 1.3 mmol) was dissolved in 30 mL trifluoroacetic acid and 10 mL sulfuric acid. N-bromosuccinimide (0.1 g, 5.4 mmol) was slowly added and the reaction was left to stir for 12 hours at room temperature. The mixture was added to 500 mL deionized H_2O and quenched with $NaHCO_3$ (approx. 1 L), then extracted with dichloromethane. The organic phase was dried with

$MgSO_4$ and the solvent removed in *vacuo.* The crude mixture was heated in chloroform and the solution decanted to afford yellow solids (Yield: 0.05 g, 7%). $^{31}P\{^1H\}$ (162 MHz, CD_2Cl_2) δ: -1.6 ppm. ^1H NMR (400 MHz, CD_2Cl_2) δ 7.88 – 7.78 (m, 2H), 7.67 (dt, J = 7.5, 3.9 Hz, 1H), 7.55 (s, 2H). ^{13}C NMR (100.6 MHz, CD_2Cl_2) δ 169.3 (d, J_{CP} = 6 Hz), 145.3 (d, J_{CP} = 10.1 Hz), 139.4 (d, J_{CP} = 11.1 Hz), 133.2 (d, J_{CP} = 3 Hz), 132.4 (d, J_{CP} = 12.1 Hz), 128.9 (d, J_{CP} = 14.1 Hz), 125.5 (d, J_{CP} = 15.1 Hz), 117.7 (J_{CP} = 9.1 Hz). HRMS (ESI): m/z = 628.6280 $[M+H]^+$ (calcd. 628.6280).

Synthesis of **4-7**

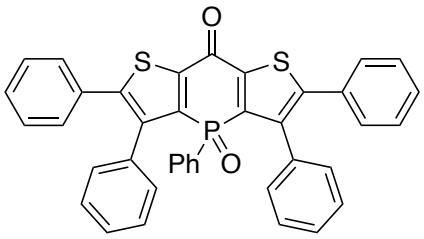

Compound **4-5** (0.1 g, 0.17 mmol), phenylboronic acid (0.21 g, 1.7 mmol) and bis(triphenylphosphine)palladium(II)-dichloride (0.02 g, 0.03 mmol) were dissolved in 4 mL dioxane. To this K_2CO_3 (0.1 g, 0.7 mmol) and 2 mL deionized H_2O were added. The mixture was heated to 98 °C for 24 hours. The solvent was removed in *vacuo* and silica column chromatography using ethyl acetate and hexanes (1:1) was done for bulk purification. Re-precipitation in acetonitrile gave bright yellow solids (Yield: 0.05 g, 45%). Single crystals for XRD were obtained via slow evaporation in acetone. $^{31}P\{^1H\}$ (162 MHz, CD_2Cl_2) δ 0.3 ppm. ^1H NMR (600 MHz, CD_2Cl_2) δ 7.31 (s), 7.34 – 7.25 (m), 7.27 – 7.22 (m), 7.25 – 7.16 (m), 7.18 – 7.11 (m), 7.02 (s), 6.93 (td), 6.79 (dd). ^{13}C NMR (150 MHz, CD_2Cl_2) δ 172.5 (d, J_{CP} = 6 Hz), 150.2 (d, J_{CP} = 13.5 Hz), 143.1 (d, J_{CP} = 9 Hz), 142.9 (d, J_{CP} = 12 Hz), 141.2 (d, J_{CP} = 100.5 Hz), 133 (d, J_{CP} = 135 Hz), 130.2 (d, J_{CP} = 10.5 Hz), 139.3 (d, J_{CP} = 103.5 Hz), 128.9 (s), 127.7 (d, J_{CP} = 15 Hz), 127.5 (s). HRMS (ESI): m/z = 621.1109 $[M+H]^+$ (calcd. 621.1112).

Synthesis of **4-8**

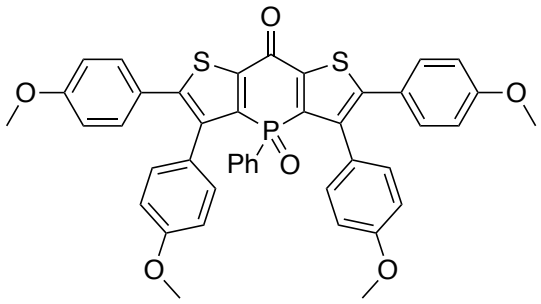

Compound **4-5** (0.07 g, 0.12 mmol), 4-methoxyphenylboronic acid (0.17 g, 1.2 mmol) and bis(triphenylphosphine)palladium(II)dichloride (0.02 g, 0.02 mmol) were dissolved in 3 mL dioxane. To this K_2CO_3 (0.06 g, 0.4 mmol) and 1 mL deionized H_2O were added. The mixture was heated to 98°C for 24 hours. The solvent was removed in *vacuo* and silica column chromatography using ethyl acetate and hexanes (3:1) was done for bulk purification. Re-precipitation in diethyl ether gave bright orange solids (Yield: 0.06 g, 73%). Single crystals for XRD were obtained via slow evaporation in acetone. $^{31}P\{^1H\}$ (162 MHz, CD_2Cl_2) δ 0.0 ppm. ^1H NMR (600 MHz, CD_2Cl_2) δ 7.25 – 7.17 (m, 9H), 6.99 (td, J = 7.6, 3.0 Hz, 2H), 6.85 (ddd, J = 13.9, 8.1, 1.4 Hz, 2H), 6.79 – 6.74 (m, 4H), 6.57 (s, 4H), 3.76 (d, J = 8.1 Hz, 12H). ^{13}C NMR (150 MHz, CD_2Cl_2) δ 172.5 (d, J_{CP} = 6 Hz), 160.1 (s), 159.2 (s), 150.2 (d, J_{CP} = 13.5 Hz), 142.1 (d, J_{CP} = 9 Hz), 141.9 (d, J_{CP} = 12 Hz), 132.13 (s), 131.1 (d, J_{CP} = 3 Hz), 130.5 (s), 130.4 (d, J_{CP} = 12 Hz), 129.6 (d, J_{CP} = 112.5 Hz), 127.5 (d, J_{CP} = 13.5 Hz), 125.5 (s), 124.8 (s), 113.9 (s), 113 (s), 55.2 (d, J_{CP} = 20 Hz). HRMS (ESI): m/z = 741.1539 $[M+H]^+$ (calcd. 741.1534).

Synthesis of **4-9**

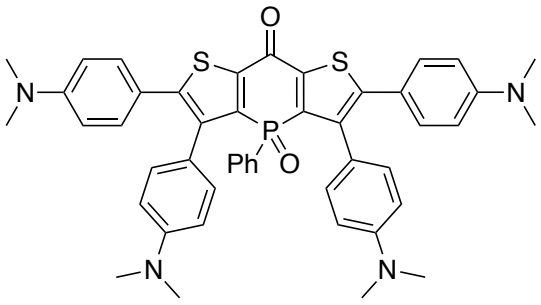

Compound **4-5** (0.2 g, 0.17 mmol), 4-(N,N-dimethylamino)phenylboronic acid pinacol ester (0.41 g, 1.7 mmol) and bis(triphenylphosphine)-palladium(II)dichloride (0.02 g, 0.03 mmol) were dissolved in 4 mL dioxane. To this K_2CO_3 (0.09 g, 0.7

mmol) and 2 mL deionized H_2O were added. The mixture was heated to 98 °C for 24 hours. The solvent was removed in *vacuo* and passed through a neutral alumina plug eluting with ethyl acetate and hexanes (1:1) for bulk purification. Re-precipitation in acetonitrile gave dark purple solids (Yield: 0.07 g, 53%). Single crystals for XRD were obtained via slow evaporation in acetonitrile. $^{31}P\{^1H\}$ (160 MHz, CD_2Cl_2) δ 0.2 ppm.^1H NMR (400 MHz, CD_2Cl_2) δ 7.16 (dd, J = 9.6, 2.6 Hz, 9H), 6.96 (td, J = 7.7, 3.3 Hz, 2H), 6.89 – 6.79 (m, 2H), 6.74 (s, 4H), 6.58 – 6.49 (m, 4H), 2.92 (d, J = 15.5 Hz, 12H, NMe_2). ^{13}C NMR (100.6 MHz, CD_2Cl_2) δ 172.3 (d, J_{CP} = 5 Hz), 150.9 (s), 150.4 (s), 149.8 (s), 142.4 (d, J_{CP} = 75 Hz), 141.5 (d, J_{CP} = 14.1 Hz), 140.8 (d, J_{CP} = 9.1 Hz), 131.5 (s), 130.6 (s), 130.5 (d, J_{CP} = 11.1 Hz), 129.8 (s), 127.3 (d, J_{CP} = 13.1 Hz), 121.7 (d, JCP = 140 Hz), 111.5 (s), 40.2 (d, J_{CP} = 40 Hz). HRMS (ESI): m/z = 793.2802 $[M+H]^+$ (calcd. 793.2800).

4.5 References

(1) Liu, Z.; Meng, L.; Jiang, Y.; Li, C.; Gu, H.; Zhao, K.; Zhang, J.; Meng, H.; Ren, Y. Hyperconjugation Engineering of π-Extended Azaphosphinines for Designing Tunable Thermally Activated Delayed Fluorescence Emitters. *J. Am. Chem. Soc.* **2025**, *147* (4), 3650–3661. https://doi.org/10.1021/jacs.4c15651.

(2) Dienes, Y.; Durben, S.; Kárpáti, T.; Neumann, T.; Englert, U.; Nyulászi, L.; Baumgartner, T. Selective Tuning of the Band Gap of π-Conjugated Dithieno[3,2-*b*:2′,3′-*d*]phospholes toward Different Emission Colors. *Chem. Eur. J.* **2007**, *13* (26), 7487–7500. https://doi.org/10.1002/chem.200700399.

(3) Mateo-Alonso, A. π-Conjugated Materials: Here, There, and Everywhere. *Chem. Mater.* **2023**, *35* (4), 1467–1469. https://doi.org/10.1021/acs.chemmater.2c03567.

(4) Romero-Nieto, C.; Durben, S.; Kormos, I. M.; Baumgartner, T. Simple and Efficient Generation of White Light Emission from Organophosphorus Building Blocks. *Adv. Funct. Mater.* **2009**, *19* (22), 3625–3631. https://doi.org/10.1002/adfm.200901540.

(5) Demay-Drouhard, P.; Baumgartner, T. Highly Luminescent 4-Pyridyl-Extended Dithieno[3,2-*b*:2′,3′-*d*]phospholes. *J. Org. Chem.* **2020**, *85* (22), 14627–14633. https://doi.org/10.1021/acs.joc.0c01369.

(6) Song, C.; Wang, Z.; Li, J.; Chen, Y.; Zhao, F.; Zhang, H. Extension of π-Conjugation and Enhancement of Electron-Withdrawing Ability at Terminal Indenedione for A-π-D-π-A Small Molecules for Application in Organic Solar Cells. *Org. Electron.* **2020**, *81*, 105679. https://doi.org/10.1016/j.orgel.2020.105679.

(7) Hindenberg, P.; Romero-Nieto, C. Phosphaphenalenes: An Evolution of the Phosphorus Heterocycles. *Synlett.* **2016**, *27* (16), 2293–2300. https://doi.org/10.1055/s-0035-1562506.

(8) Hindenberg, P.; Rominger, F.; Romero-Nieto, C. Phosphorus Post-Functionalization of Diphosphahexaarenes. *Chem. Eur. J.* **2019**, *25* (57), 13146–13151. https://doi.org/10.1002/chem.201901837.

(9) Wu, S.; Yan, Y.; Hou, H.; Huang, Z.; Li, D.; Zhang, X.; Xiao, Y. Polarity-Sensitive and Membrane-Specific Probe Quantitatively Monitoring Ferroptosis through Fluorescence Lifetime Imaging. *Anal. Chem.* **2022**, *94* (32), 11238–11247. https://doi.org/10.1021/acs.analchem.2c01737.

(10) Bergström, M.; Suresh, G.; Naidu, V. R.; Unelius, C. R. *N* -Iodosuccinimide (NIS) in Direct Aromatic Iodination. *Eur. J. Org. Chem.* **2017**, *2017* (22), 3234–3239. https://doi.org/10.1002/ejoc.201700173.

(11) Rajesh, K.; Somasundaram, M.; Saiganesh, R.; Balasubramanian, K. K. Bromination of Deactivated Aromatics: A Simple and Efficient Method. *J. Org. Chem.* **2007**, *72* (15), 5867–5869. https://doi.org/10.1021/jo070477u.

(12) Kreuzer, F.; Aubele, A.; Mena-Osteritz, E.; Bäuerle, P. Synthesis and Reactivity of Dithienopyrazines. *Eur. J. Org. Chem.* **2023**, *26* (13), e202300023. https://doi.org/10.1002/ejoc.202300023.

(13) Jabbarpoor, M.; LeBlanc, J.; Chen, Z.; Cadwallader, D.; Le, C. M. Pd-Catalyzed Suzuki-Type Cross-Coupling of 2-Pyridyl Carbamoyl Fluorides. *Chem. Commun.* **2024**, *60* (66), 8700–8703. https://doi.org/10.1039/D4CC02431A.

(14) Belyaev, A.; Chen, Y.; Liu, Z.; Hindenberg, P.; Wu, C.; Chou, P.; Romero-Nieto, C.; Koshevoy, I. O. Intramolecular Phosphacyclization: Polyaromatic Phosphonium P-Heterocycles with Wide-Tuning Optical Properties. *Chem. Eur. J.* **2019**, *25* (25), 6332–6341. https://doi.org/10.1002/chem.201900136.

(15) Bamfield, P.; Hutchings, M. 7.1 Solvent Polarity and Solvatochromic Shifts.

(16) Kim, O.-K.; Lehn, J.-M. Solvatochromism of Non-Linear Optical Chromophores Containing the Dithienothiophene Group in Donor-Acceptor Molecules. *Chem. Phys. Lett.* **1996**, *255* (1–3), 147–150. https://doi.org/10.1016/0009-2614(96)00358-2.

(17) Cerón-Carrasco, J. P.; Jacquemin, D.; Laurence, C.; Planchat, A.; Reichardt, C.; Sraïdi, K. Solvent Polarity Scales: Determination of New $E_T(30)$ Values for 84 Organic Solvents. *J. Phys. Org. Chem.* **2014**, *27* (6), 512–518. https://doi.org/10.1002/poc.3293.

(18) Bonaccorso, C.; Cesaretti, A.; Elisei, F.; Mencaroni, L.; Spalletti, A.; Fortuna, C. G. New Styryl Phenanthroline Derivatives as Model D−π−A−π−D Materials for Non-Linear Optics. *ChemPhysChem.* **2018**, *19* (15), 1917–1929. https://doi.org/10.1002/cphc.201800391.

(19) Laurence, C.; Mansour, S.; Vuluga, D.; Sraïdi, K.; Legros, J. Theoretical, Semiempirical, and Experimental Solvatochromic Comparison Methods for the Construction of the α_1 Scale of Hydrogen-Bond Donation of Solvents. *J. Org. Chem.* **2022**, *87* (9), 6273–6287. https://doi.org/10.1021/acs.joc.2c00526.

(20) Ren, Y.; Baumgartner, T. A Structure-Property Study toward π-Extended Phosphole Chromophores with Ambipolar Redox Properties. *Can. J. Chem.* **2016**, *94* (4), 297–304. https://doi.org/10.1139/cjc-2015-0347.

Chapter 5: Conclusions and Future Outlook

5.1 Conclusions

Overall, the main focus of this thesis was to study the underexplored dithienoketophosphinine system and its three sites of modification.

Chapter 2 covers various modifications of the phosphorus lone pair and the observed changes imposed on the system. All species reported in this chapter are non-emissive but experience shifts in their absorption spectra and in their redox properties. All compounds show relatively low reversible reduction potentials, except for the gold chloride functionalized species. The frontier molecular orbitals also change in energy and delocalization with the various functionalizations. The future for this modification avenue is the fine tuning of the properties by adding various alkyl and aryl substituents, as well as metals and to further explore the alteration of the system.

Chapter 3 introduces a concept not attainable in the dithienophosphole system – keto-modification. The modification of choice was Knoevenagel condensation introducing dicyanomethylene groups to create a stronger acceptor environment. The three compounds reported differ in their phosphorus centre substituent (oxide, lone pair, methyl). These compounds are also non-emissive in nature, however, both the dicyanomethylene moiety and the change of the substitution pattern at the phosphorus centre cause a red shift in absorption from the compounds reported in Chapter 2. The LUMO for these systems is lower in energy and the low reduction events with robust reversibility proved them to be better acceptors than the species reported in Chapter 2.

Chapter 4 reports a series of cross-coupled compounds with four sites of cross-coupling and varying in the donating/accepting ability of the introduced aryl groups. The compounds reported in this section are emissive unlike those in the previous two chapters. The red shifts seen in these species varied from blue to near-IR and displayed solvatochromism as a result of their charge-

transfer character. The electron-accepting qualities were retained, albeit at higher reduction potentials than those of the compounds reported in Chapters 1 and 2.

Although this thesis covers various key modifications and their impact on the optical and electrochemical properties of the dithienoketophosphinine, the opportunities for the dithienoketophosphinine system are vast. The next section presents future projects inspired by the work presented in this thesis to further develop our understanding of the dithienoketophosphinine system. Although the future work presented is not exclusive to these systems, it highlights some key concepts that should be tackled when creating these new species. Each potential compound comprises a brief inspiration, however, the true properties can only be revealed once the respective species are made.

5.2 Future outlook

5.2.1 Chemical reductions

For all of the dithienoketophosphinine modified species in the previous three chapters, excellent reversibility and relatively low reduction potentials were observed for most of the species. Additional to the cyclic voltammetry experiments performed, more in-depth characterizations are required to gain a deeper understanding on the reduced species. One approach is performing spectroelectrochemistry on the dithienoketophosphinine derivatives introduced in Chapters 2, 3 and 4, allowing for the comparison of the respective absorption spectra for each isolated redox state of the species.[1,2] A complementary approach involves chemical reduction of the species with appropriate reducing agents that can target the various redox states. Initial reducing agents that

have been applied to these systems are cobaltocene, and sodium metal with 15-crown-5.[2,3] Addition of these reagents causes changes in the colour of the solution from tan to blue or yellow to green to orange for the second species. Complementary to chemical reduction is electron paramagnetic resonance (EPR) spectroscopy that can be performed to understand the coupling of the radical to the various nuclei on the compound in conjugation with obtaining calculations on spin density maps to get a full understanding on the delocalization of the electrons once added to the system. Single-crystal XRD structures of the resulting species are also an asset for understanding the conformational changes on the system when an electron is added and observe the integrity of the charged state as has been done in many examples in the literature (mentioned in Chapter 3 with triarylborane systems as well).[2]

5.2.2 Solid state emission

To be applicable to many real-life applications, the materials used as chromophores are usually most useful in an aggregated state such as films or crystals.[4] The tetra-cross-coupled species reported in Chapter 4 all display solid state emission as shown in Figure 5-1.

Figure 5-1. Solid state emission of cross coupled species from Chapter 4. From left to right (**4-6**, **4-7**, **4-8**, **4-9**).

In this context, a known issue with materials used as chromophores is aggregation caused quenching (ACQ). In particular, when molecules are in the aggregated state, the interactions of neighbouring molecules promote non-radiative processes otherwise not seen in solution, thus making some compounds emissive only in solution.[4] The next steps for this project are to quantify the solid-state emission through processing the powders into thin films and obtaining the absorption, emission and quantum yields to gauge their usefulness in the solid state.

5.2.3 4-Pyridyl Functionalized Dithienoketophosphinine

As discussed in Chapter 1, there are many benefits to having pyridine-type systems incorporated into phosphorus-based scaffolds, namely the 4-pyridyl dithienophosphole (**1-14)** inspired by viologens (**1-18**) that displays improved electron-acceptor and redox properties.[1,5]

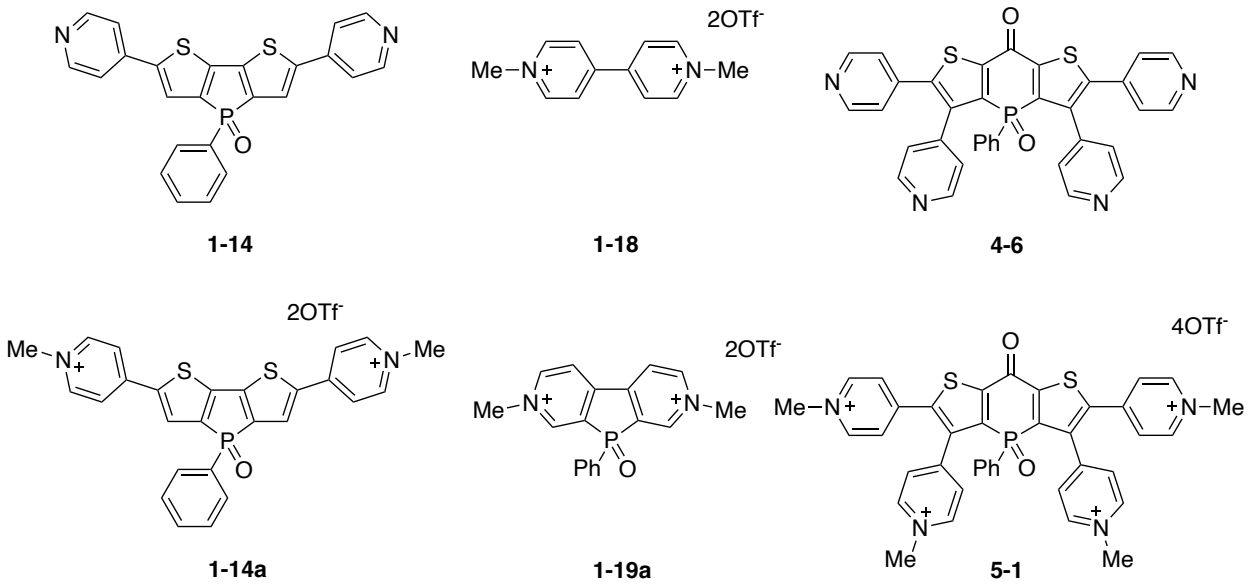

Figure 5-2. 4-Pyridyl dithienophospholes **1-14** and **1-14a**; viologen and phosphaviologen **1-18** and **1-19a**; 4-pyridyl extended dithienoketophosphinine **4-6** and methylated congener **5-1**.[1,5]

In Chapter 4, the 4-pyridyl tetra cross-coupled species (**4-6**) was only briefly reported due to a lack of purity thus far. Based on DFT calculations (see Figure 5-3) **4-6** appears to be a strong acceptor compound when compared to the other species reported in Chapter 4 with a LUMO energy of -3.34 eV. The unique aspect of integration of pyridyl groups is the accessibility of the lone pair at the nitrogen atom to be further functionalized as seen in our previous work. A common approach in our group has been methylation of the nitrogen centres to create cationic species, which are more electron accepting (**1-14a** and **1-19a;** Figure 5-2).[1,5] Thus a tetra-methylated species **5-1** can be a future derivative of **4-6.** Based on DFT calculations the LUMO energy of **5-1** is -4.73 eV, making it an even stronger acceptor than any of the other cross-coupled species and of great interest for the future of this project. Next steps involve isolation of **4-6** and methylation with methyl triflate to access **5-1.**

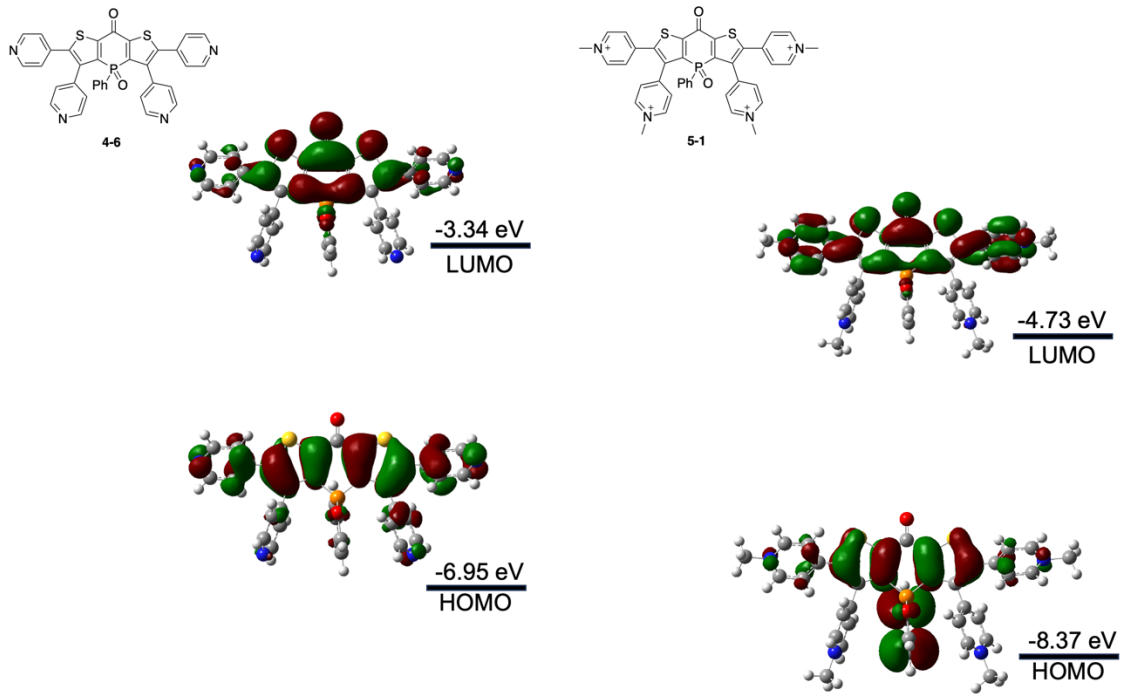

Figure 5-3. Frontier molecular orbitals of **4-6** and **5-1** with respective HOMO and LUMO energies (eV). Level: B3LYP/6-31G+(d) using a PCM solvation model in CH_2Cl_2.

5.2.4 Dicyanomethylene Functionalization of Tetra-substituted Species

Chapter 3 reported the increase of the electron-acceptor character of the species by addition of the dicyanomethylene moiety in the *para* position to the phosphorus centre in the dithienophosphinine ring. In Chapter 4 four-fold cross-coupling reactions that maintained reversibility in redox behaviour of the species while also being emissive were reported. Merging the two modifications shown in Chapters 3 and 4 to create compound **5-2** can thus be envisioned as well (Figure 5-4A). Preliminary studies successfully afforded the tetra-phenyl-extended dicyanomethylene-phosphinine and a solid-state structure has been acquired (Figure 5-4B). The ^{31}P NMR resonance is -0.6 ppm and the emission of this species is green, as seen in Figure 5-4C. The DFT calculations suggest that **5-2** with a LUMO of -3.59 eV is an even stronger acceptor than **4-6** (LUMO: -3.34

eV). Its optical and electrochemical data will also be of interest. Extension to other compounds, such **5-3**, **5-4**, and **5-5** to increase the accepting nature for **5-3** or to introduce a stronger donor-acceptor interaction for **5-5** and studying the resulting properties are also valuable targets (Figure 5-5).

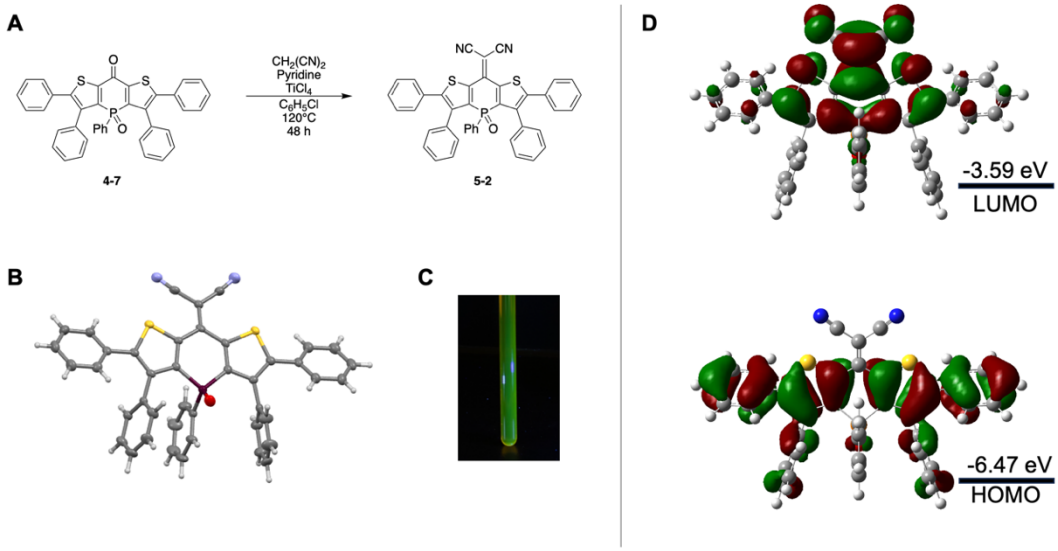

Figure 5-4. (A) Reaction conditions to prepare compound **5-2**; (B) solid-state structure of **5-2** thermal ellipsoids with 50% probability; (C) emission of **5-2** in $CDCl_3$; (D) frontier molecular orbitals of **5-2** with respective HOMO and LUMO energies (eV). B3LYP/6-31G+(d) level of theory using a PCM solvation model in CH_2Cl_2.

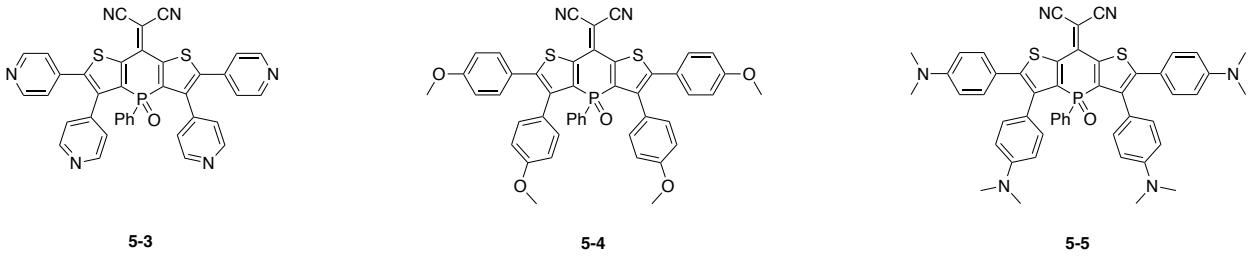

Figure 5-5. Proposed tetra-cross-coupled dithienophosphinine systems with dicyanomethylene functionality.

5.2.5. Analyte Sensing

Previously reported dithienophospholes, with dimethylaminophenyl and pinacol borane groups were reported to have use in sensing applications (**4-3** Scheme 5-1; **5-7** Scheme 5-2).[6,7] Both compounds have accessible sites (N and B) that can be leveraged for such applications. Compound **4-3** was employed in acid sensing wherein the protonation of the lone pair on the nitrogen induces a blue shift in the emission when creating compound **4-3a** (Scheme 5-1A). The use of amines is very applicable in the field of acid sensing especially when used as a chromophore for applications in sensing acid waste in the environment.[8] Seeing the applicability of the dimethylaminophenyl functionalized dithienophosphole, the same approach was qualitatively applied to the dimethylaminophenyl-functionalized dithienoketophosphinine from Chapter 4 by adding a few drops of hydrochloric acid (Scheme 5-1B). Interestingly, just like the dithienophosphole, compound **4-9** experiences a blue shift in emission upon addition of the acid almost immediately as shown in Scheme 5-1B. The next steps here would be proper titration of **4-9** with acids and to obtain their UV-vis/emission profiles to understand how many protonated species can potentially be isolated, with **5-6** being one of them (Scheme 5-1B). The B(pin)-functionalized dithienophopshole **5-7** was reported to be used in fluoride ion sensing to form **5-7a**. The development of fluoride-ion sensors especially as chromophores is quite interesting as very small amounts of fluoride can be detected and repressed by a shift in emission. This is of great importance to the dental care industry, medical treatments, and fluoride in water supply.[7] Seeing the value of sensing fluoride ions and the success B(pin) groups have in achieving this target, another species than can be studied in a similar manner to the acid sensors mentioned earlier is a tetra-pinacol borane-substituted dithienoketophosphinine **5-8** towards **5-8a** (Scheme 5-2B) .

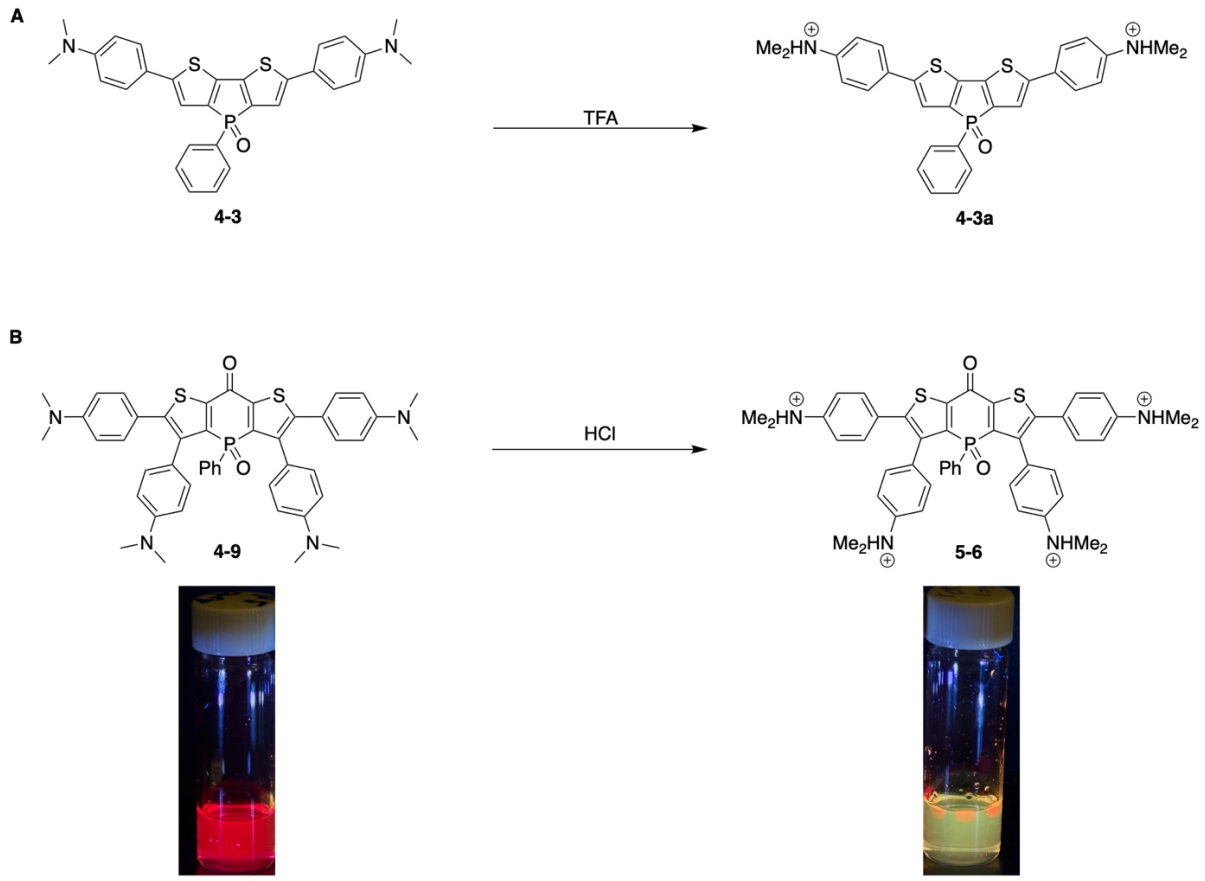

Scheme 5-1. Previously reported dimethylamino-functionalized dithienophosphole protonation (A);[6] Proposed protonation of dimethylamino-functionalized dithienoketophosphinine and the respective emissions after addition of acid (B).

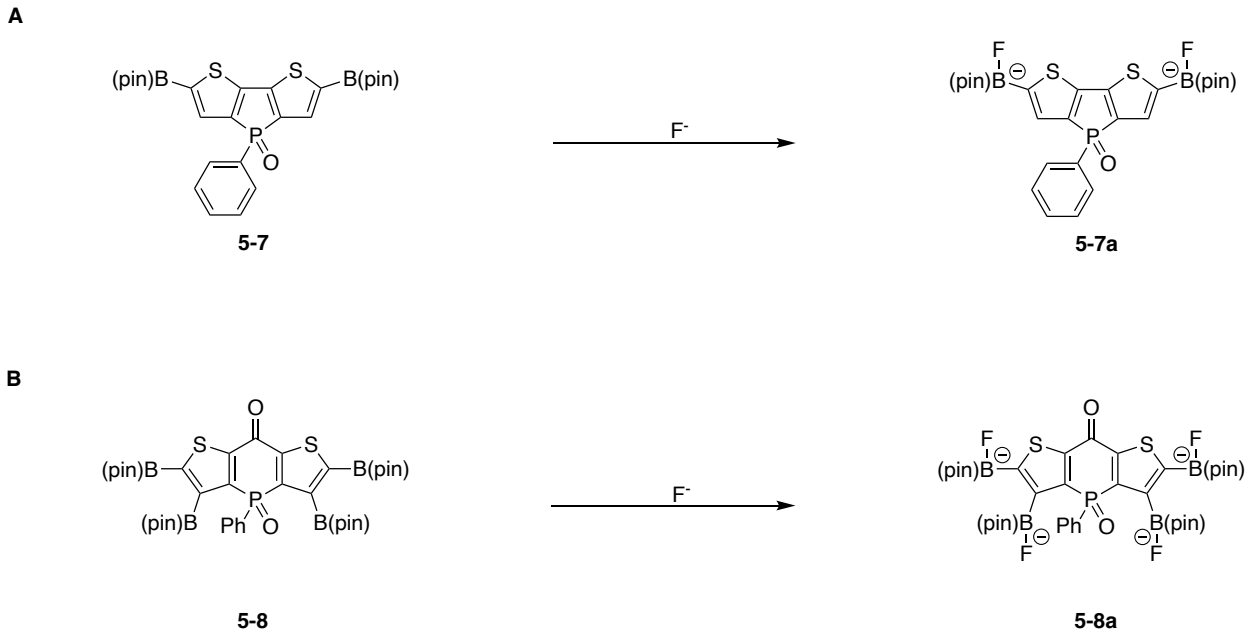

Scheme 5-2. (A) Previously reported B(pin)-functionalized dithienophosphole **5-7** and fluoride coordinated species **5-7a**;[7] (B) proposed B(pin)-functionalized dithienoketophosphinine **5-8** and fluoride coordinated species **5-8a**; (pin: pinacolate).

5.2.6 Nitro-substituted Species

Nitrobenzenes are well known redox-active species and have been used in battery applications and other energetic materials.[9,10] The excellent electrochemical reversibility and one- or two- electron acceptance, while remaining stable, makes them intriguing materials to study alongside our already existing electron-accepting dithienoketophosphinines. A simple approach to incorporate nitro-benzene type motifs into the dithienoketophosphinine scaffold would involve four-fold cross-coupling with either 4-nitro or 3-nitro benzeneboronic acid (Scheme 5-3A,B). Despite the potential, but overall low, risk of being explosive, species **5-9** and **5-10** could provide access to powerful n-type materials.

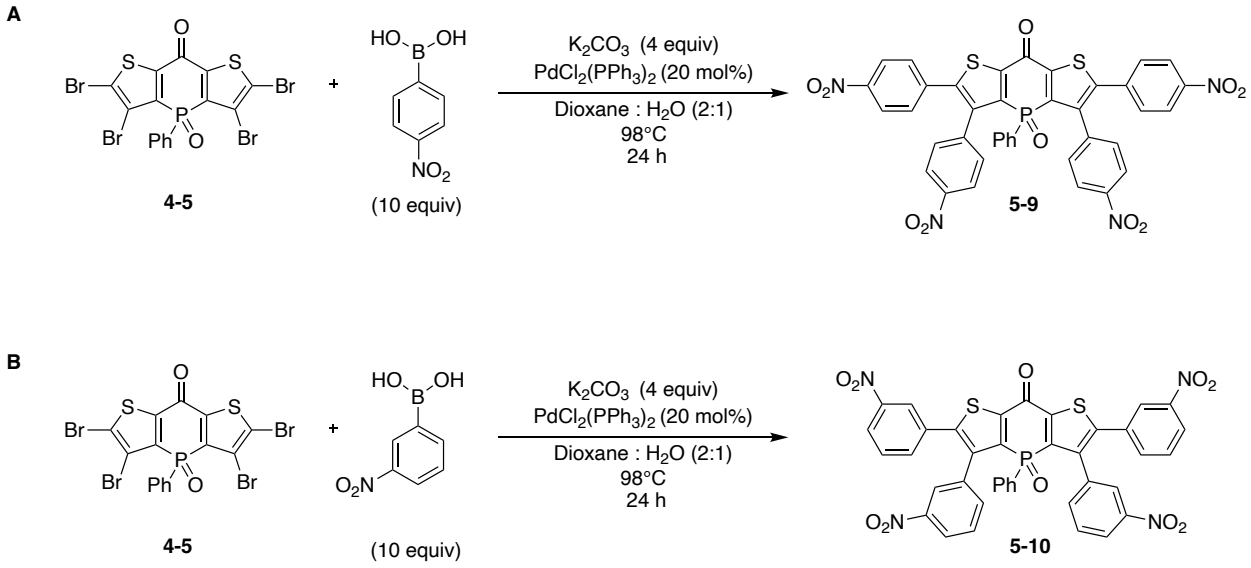

Scheme 5-3. Proposed reaction toward 4-nitrobenzene- and 3-nitrobenzene-functionalized dithienoketophosphinines.

5.2.7 Addition of Cationic Phosphonium Groups on Dithieno-backbone

By now, it is established that the dithienoketophosphinine is a strong acceptor compound that can be leveraged into an even stronger acceptor compound via incorporation of cationic centres at the core of the backbone, resulting in a strong stabilization of the LUMO by induction.[11] A common motif used in achieving this is the addition of triethylphosphonium groups. This methodology has been applied by Cao et al. wherein they attach triethylphosphanes onto pyrometallic diimides **5-11** to form **5-12** (Scheme 5-4). In addition to altered optical and structural features, the functionalized and unfunctionalized species had two reversible reductions. The unfunctionalized species has reductions at -1.35 V and -1.56 V (vs Fc/Fc^{+}) that, upon addition of the triethylphosphane group, significantly shift to -0.52 V and -1.17 V (vs Fc/Fc^{+}), respectively.[11] For this reason the related species **5-13** with expectedly significantly enhanced acceptor character should be accessible in similar fashion. Based on DFT calculations shown in Figure 5-6, the

LUMO energy of **5-13** is-5.04 eV, substantially lower than any of the species reported thus far in this thesis, making it an impactful target as an n-type system.

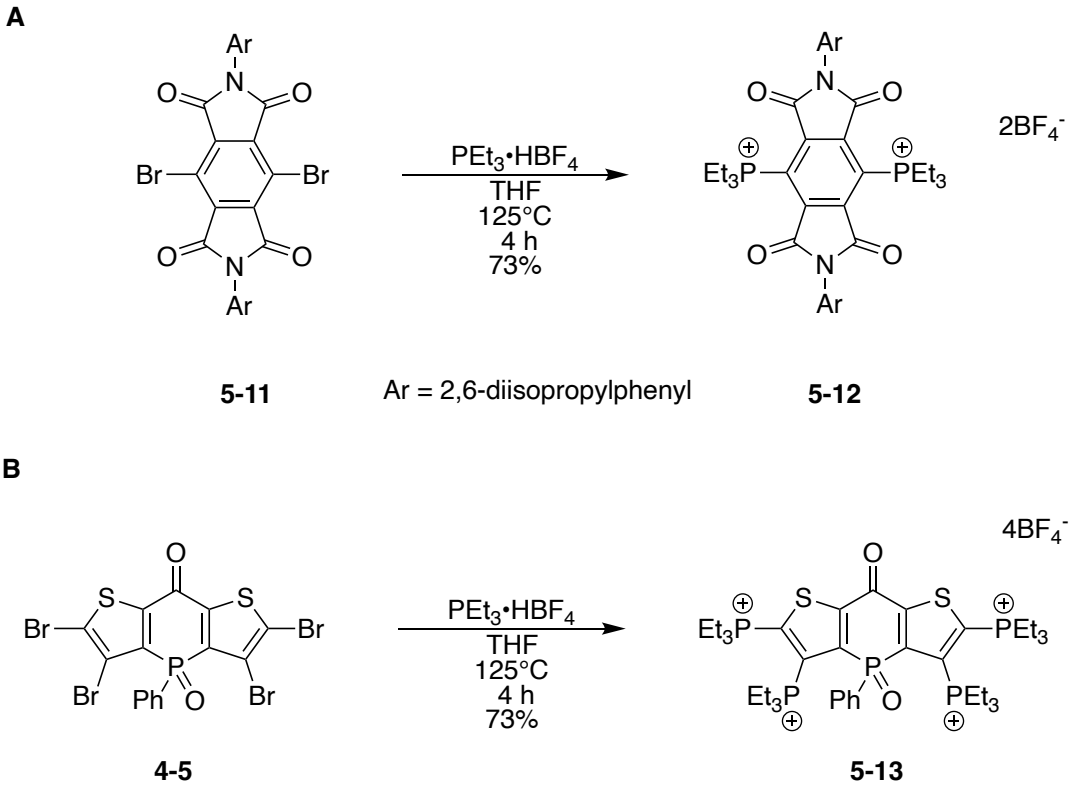

Scheme 5-4. Addition of cationic side groups to pyrometallic diimides reported by Cao et al.[11]

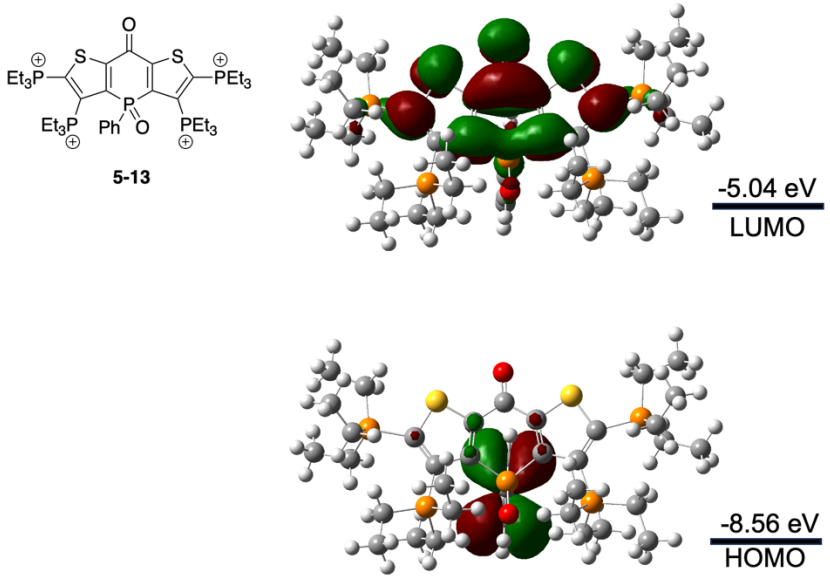

Figure 5-6. Frontier molecular orbitals of **5-13** with respective HOMO and LUMO energies (eV). Level: B3LYP/6-31G+(d) using a PCM solvation model in CH_2Cl_2.

5.2.8 Polycyclic Aromatic Hydrocarbon-type Dithienoketophosphinines

Polycyclic aromatic hydrocarbons are π-conjugated systems with at least two fused rings with many sp^2 carbons.[12–15] Structurally they can be planar, bent, bowl-shaped and various other distortions from planarity. Throughout the years, many main-group incorporated systems have been reported with various intriguing optical, structural, and electrochemical features. Examples of these systems can be found throughout the chapters of this thesis; the examples by the Romero-Nieto group on phosphaphenalenes and phosphahexaarenes are most similar.[16,17] A very recent example from our group reports a series of π-extended vat orange 3 systems containing fused six-membered phosphorus heterocycles (Figure 5-7A), falling into the category of nanographenes and polycyclic aromatic hydrocarbons.[18] The reported species have interesting optical features in solution as well as the solid state and generally low-energy emissions (>550 nm). The redox properties ranged between -2.04 V and -1.24 V (vs Fc/Fc^+) and, based on the environment of crystallization, the organization of the system in the solid state was impacted. Seeing the value of PAH type systems and main-group element incorporation, turning the tetra-cross-coupled products presented in Chapter 4 into PAH type systems **5-14** to **5-17** can be envisioned (Figure 5-7B,C). The target compounds would vary in their peripheral donor/acceptor strength, however, depending on the distortion from planarity or supramolecular packing, different optical features may arise. The formation of these systems can potentially be accomplished through Scholl reaction conditions using $AlCl_3$ and heat as a starting point, however, the exact required conditions will need to be explored in depth.[19,20]

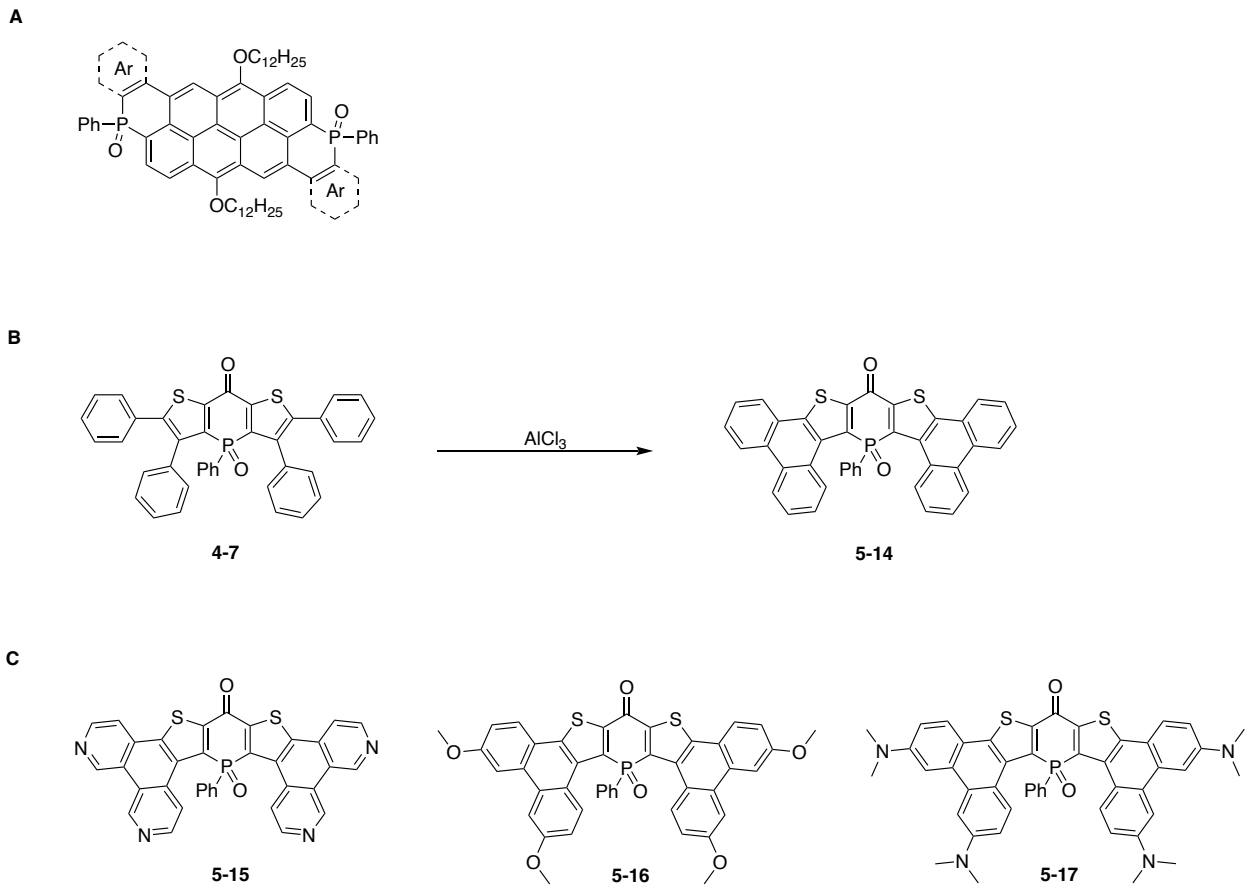

Figure 5-7. Phosphorus-incorporated vat orange 3 systems reported by our group (A); Formation of polycyclic aromatic hydrocarbon type dithienoketophosphinine **5-14** with generic Scholl reaction conditions (B); Proposed dithienoketophosphinine systems **5-15** to **5-17**.

5.2.9 Keto-modifications of Dithienoketophosphinines with Donor Groups

A final proposed series of compounds based on the dithienoketophosphinine system is an alternative to the electron-accepting qualities sought after in Chapter 3 with the dicyanomethylene functionalities. A well-studied building block in the field of supramolecular chemistry is tetrathiafulavelene (TTF).[21] It is known for its reversible two-electron oxidations and has been incorporated into different polycyclic aromatic hydrocarbons. Typically, the TTF-incorporated species display stronger absorptions with lower oxidation potentials. The TTF-motif can be

introduced onto carbonyl groups using Horner-Wadsworth-Emmons (HWE) reactions with the respective phosphonate reported by Nielson et al. to turn **5-18** into **5-19** (Scheme 5-5A). Compound **5-19** has lower oxidation potentials that are attributed to the electron donating character of the TTF motif and displays different absorption and emissions after charge/discharge cycles. When the TTF motif is present on an electron accepting system, an innate charge-transfer character arises and the dithienoketophosphinine the keto group would be an ideal site for functionalization along these lines as well (Scheme 5-5B; **5-20**). This could lead to opposing qualities to that of the dicyanomethylene functionalized species presented in Chapter 3 and may introduce reversible oxidation as well as reduction events, i.e., a true ambipolar species. Although enhanced electron-acceptor character is the goal, broadening the properties of the dithienoketophosphinine to various extremes would solidify its functionality and its ability to be catered to many different applications.

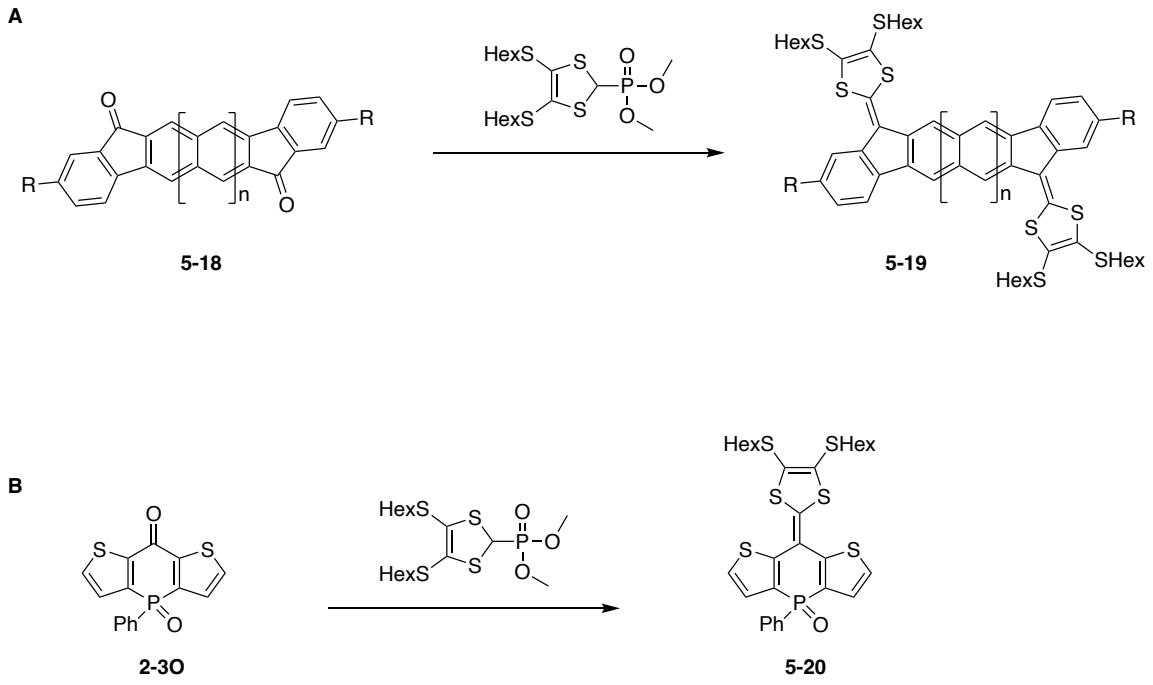

Scheme 5-5. (A) Horner-Wadsworth-Emmons (HWE) reaction performed by Nielson at all to form TTF-functionalized **5-18**; (B) proposed dithienoketophosphinine with TTF-type functionality.

Overall, the preceding chapters of this thesis have shown the versatility of the dithienoketophosphinine system at its initial stages. Although much knowledge has been attained from the various modifications performed on the key three sites on the dithienoketophosphinine scaffold, this chapter emphasizes that there is much work left to be done to ultimately fully harvest all of the properties of this highly intriguing functional molecular system.

5.3 References

(1) Stolar, M.; Borau-Garcia, J.; Toonen, M.; Baumgartner, T. Synthesis and Tunability of Highly Electron-Accepting, N-Benzylated "Phosphaviologens." *J. Am. Chem. Soc.* **2015**, *137* (9), 3366–3371. https://doi.org/10.1021/ja513258j.

(2) Liao, G.; Chen, X.; Qiao, Y.; Liu, K.; Wang, N.; Chen, P.; Yin, X. Highly Electron-Deficient Dicyanomethylene-Functionalized Triarylboranes with Low-Lying LUMO and Strong Lewis Acidity. *Org. Lett.* **2021**, *23* (15), 5836–5841. https://doi.org/10.1021/acs.orglett.1c01983.

(3) Mahoney, E. R.; Boudjelel, M.; Shavel, H.; Krzyaniak, M. D.; Wasielewski, M. R.; Malapit, C. A. Triphenylphosphine Oxide-Derived Anolyte for Application in Nonaqueous Redox Flow Battery. *J. Am. Chem. Soc.* **2025**, *147* (2), 1381–1386. https://doi.org/10.1021/jacs.4c07750.

(4) Bera, M. K.; Pal, P.; Malik, S. Solid-State Emissive Organic Chromophores: Design, Strategy and Building Blocks. *J. Mater. Chem. C.* **2020**, *8* (3), 788–802. https://doi.org/10.1039/C9TC04239C.

(5) Demay-Drouhard, P.; Baumgartner, T. Highly Luminescent 4-Pyridyl-Extended Dithieno[3,2-*b*:2′,3′-*d*]phospholes. *J. Org. Chem.* **2020**, *85* (22), 14627–14633. https://doi.org/10.1021/acs.joc.0c01369.

(6) Romero-Nieto, C.; Durben, S.; Kormos, I. M.; Baumgartner, T. Simple and Efficient Generation of White Light Emission From Organophosphorus Building Blocks. *Adv. Funct. Mater.* **2009**, *19* (22), 3625–3631. https://doi.org/10.1002/adfm.200901540.

(7) Neumann, T.; Dienes, Y.; Baumgartner, T. Highly Sensitive Sensory Materials for Fluoride Ions Based on the Dithieno[3,2-*b* :2′,3′-*d*]phosphole System. *Org. Lett.* **2006**, *8* (3), 495–497. https://doi.org/10.1021/ol052911p.

(8) Makkad, S. K. Amine Decorated Polystyrene Nanobeads Incorporating π-Conjugated OPV Chromophore for Picric Acid Sensing in Water. *RSC Adv.* **2020**, *10* (11), 6497–6502. https://doi.org/10.1039/C9RA09852F.

(9) Liu, B.; Tang, C. W.; Zhang, C.; Jia, G.; Zhao, T. Cost-Effective, High-Energy-Density, Nonaqueous Nitrobenzene Organic Redox Flow Battery. *Chem. Mater.* **2021**, *33* (3), 978–986. https://doi.org/10.1021/acs.chemmater.0c04118.

(10) Harter, L.; Bélanger-Chabot, G.; Rahm, M. Dinitroacetylene: Can It Be Made? *Propellants Explos. Pyrotech.* **2025**, *50* (4), e12019. https://doi.org/10.1002/prep.12019.

(11) Leake Gebresilassie, F.; Ji Kim, M.; Castellanos, D.; Broderick, C. H.; Ngo, S. M.; Young, V. G.; Cao, D. D. Bisphosphonium Benzene Diimides. *Chem. Eur. J.* **2024**, *30* (57), e202402791. https://doi.org/10.1002/chem.202402791.

(12) Delouche, T.; Roisnel, T.; Dorcet, V.; Hissler, M.; Bouit, P. Mixing Polyaromatic Scaffolds and Main Group Elements: Synthesis, Coordination and Optical Properties of Naphthyl-Fused Heteropines. *Eur. J. Inorg. Chem.* **2021**, *2021* (11), 1082–1089. https://doi.org/10.1002/ejic.202001097.

(13) Ripani, L.; Bombonato, E.; Paolucci, F.; Marcaccio, M. Electron Transfer in Polyaromatic Hydrocarbons and Molecular Carbon Nanostructures. *Curr. Opin. Electrochem.* **2022**, *35*, 101065. https://doi.org/10.1016/j.coelec.2022.101065.

(14) Wu, J.; Pisula, W.; Müllen, K. Graphenes as Potential Material for Electronics. *Chem. Rev.* **2007**, *107* (3), 718–747. https://doi.org/10.1021/cr068010r.

(15) Feng, X.; Wu, J.; Ai, M.; Pisula, W.; Zhi, L.; Rabe, J. P.; Müllen, K. Triangle-Shaped Polycyclic Aromatic Hydrocarbons. *Angew. Chem. Int. Ed.* **2007**, *46* (17), 3033–3036. https://doi.org/10.1002/anie.200605224.

(16) Hindenberg, P.; López-Andarias, A.; Rominger, F.; de Cózar, A.; Romero-Nieto, C. A Guide for the Design of Functional Polyaromatic Organophosphorus Materials. *Chem. Eur. J.* **2017**, *23* (56), 13919–13928. https://doi.org/10.1002/chem.201701649.

(17) Hindenberg, P.; Rominger, F.; Romero-Nieto, C. Phosphorus Post-Functionalization of Diphosphahexaarenes. *Chem. Eur. J.* **2019**, *25* (57), 13146–13151. https://doi.org/10.1002/chem.201901837.

(18) Dadgaryeganeh, R.; LeBlanc, J.; Pradhan, E.; Miao, D.; Hussein, A.; Hunter, H. N.; Zeng, T.; Romero-Nieto, C.; Baumgartner, T. From Flat to Twisted – Multifunctional Phosphacyclic Nanocarbons Based on Vat Orange 3. *Chem. Sci.* **2025**, *16* (8), 3680–3692. https://doi.org/10.1039/D4SC07106A.

(19) Jassas, R. S.; Mughal, E. U.; Sadiq, A.; Alsantali, R. I.; Al-Rooqi, M. M.; Naeem, N.; Moussa, Z.; Ahmed, S. A. Scholl Reaction as a Powerful Tool for the Synthesis of Nanographenes: A Systematic Review. *RSC Adv.* **2021**, *11* (51), 32158–32202. https://doi.org/10.1039/D1RA05910F.

(20) Rempala, P.; Kroulík, J.; King, B. T. Investigation of the Mechanism of the Intramolecular Scholl Reaction of Contiguous Phenylbenzenes. *J. Org. Chem.* **2006**, *71* (14), 5067–5081. https://doi.org/10.1021/jo0526744.

(21) Granhøj, J.; Zalibera, M.; Malček, M.; Bliksted Roug Pedersen, V.; Erbs Hillers-Bendtsen, A.; Mikkelsen, K. V.; Rapta, P.; Brøndsted Nielsen, M. Extended Tetrathiafulvalenes with Fluoreno[3,2-*b*]fluorene and Diindeno[1,2-*b*:1′,2′-*i*]Anthracene Cores. *Chem. Eur. J.* **2024**, *30* (5), e202302688. https://doi.org/10.1002/chem.202302688.